This is to certify that the
dissertation entitled

DETECTING INTRACELLULAR METABOLITES AND THE RESULTING CELL FUNCTION BY MERGING MICROFLUIDIC AND MICROTITRE PLATE TECHNOLOGIES.

presented by

Nicole Villiere Tolan

has been accepted towards fulfillment
of the requirements for the

Ph.D. degree in Chemistry

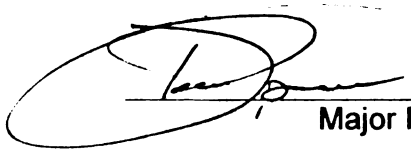

Major Professor's Signature

8-28-09

Date

MSU is an Affirmative Action/Equal Opportunity Employer

DETECTING INTRACELLULAR METABOLITES AND THE RESULTING CELL FUNCTION BY MERGING MICROFLUIDIC AND MICROTITRE PLATE TECHNOLOGIES.

By

Nicole Villiere Tolan

A DISSERTATION

Submitted to
Michigan State University
in partial fulfillment of the requirements
for the degree of

DOCTOR OF PHILOSOPHY

Chemistry

2009

ABSTRACT

DETECTING INTRACELLULAR METABOLITES AND THE RESULTING CELL FUNCTION BY MERGING MICROFLUIDIC AND MICROTITRE PLATE TECHNOLOGIES.

By

Nicole Villiere Tolan

Recent advancements have been made in our group to better mimic the blood vessels found *in vivo* in order to obtain a multicellular system that incorporates the relevant aspect of flow into an *in vitro* platform. By combining flow channels that approximate these vessels *in vivo* with an array of wells onto a single microfluidic device, we demonstrate an enabling system capable of merging microfluidic and microtitre plate technologies. This platform is used to monitor various aspects of the *in vivo* system that control vasodilation as it pertains to diabetes mellitus and the complications associated with the disease. This research has focused on the specific role of the erythrocyte or red blood cell (RBC) as it relates to hyperglycemic conditions and antioxidant status of the cell. The role of RBCs in controlling vascular caliber is discussed, detailing the concepts of RBC deformability and how glucose metabolism and antioxidant status affects adenosine triphosphate (ATP) release and its ability to stimulate subsequent nitric oxide (NO) production, a known vasodilator.

First, this device is used to measure both intracellular glucose metabolites and the resulting effect on RBC function. Specifically, this device is employed to monitor the antioxidant status of the cell while simultaneously determining the effect on ATP release, a known stimulus of NO production in endothelial cells, which is a major determinant in

vasodilation. Here, the affects of inhibitors on the pentose phosphate and polyol pathways for glucose metabolism, as well as the influence of hyperglycemic conditions, on the RBC antioxidant ability and the resulting ATP release are shown.

This multicellular device, incorporating flowing RBCs and a cultured endothelium, is used to determine the mechanisms of action for various stimuli of RBC-derived ATP release and the subsequent stimulation on endothelium-derived NO production. This plays an important role in the ability to monitor the final effect these substances have on the mechanism for NO production as it pertains to the complications associated with diabetes, specifically, hypertension and cardiovascular disease.

Moreover, preliminary results illustrating the importance of such a flow-based device for monitoring the specific mechanism of action for two pharmaceuticals, pentoxyfilline (trental) and iloprost, are presented. Only by employing a flow-based system could the mechanism for trental-induced ATP release be shown effective, speculating that the increase vasodilation observed *in vivo*, acts by way of mechanical deformation-induced ATP release.

This research demonstrates the need for incorporating such a flow-based system into the current technologies used for drug discovery in order to combat the exponential increase in healthcare costs and the ability to implement a more individualized method for clinical testing. With appropriate dimensions, identical to the microtitre plates utilized today, automation and detection methods for drug discovery and clinical diagnosis processes could be implemented.

DEDICATION

To all of those that have affected my life in one way or another,

to help me end up here, where I am today.

ACKNOWLEDGMENTS

I would like to acknowledge Dr. David Green and Dr. Cliff Harris of Albion College for their undying devotion to undergraduate education; it is to them I owe all future aspirations from that point. My interest in the sciences only began upon their teachings and has continued to grow with their guidance. To my family, I owe the utmost appreciation and recognition of their support, as my education has always, and always will be, a priority.

I owe much gratitude to my graduate advisor, Dr. Dana Spence, as well as my past and present lab-mates in the Spence group. Without the opportunity to apply myself to an unbelievably worthy area of research, I do not feel that I would have put forth enough dedication to continue on to obtain my degree. It is to Dr. Spence I owe the most appreciation, he has made a large contribution to the sciences and I can only foresee his findings to play an integral role in the medicinal arena in the future. To all the students of the Spence Group, past and present, I have enjoyed working with such an intelligent, hard working, and self-motivated group. To those I gain great knowledge from, especially Luiza and Ajith, I look forward to future discussions of our research as we move onto new areas of study. Your help and support has been essential for me.

Finally to my husband Nick, your love and patience, support and thoughtfulness, has enabled me to achieve this degree. It is to you I owe the most important moment in my life, thus far. Together, three as one, we are unbreakable.

TABLE OF CONTENTS

LIST OF TABLES

LIST OF FIGURES

CHAPTER 1: INTRODUCTION

The motivation behind the work presented here is the incorporation of analytical methods to determine biologically relevant processes and mechanisms. Specifically, advancements have been made to better mimic the *in vivo* resistance vessels by employing an *in vitro* platform in order to conduct various analytical measurements on blood analytes. Specific attention has been given to perform complete and appropriate sample handling, analytical measurements, and accurate data interpretation of biological analyses of bulk cell samples.[1] Here, biological systems related to diabetes and the main complications associated with the disease are monitored and discussed in great detail. Research has been performed and methods have been developed to monitor various intracellular metabolites as well as intercellular communication between multiple cell types, which may play a key role in complications associated with diabetes, especially hypertension.

Microfluidic technology has fallen short of fulfilling the promises of integrating high throughput analyses within a flow-based platform. It is speculated that this may be due to a lack of standard dimensions which are, currently in place for microtitre plates. Standardized dimensions has allowed for the incorporation of automation technologies, such as liquid handling and plate readers. The goal of this work is to incorporate the requirements for individual assays onto one microfluidic device, examining multiple glucose metabolism pathways in a high throughput system, while also monitoring overall cell function as it pertains to cell-to-cell communication. The research aims were to demonstrate the integration of multiple pathways involved in glucose metabolism,

providing more information as to the mechanism of cell function that contributes to diabetic complications.

The development of a high throughput, simultaneous method of addressing various aspects of a single RBC sample will allow for a specific diagnosis of the glucose metabolism malfunction that results in inadequate blood flow that is typically observed in diabetic patients. The specific aims concentrated on evaluating both the pentose phosphate and polyol pathways by inhibiting glucose 6-phosphate dehydrogenase (G6PD) and aldose reductase (AR), while monitoring the resulting levels of reduced nicotinamide adenine dinucleotide phosphate (NADPH), glutathione (GSH), sorbitol (SORB) as well as the resulting released ATP. This research also demonstrates the ability to then monitor on a separate microfluidic array (μFA) the intracellular NO production within cultured bPAECs as a result of pharmaceutically and shear-induced ATP release from the RBC.

1.1 DIABETES MELLITUS

According to the American Diabetes Association (ADA), diabetes is classically presented with symptoms of polyuria (excessive urination), polydipsia (excessive thirst), and unexplained weight loss. Diabetes is classified as a group of metabolic disorders that may also be presented with polyphagia (excessive hunger), blurred vision, growth impairment, ketoacidosis, nonketotic hyperosmolar syndrome and often times results in susceptibility to infection. It is caused by individual instances of reduced insulin secretion or insulin efficacy, or a combination of the two and it is often difficult to determine the original cause of hyperglycemia (high blood sugar). The two accepted

methods for diagnosing diabetes are the fasting plasma glucose test (FPG), where no caloric intake is sustained for 8 hrs prior to glucose measurement, and the oral glucose tolerance test (OGTT), where plasma glucose levels are measured two hours after administering 1.75 g glucose per kg body weight. Diabetes is confirmed when FPG levels are above 126 mg/dL or when plasma glucose levels are at or above 200 mg/dL for an OGTT. Another common marker of diabetes is the glycosylated hemoglobin (A1C) test. Levels less than 7% are associated with microvascular disease prevention and indicates the amount of hemoglobin glycated due to elevated plasma glucose levels.[2] An A1C level of 6% is synonymous to an average blood plasma glucose level of approximately 120 mg/dL and is used to gauge control of blood glucose in diabetes patients.[3]

Pre-diabetes, as described by the Center for Disease Control and Prevention (CDC), is a condition in which a person has elevated risk of developing type II diabetes, heart disease and stroke. Pre-diabetes is indicated by resulting FPG and OGTT levels between 100-125 mg/dL and 140-199 mg/dL, respectively. The resulting impaired fasting glucose (IFG) and impaired glucose tolerance (IGT) are associated with metabolic syndrome and typically accompanied by normal levels of A1C. In 2007, the CDC reported that 23.6 million people in the United States were affected by diabetes and concluded that 17.9 million were diagnosed, leaving 5.7 million undiagnosed and unaware of their disease.[4] The ADA outlines the various degrees of blood glucose levels present in the three main classifications of diabetes, type 1, type 2, and gestational diabetes, shown in table 1.1.[5]

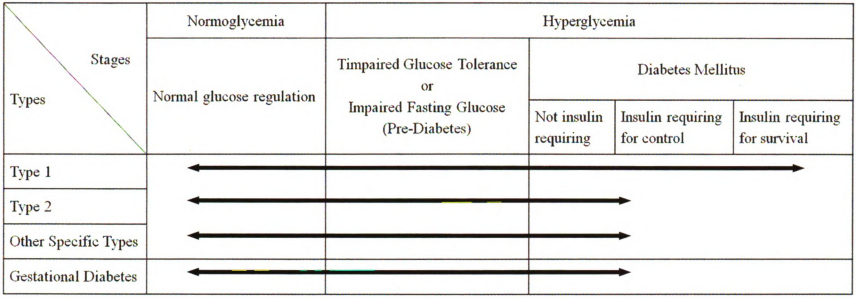

Table 1.1 Degree of glycemic ranges present in each individual type of diabetes from normal blood glucose levels to a hyperglycemic condition, which coincides with insulin dependence as a result from impaired glucose tolerance or fasting glucose levels. Both type 1 and type 2 diabetics often require insulin for blood glucose control, suggesting a resistance to insulin as well as a reduction in insulin secretory response.

1.1.1. THREE MAIN CLASSIFICATIONS OF DIABETES

Insulin-dependent diabetes mellitus (IDDM), commonly known as type 1 diabetes and previously referred to as juvenile-onset diabetes, is associated with a lack of insulin production, a hormone necessary for glucose clearance from the blood stream. Type 1 diabetes represents only about 5-10% of all the reported cases of diabetes. It typically develops in children, however, it can occur at any age, ultimately resulting in the necessity of insulin therapy for survival. In the case of type 1 diabetes, insulin is no longer produced by the beta cells (β-cells) of the pancreas due to the autoimmune destruction of these cells.[5-7] The trigger for this autoimmune response leading to the damage of the β-cells has been explained as a polygenetic disposition[8] resulting from multifactoral environmental effects, which may include viral infection.[9-11] The β-cells are contained within the islets of Langerhans, which are located in the pancreas, serving to produce and secrete insulin into the blood stream in response to elevated blood glucose levels.

It is thought that the susceptibility to autoimmune destruction of the β-cells is due to upregulation of both Major Histocompatability Complex (MHC) class I molecules and interferions as a result of viral infection-induced inflammation. The MHC is a region of the human genome that is responsible for encoding for proteins that are involved in the immune system, including autoimmunity. Interferions are proteins produced by the cells that comprise the immune system and are responsible for cell signaling that is necessary for the destruction of foreign bodies or malfunctioning cells which commonly include viruses, parasites, and tumor cells.

It has been reported[5] that 85-90% of all patients diagnosed with type 1 diabetes presents with at least one autoantibody marker, either to insulin, glutamic acid decarboxylase (GAD) or tyrosine phosphatases (IA-2 and IA 2β). GAD and tyrosine phosphatases are class of enzymes that have been of particular interest to research of diabetes because these enzymes are typically targeted by autoantibodies in diabetes patients. There are many genetic predispositions for β-cell destruction leaving type 1 diabetics prone to various other autoimmune disorders such as, but not limited to, Grave's disease, Hashimotos's thryroiditis, Addington's disease, vitiligo, celiac sprue, autoimmune hepatitis, myasthenia gravis, and finally, pernicious anemia.[5] The rate of β-cell destruction is variable, typically vigorous in infants and children, where as a much slower reduction of β-cell mass is observed in adults.

As β-cell mass decreases and insulin production is reduced, ketoacidosis, typically symptomatic of type 1 diabetes, occurs as the formation of ketone bodies are produced via ketosis. Here, the body resorts to metabolism of fatty acids and the deamination of amino acids, resulting in an eventual acidification of the blood leading to the symptoms associated with diabetes, as well as nausea and vomiting, abdominal pain, shortness of breath, sweet fruit- or acetone-scented breath as well as confusion. The amount of insulin secreted is typically determined by indirectly measuring the amount of C-peptide within the peripheral circulation.

C-peptide has been used as a means to classify diabetes type because it is secreted in equimolar amounts with insulin from the pancreatic beta cells. Proinsulin is produced in the β-cells and is comprised of insulin and C-peptide, which is the C-chain that connects the A- and B-chains of insulin. Comprised of 31 amino acids, C-peptide is

cleaved from the active form of the hormone as it is secreted into the pancreatic islets. It is measured to determine insulin secretion for several reasons, but importantly, because its concentration within the peripheral circulation reflects the original proinsulin production due to increased half-life, compared to insulin, which is typically extracted by the liver due to its bioactivity.

Non-insulin dependent diabetes mellitus (NIDDM) or type 2 diabetes, previously described as adult-onset diabetes, is classified as an insulin resistance, where the insulin that is produced is not properly utilized by the cells comprising the peripheral tissues of the body. This lack of insulin activity results in hyperglycemia, increasing both FPG and A1C levels. Type 2 diabetes accounts for approximately 90 to 95% of all cases of diabetes and can also result in a reduction of relative insulin secretion as the disease progresses, further requiring antihyperglycemic medication or insulin along with an insulin sensitizer.

While autoimmune β-cell destruction does not occur in type 2 diabetes, β-cell dysfunction due to hyperglycemia may be responsible for the reduced insulin secretion and can be at least partially restored upon lowering blood glucose levels.[12] Measuring the concentration of β-cells within the pancreas often varies across different methods, however, the concentration of β-cells in the pancreas of type 2 diabetic patients is characteristically reduced by approximately 40-60% when compared to those found within the pancreas of healthy non-diabetic patients.[13] This decrease is thought to be due to an upset of the balance between the loss (through apoptosis) and regeneration (through replication or differentiation of precursors) of β-cells. Commonly, patients diagnosed

with type 2 diabetes are obese or have an increased percentage of body fat that is associated with insulin resistance.

Hyperglycemia typically presents in a more gradual fashion in type 2 diabetes and rarely results in ketoacidosis, although when it does occur, it typically is due to an onset of another illness or infection. Unlike type 1 diabetes, the genetic profiles that are associated with type 2 diabetes are more complex and are currently obscurely defined. The risk of developing type 2 diabetes is increased with age, obesity, lack of physical activity and is also elevated among individuals of certain racial or ethnic background (Hispanic/Latino Americans, Native Hawaiians, American Indians, Asian Americans, African Americans and Pacific Islanders).[5]

Gestational diabetes mellitus (GDM) is defined as any sort of glucose intolerance that is first diagnosed during pregnancy and is described as a disorder of carbohydrate metabolism.[14] The resulting glucose intolerance and lack of insulin secretion typically only occurs during the term of pregnancy and are characteristically alleviated upon delivery. However, the risk of sustaining glucose intolerance in the form of type 2 diabetes, even after child birth, is elevated in comparison to non-GDM individuals.[15] GDM is more frequently diagnosed in women of African American, Hispanic/Latino American, and American Indian ethnic background. It was reported that on average, 4% of all pregnancies in the US are complicated by GDM, although it represents 90% of all pregnancy complications[5]. GDM is usually diagnosed within the third trimester of pregnancy where diet modification and or insulin therapy can control hyperglycemia. Treatment for hyperglycemia during pregnancy is necessary to avoid complications in the infant as well as reduce the risk of spontaneous abortion.

Diabetes outside of these three main classifications include maturity-onset diabetes of youth (MODY), genetic predisposition to ineffective insulin action, endocrinopathies, drug- or chemical-induced diabetes, and those affected by damage to, or disease of the pancreas, representing an estimated 1-5% of all cases of diagnosed diabetes. In the case of MODY, patients are affected by a monogenetic defect in β-cell function that is typically displayed as hyperglycemia before the age of 25 years. Here, there are minimal or no defects in insulin action and the impaired insulin secretion is most commonly due to a mutation in chromosome 12 (the hepatic transcription factor (HNF)-1α), or a mutation in chromosome 7p (the glucokinase gene).[5] In the past, the genetic defect in insulin action was described as "type A" diabetes, and is a metabolic disorder of hyperinsulinemia and modest hyperglycemia, resulting in severe diabetes.

Endocrinopathies, or diseases that are dependent upon the endocrine gland, may result in an insulin resistance due to elevated levels of various hormones such as growth hormone, cortisol, glucagon and epinephrine. Here, the diabetic condition is typically found with some sort of pre-existing defect in insulin action and once hormone levels are balanced, the hyperglycemic condition is resolved.[5]

Various drugs, such as nicotinic acid, glucocorticoids and α-interferons have been reported to impair insulin effectiveness. Numerous infections and viruses have also been correlated with an insulin inactivity, the most common of which are, congenital rubella, coxsackievirus B, cytomegalovirus, adenovirus and mumps. Finally, damage to the pancreas either through pancreatitis, physical trauma, infection, or pancreatic carcinoma, has been shown to result in insufficient insulin production and hyperglycemia. It has been noted[5] that this damage need not be extensive to greatly diminish insulin secretion

and must involve another pathway besides physical reduction in β-cell mass because cancer of only a small portion of the pancreas has been shown to result in diabetes.

1.1.2 COMPLICATIONS ASSOCIATED WITH THE DIABETES

Diabetic patients often suffer from one or more related complications including, but not limited to, blindness, kidney damage, nerve damage, periodontal disease, pregnancy complications, heart disease, stroke, and cardiovascular disease. Detailed information regarding the complications associated with diabetes and their US statistics are derived from the Center for Disease Control and Prevention's Diabetes National Fact Sheet for 2007.[4]

Diabetic retinopathy is the leading cause of blindness in diabetics 20-74 years of age and was reported to result in 12,000 to 24,000 new cases of blindness each year. It is classified as non-inflammatory damage to the retina, resulting from dysfunction and eventually bleeding from the capillaries of the eye. It has been reported that nearly all patients diagnosed with type 1 diabetes and more than 60% of those diagnosed with type 2 diabetes will be diagnosed with retinopathy within 20 years of diagnosis.[16]

Nephropathy, or kidney disease, is also predominantly associated with diabetes as it is the leading cause for renal failure, eventually resulting in the requirement for chronic dialysis or kidney transplant. By monitoring the concentration of albumin (the most abundant blood plasma protein) and creatinine (produced as creatinine phosphate from the muscle, is broken down) excretion in the urine, the severity of renal failure can be determined.[17]

It was estimated in 2007 that 60-70% of people with diabetes have mild to severe peripheral neuropathy, or nerve damage resulting in numbness or pain in the hands and feet. In severe cases, neuropathy can progress to form ulcers where the need for amputation occurs. It was reported that more than 60% of nontraumatic amputations are associated with diabetes-related neuropathy. Autonomic neuropathy, results in gastrointestinal and sexual dysfunction. Periodontal (gum) disease has been reported to affect 33% of diabetics where it is twice as common in young adults, and three times more likely to occur as poorly controlled A1C levels increase (>9%).

Approximately 5-10% of pregnancy complications due to GDM result in serious birth defects and an increase in the number of spontaneous abortions resulting from poorly controlled glycemia prior to conception or during the first trimester of pregnancy. As in the case of GDM, as with diabetes in general, there has been a reported increased incidence of vascular disease that is presented as endothelial dysfunction, increased oxidative stress, and general over expression of inflammatory responses.[18]

Oxidative stress is defined as a disruption in the balance between the production of reactive oxygen species (ROS) and the antioxidant defenses. Superoxide anion (O_2^-), hydrogen peroxide (H_2O_2), hydroxyl radical (OH^-) and peroxynitrate ($OONO^-$) are all examples of ROS that have been correlated to the oxidation of membrane lipids that are thought to play an integral role in the development of atherosclerosis.[19] Research has indicated increased concentrations of ROS may impair NO signaling which could then reduce endothelium-dependant vasodilation, increase platelet aggregation and the expression of adhesion molecules leading to neutrophil migration to the endothelium and proliferation of smooth muscle cells.

There are long-term complications that are associated with the continued hyperglycemic conditions that are found in diabetes, and often results in a combination of the complications associated with hypertension. Along with hypertension, or high blood pressure, are increased occurrences of cardiovascular, peripheral arterial and cerebrovascular disease. The complications typically associated with type 2 diabetes are more frequently due to micro- and macrovascular disorders. Microvascular disease is a condition of the resistance vessels where plaque formation, constriction of the arteries, or damage to the lining of these vessels can occur.

It has also been reported that there is a substantial increased risk for cardiovascular disease in people with type 1 and type 2 diabetes compared to healthy controls.[17,19] Moreover, among those diagnosed with diabetes, at least 65% will die from a heart attack or stroke. According to the CDC, cardiovascular diseases include various forms of heart and blood vessel dysfunctions such as high blood pressure, coronary heart disease, stroke, and heart failure.[4] A heart attack, or myocardial infarction, is described as the blockage of blood flow to a portion of the heart and upon lack of oxygen (O_2), often results in permanent damage to the heart muscle. The blockage of proper blood flow is typically a disturbance of plaque buildup in a coronary artery, which is due to atherosclerosis.

Atherosclerosis is defined as the narrowing of the coronary arteries due to a combination of buildup of plaque, deposits of fat, cholesterol and platelets within the vessels comprising the circulation system, and hardening of the arteries due to calcification. Stroke, resulting in a loss of brain function is due to a disturbance of blood flow to the brain which results either from a blood clot or bleeding into the tissue of the

brain from a break in the blood vessel. It has been suggested in the literature that an increase in oxidative stress, as with patients diagnosed with diabetes and sustained hyperglycemia, is directly correlated with an adverse affect on the vascular system and an increase in atherosclerosis.[19]

Dyslipidemia, a condition in which there is an increased level of lipids found in the circulation system, often arises due to prolonged elevated levels of insulin, as in the case of type 2 diabetes. The elevated levels of lipids within the blood stream combined with hypertension, increases the risk of type 2 diabetics to have two to five times higher risk of cardiovascular disease.[4] Uncontrolled hyperglycemia has been associated with biochemical imbalances that can lead to diabetic ketoacidosis as well as hyperosmolar (nonketotic) comas and put individuals at higher risk of illnesses, increasing the prognosis and likely hood of mortaility.

1.1.3 CURRENT THERAPIES AND TREATMENTS

It has been reported[4] that patients diagnosed with type 1 or type 2 diabetes, combined, take insulin only (14%), insulin and oral medication (13%), oral medication only (57%) or neither (16%). The US department of Health and Human Services recently compared the various oral antihyperglycemics classifying each as biguanides, sulfonylureas, thiazolidinediones (TZDs), and finally, alpha-glucosidase inhibitors. These oral medications all work to reduce blood glucose levels by either inhibiting the glucose production in the liver or carbohydrate absorption in the small intestine or by increasing insulin secretion or glucose uptake. These medications more effectively

decrease hyperglycemia, which is monitored by A1C levels, by using combinatorial therapies.

The Diabetes Control and Complications Trail (DCCT)[20] involved 1,500 type 1 diabetic patients and evaluated the affect of strict blood glucose control, maintaining levels approximate to those found in healthy non-diabetics, on complications such as retinopathy, neuropathy, and cardiovascular disease. It was determined that when maintaining normoglycemic levels by increased frequency in insulin injections, as compared to conventional treatment protocols, there was a correlated decrease in retinopathy, microalbuminuria and clinical neuropathy. It was also reported that the main side effect of stringent regulation of glucose levels was severe hypoglycemia, 11 people died, and 32 people were suspended from the clinical trial due to an evaluation deeming continued participation hazardous.

In a separate, but similar study, the Epidemiology of Diabetes Interventions and Complications (EDIC) research group performed a long-term (17 year) follow up study of the original DCCT.[17] It was determined that long-term risk of cardiovascular disease, including the incidence of non-fatal myocardial infarction, stroke, and death from cardiovascular disease, was reduced by more than 50% with the use of the previously adopted (DCCT) intensive treatment protocol when compared to the conventional treatment protocol. Specifically, there was a significant increase of developing cardiovascular disease in those patients administered conventional treatment with age, duration of diabetes, presence of retinopathy, current smoking status, body mass index, lipoprotein cholesterol, A1C, and albumin secretion levels.

1.2 RBCs: MORE THAN JUST OXYGEN CARRIERS

While one of the main functions of the RBC is to transport O_2 to the tissues surrounding the macro- and microvasculature system and uptake the carbon dioxide (CO_2) produced as waste from respiring cells, this highly specialized cell may also be involved in glucose clearance from the blood stream, and functions as a component necessary for vasodilation. The RBC, as reviewed by Bossi and Giardina,[21] is a simplistic biconcave cell that lacks a nucleus and intracellular organelles. Commonly referred to as a bag of hemoglobin (Hb), the RBC contains three main classes of this most abundant tetramer, the major adult Hb (HbA), the minor adult Hb (HbA2) and fetal Hb (HbF) each of which are comprised of a pair of α and β subunits, except for HbF which contains two α and two γ subunits. Both the α and β subunits contain a highly conserved hydrophobic heme pocket that binds to an iron atom through four pyrrole nitrogens and one axial bond to a histidyl residue of the polypeptide chain. The sixth bond to the ferrous iron atom (Fe^{2+}) is in the axial position and serves as the O_2 binding site. There are two separate intersubunit contacts, the $\alpha1$-$\beta1$ and the $\alpha1$-$\beta2$, where the differing subunit connections are hydrophobic in nature as compared to the two identical chain interactions, being polar.

The ability of hemoglobin to bind to O_2 is characterized by a sigmoidal binding curve that results from cooperative binding between each of the four O_2 binding sites. There are two separate conformations of hemoglobin, the tense (T) state deoxygenated structure and the relaxed (R) oxygenated structure. The T-state has a low affinity for O_2 and a high affinity for molecules found in the bloodstream such as carbon dioxide, organic phosphates, and protons. The alkaline Bohr effect, provoking the release of

protons above a pH of 6, results in Hb readily binding to O_2, shifting the conformation to the high-affinity relaxed R-state. The binding of Hb to the CO_2 that is produced from respiring tissues is inversely, yet equally, as important as the transport of O_2. The transport of CO_2 is achieved through either a direct binding to Hb or indirect method of hydrating CO_2, both of which are reversed in the lungs.

1.2.1 GENERAL STRUCTURE AND FUNCTION

When transversing the microvasculature system, red blood cells (RBCs), with inner diameters of 5-8 μm, are able to undergo cellular deformation to pass through capillaries with internal diameters ranging from 3-8 μm.[22,23] This cellular deformability is highly dependent on the cytoskeletal membrane proteins as well as the surface area to volume ratio. The RBC membrane is comprised of approximately 52% protein, 40% lipids, and 8% carbohydrates, all of which are important for the biconcave disc shape that allows the RBC to undergo considerable deformation without affecting cellular function or vitality. The lipid membrane is composed of a bilayer where the core is hydrophobic from the two fatty acid chains facing in towards one another, while the hydrophilic polar head groups face outward, towards the lumen, and inward, towards the cytoplasm of the cell.

There are over 100 different proteins that make up the RBC membrane, and include spectrin, adducing, protein 4.1, and ankyrin. These proteins are oriented such as to maintain membrane asymmetry, which is only compromised by membrane lipids that can undergo transverse diffusion and undergo outward translocation. The outer leaflet is mostly composed of phosphatidylcholines and sphingomyelins, where as the inner leaflet

of the cell has highest concentrations of phosphatidylserines and phosphatidylethanolamines. It is the job of both the ATP-dependant translocases and the aminophospholipid translocase, to revert back any phospholipids and aminophospholipids, respectively, that undergo outward translocation, playing an important role in apoptosis and cellular signaling for phagocytosis. Apoptosis, or programmed cell death, of the RBC can occur through the process of erythrophagocytosis where various morphological changes to the RBC result in identification and ingestion by macrophages. This process is mediated by oxidative stress, activating scramblase-1, controlling outward translocation of phosphatidylserines, and inhibiting aminophospholipid translocase.[24] It has been stated[21] that any sort of gene mutation or oxidative damage that results in a defect of any of the membrane proteins involved in the cellular membrane will change the cell volume and affect cellular deformation and influence premature cell death.

A significant positive correlation between membrane lipid peroxidation, induced through *in vitro* hyperglycemic conditions, and osmotic fragility has also been reported.[25] The relationship between these compromising affects on RBCs were shown to be directly dependent on oxidant stress due to the reversibility upon addition of fluoride, a known glucose metabolism inhibitor, vitamin E, a known antioxidant, *para*-chloromercurobenzoate and metyrapone, both known to inhibit the oxidizing manner of the cytochrome P-450 system, as well as dimethylfuran, diphenylamine, and thiourea, all serving as O_2 radical scavengers.

It has been demonstrated that there is a significant increase in glycosylation of RBC membrane proteins obtained from diabetic patients in comparison to healthy non-

diabetic controls.[26] Among the membrane proteins affected, spectrin was shown to undergo the most oxidative damage resulting from the free radicals generated when proteins were subjected to sustained hyperglycemic conditions. Spectrin comprises the bulk of the membrane skeleton of the RBC and it is the hexagonal lattice of the tetramer, associated with integral actin filaments, which allows for a rugged, yet flexible cellular membrane.[22,24] Studies have shown that structural abnormalities of the RBCs obtained from people with type 2 diabetes include distorted distribution of spectrin moieties and membrane-bound insulin receptor.[27] Spectrin is a polypeptide that when subjected to oxidation, resulting in the formation of disulfide bonds between chains, has been shown to reduce shear-based deformation.

In the case of type 2 diabetes the hyperglycemic conditions as illustrated in figure 1.1, result in an increase in oxidant stressors leading to glucose oxidation, protein glycation and an increase in advanced glycation endproducts (AGEs).[19,28] The morphological changes that take place in the RBC due to oxidant stress can lead to decreased deformability, increased membrane viscosity, increased aggregation, membrane lipid peroxidation, and phosphatidylserine externalization. Scanning electron microscopy was used to determine the morphological changes of RBCs obtained from type 2 diabetics when compared to healthy donors, illustrating both the acanthocytes, typically observed in patients with hyperinsulinemia, as well as cup forms, which are often found in patients with cardiovascular disease.[27] The rearrangement and redistribution of spectrin throughout the cytoskeleton of RBCs obtained from patients with diabetes was observed using fluorescence spectroscopy and these findings suggest

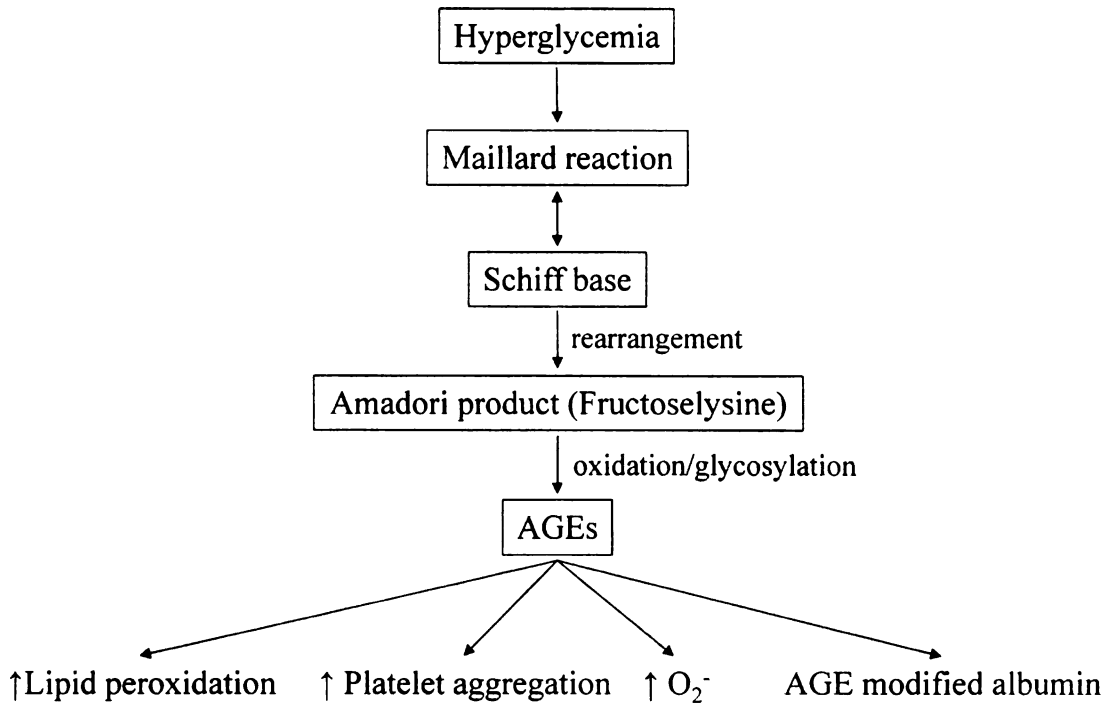

Figure 1.1 Illustration of the formation of advanced glycation endproducts (AGEs) and reactive oxygen species result from maintained hyperglycemic conditions. This image is modified from Stephens *et al*, linking oxidative products to the cellular processes that are speculated to result in the complications associated with diabetes.

that oxidative damage could lead to better understanding the severity of the associated complications.

It has been demonstrated that there is a significant reduction in the deformation of RBCs obtained from patients with diabetes when compared to those obtained from healthy, non-diabetic controls.[23,26] Within the circulation, RBCs exhibit non-Newtonian flow and concentrate in the center of the circulation vessels thereby minimizing the resistance to flow. This phenomenon is known as the Fahraeus-Lindqvist effect.[29] This effect leads to a decrease in the viscosity of the RBC solution as it passes through decreasing vessels. It has been the main explanation for the ability of the RBC, with approximate inner diameters ranging from 5-8 μm, to undergo mechanical deformation against one another within the vasculature system, having inner diameters ranging anywhere from 75 to 100 μm.

Under significant shear stress, the RBCs form ellipsoids from which the elongation, a measure of deformability, can be derived.[22] The deformability of RBCs subjected to various thiol reactive SH-reagents, resulting in disulfide formation between membrane proteins, was determined by Bossi and Gardinia. It was concluded that diamide, specific for oxidizing SH groups in spectrin, only induces a small fraction of dimerization, yet lends to a 50% decrease in RBC deformation. This exemplifies that even a small change in the number of disulfide bonds, from the native form of spectrin, will greatly affect the shear resistance of the RBC membrane.

1.2.2 MECHANICAL DEFORMATION-MEDIATED ATP RELEASE

Research has shown that RBCs play an essential role in the circulation, not only in carrying O_2 throughout the body, but also in the mechanism of vasorelaxation of the systemic and micro circulation. It has been suggested that the ability of the RBC to communicate the need for O_2 from the tissue to the vasculature, increasing blood flow and ultimately the supply of O_2 is mediated by the ability of the RBC to release adenosine triphosphate (ATP).[30-33] It has been well established that the ability of RBCs to release ATP upon mechanical deformation is a necessary factor for the stimulation of nitric oxide (NO) synthesis in the endothelium lining the luminal surface of the vasculature which will be detailed in a subsequent chapter.

It was shown that in isolated perfused rabbit lungs, the presence of rabbit RBCs was required in order to induce the stimulation of NO, resulting in vasodilation.[34] Further validating a relationship between RBC-derived ATP release and the control of vascular caliber, studies have shown that upon interluminal addition of 10 μM ATP into the arterioles of a hamster retractor muscle, significant vasodilation occurred[30] and separately, studies have also been performed, demonstrating that the presence of RBCs was necessary for a resulting increase in vascular caliber under low O_2 tension conditions.[33]

It has been concluded that the RBCs ability to release low micromolar concentrations of ATP, as a result of low O_2 tension as well as a change in pH, will increase vascular caliber and increase blood flow,[30,32] thereby altering the distribution of RBCs throughout the vascular system and ultimately increasing the supply of O_2 to localized tissues where it is in needed. Further studies, applying ATP to the intraluminal side of arterioles and the resulting vasodilation, demonstrated that the release of low

nanomolar amounts of ATP from RBCs *in vivo is* responsible for the vasodilation mechanism of resistance vessels.[31]

ATP release from RBCs has been previously measured in a continuous flow system by employing the luciferin/luciferase assay, which has also been employed in this research and will be discussed in detail in subsequent chapters.[35] By using various internal diameter fused silica microbore tubing and by varying the length of tubing, increasing ATP release was shown to correlate with the increased shear stress. This flow-based system, employing tubing with inner diameters ranging from 25-75 μm closely mimics the arterioles (10-100 μm) found *in vivo*, where the primary control of vascular resistance takes place. This experimental set up is an advancement in comparison to previous filtration methods for measuring deformation-induced ATP release. Filtration methods require an off-line approach to determine ATP release, employing the luciferin/luciferase assay, inherently reducing sample throughput. Also this method strays from an *in vivo* approximation since it is only applicable to hematocrits (volume percent RBCs in buffer) above 5% and less than 20% to allow for proper signal intensity and to prevent clogging, respectively.[34,36]

The mechanical deformation of RBCs has also been evaluated using a pressure-based system in which varying hematocrit RBC samples as well as chemically stiffened RBC samples were compared to each other and correlated to the mechanically-induced ATP release.[29] By replacing the filter, as used in previously mentioned studies, with a 15 cm section of 25 μm microbore tubing, the RBC deformation and resulting ATP release was determined. As the number of RBCs within the tube increases (as with increasing hematocrit) the RBCs are able to absorb pressure placed on the system as the flow is

increased to 10 μL/min. Thus, the time required for the system to reach half pressure of equilibrium is proportional to the deformability of the RBC sample and the subsequent deformation-induced ATP release was measured in the effluent.

1.2.3 G-PROTEIN COUPLED SIGNAL TRANSDUCTION PATHWAY

The proposed mechanism for the release of ATP from RBCs includes the activation of the receptor-mediated membrane-bound heterotrimeric G-proteins (G_s or G_i) (figure 1.2).[37-39] This occurs as either mechanical deformation of the RBC membrane changes the conformation of the G-protein coupled receptor (GPCR) or through the pharmaceutical stimulation as iloprost can bind to the prostacyclin receptor (IPR).[39] It has been reported in the literature that activation of either G_s or G_i will result in increased 3'5'-cyclic adenosine monophosphate (cAMP) upon activation of adenylyl cyclase (AC), subsequently initiating the phosphorylation of the cystic fibrosis transmembrane conductance regulator (CFTR) by protein kinase A (PKA).[40] Sprague *et al.* effectively demonstrated this signal transduction pathway by monitoring the reduced ATP release from RBC when G_s was inhibited with pertussis toxin.

Separately, the dependence of ATP release (in response to mechanical deformation) on the CFTR protein was studied by monitoring the ATP release from RBCs that were treated with two chemically dissimilar CFTR inhibitors (glybenclamide and niflumic acid) as well as RBCs obtained from cystic fibrosis (CF) patients.[36] It was demonstrated that when CFTR is either chemically inhibited or genetically deficient, as in the case of CF patients, there is a decrease in the concentration of ATP that is released when RBCs are passed through filters ranging from 5-12 μm in diameter. Importantly, it

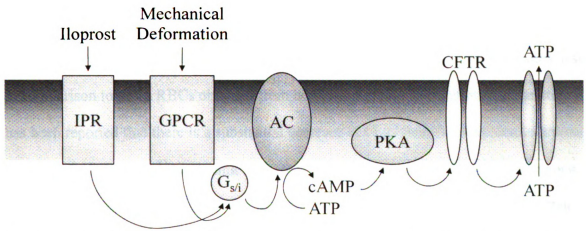

Figure 1.2 G-protein coupled signal transduction pathway involving either the mechanical deformation or pharmaceutical-induced ATP release as either the G-protein coupled receptor (GPCR) or the prostacyclin receptor (IPR) activates G-protein (G_s). Upon activation, adenylyl cyclase (AC) will convert intracellular ATP to 3'5'-cyclic adenosine monophosphate (cAMP), stimulating the phosphorylation of the cystic fibrosis transmembrane regulator (CFTR) by protein kinase A (PKA).

was also demonstrated here by monitoring red cell transit time (RCTT), that there was no decrease in RBC deformability, concluding that the ATP release is directly dependant on the action of CFTR. It is also worth noting that the concentration of intracellular ATP within RBCs was determined to be statistically similar whether they were obtained from healthy controls or CF patients, as well as, after chemical treatment. Here unpublished data also demonstrated that the incubation with either glybenclamide or niflumic acid did not directly affect the potassium-sensitive ATP channels by showing that inhibition with cromakalim did not affect the RBC deformability or the concentration of deformation-induced ATP release.

It has been shown that ATP release from the RBCs of people with type 2 diabetes,[37,41] primary pulmonary hypertension,[42] and cystic fibrosis[36] is significantly less in comparison to those RBCs obtained from healthy controls. Throughout the literature it has been reported that there is a substantial decrease in G_i expression in numerous animal models of diabetes,[43-47] including rats that have been administered streptozotocin, resulting in β-cell destruction. A decreased expression of G_i in the platelets and RBCs from type 2 diabetics,[37] decreasing vascular circulation and inadequate O_2 delivery throughout the circulation system, is thought to be the reason for hypertension complications that are associated with the disease, resulting in poor wound healing that often times requires limb amputations.[40] It was reported that there is a decreased cAMP generation and ATP release from RBCs as A1C levels increase in response to mastoparan 7 (activates G_i), providing a possible explanation for the increase incidence of vascular complications as A1C levels increase in type 2 diabetes.

1.2.4 ENDOTHELIUM-DERIVED RELAXING FACTOR: NO

In 1998 Furchgott, Ignarro and Murad were jointly awarded the Nobel Prize in Physiology or Medicine for demonstrating that NO is a signaling molecule in the cardiovascular system. Specifically, Furchgott and Zawadzki[48] discovered that in order to induce rabbit thoracic aorta relaxation through the perfusion of acetylcholine (ACh), the endothelial lining within the aortic ring was required. This demonstrated that ACh elicits a response of the endothelial lining that in turn, induces smooth muscle relaxation and that without the mediation of the endothelium, ACh will induce a constriction of the smooth muscle. The sandwich experiment, as illustrated in figure 1.3 was used to transfer the biologically active substance to a biodetector. Specifically two rabbit aortic strips, one devoid of the endothelial lining, were placed lumen-side together, the resulting vasodilation in the strip without endothelial cells was due to the endothelium derived relaxing factor (EDRF) produced in the strip with the intact lining. Several other experiments were explained in a review by Moncada[49] where the EDRF from the endothelium of either an isolated rabbit aortas or cultured endothelium, was transferred to rabbit aortic strips, vascular rings or canine coronary arteries, inducing vasodilation in the ladder biological detector. It was then determined that NO was the endogenous vasodilator that was responsible for the resulting relaxation upon the perfusion of various agonists such as ACh and bradykinin.[50]

NO has been reported throughout the literature to not only elicit relaxation of smooth muscle cells comprising the cardiovascular system, but also demonstrated to inhibit platelet aggregation, adhesion to endothelium, as well as revert platelet activation and disaggregate thrombosis formations.[51] Thrombosis is the process by which the body

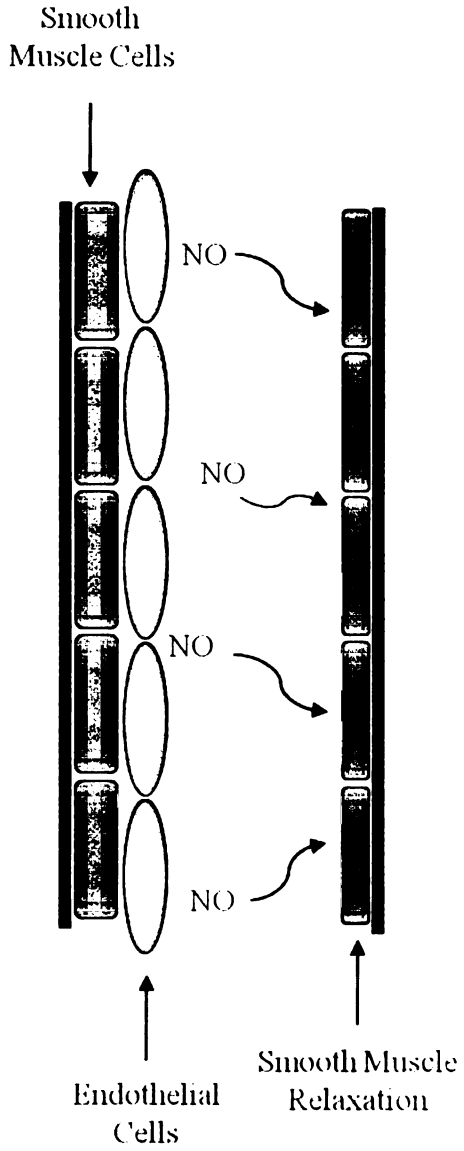

Figure 1.3 Illustration of the sandwich experiment conducted by Furchgott and Zawadzki where the endothelium-derived relaxing factor (EDRF), later to be determined as nitric oxide (NO), from the endothelial cells of one rabbit aortic strip were exposed to the smooth muscle cells on the second strip, devoid of the endothelial lining. Here, the exposed smooth muscle cells, acting as a biological detector, underwent relaxation from the biologically active vasodilator transferred.

recruits platelet aggregation in order to stop hemorrhaging from lesions in the vascular system. Research in our group has focused on monitoring the NO that is produced by the endothelium or platelets themselves and how it can prevent platelet activation and aggregation.[52,53]

1.2.5 ATP-MEDIATED NO PRODUCTION

Once ATP is released from the RBC, it can bind to the P_{2Y} purinergic receptor that is found on the membrane of the endothelial cells that line the luminal surface of circulatory vessels. Subsequently, as illustrated in figure 1.4, NO is produced when vascular endothelium nitric oxide synthase (eNOS) converts L-arginine to L-citrulline upon activation of the Ca^{2+} dependent calmodulin protein, which is bound to the eNOS enzyme.[49,50,54] NO can diffuse back out into the circulation where it can affect other cell types of the vascular system, or it can also diffuse through the underlying smooth muscle cells where it binds to soluble guanylate cyclase (sGC) and stimulates the production of cyclic guanylate monophosphate (cGMP).[55] This cGMP has been shown to reduce the concentration of intracellular Ca^{2+}, preventing crossover of myosin and actin, ultimately inducing smooth muscle relaxation.[54,56]

Smooth muscle contraction and relaxation is mediated via a Ca^{2+}-dependent mechanism that involves the phosphorylation of myosin light chain (MLC) by MLC kinase.[57] During contraction, an intracellular increase of Ca^{2+}, binding with the acidic protein calmodulin, activates that MLC kinase. Upon phosphorylation, the cycling of the myosin cross-bridges with actin is initiated with the release of energy from ATPase

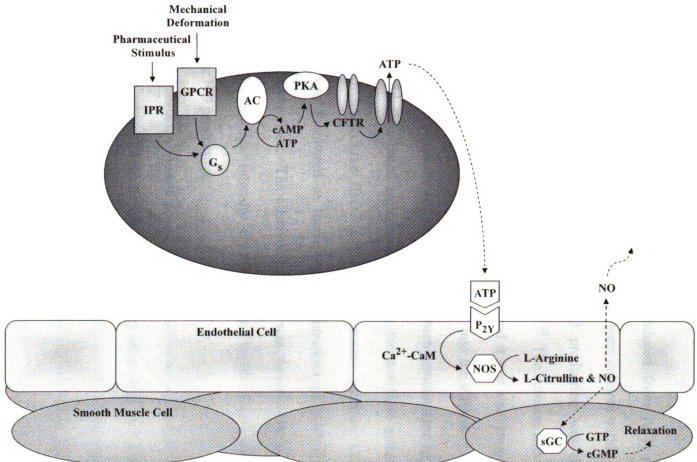

Figure 1.4 ATP-stimulated vasodilation mechanism and the production of nitric oxide (NO) resulting from ATP binding to the P_{2Y} receptor located on the endothelial lining of the vascular system. Upon activation of endothelial nitric oxide synthase (NOS) by calcium-dependent calmodulin (Ca^{2+}-CaM), L-arginine is converted to L-citrulline and NO which can then diffuse to the smooth muscle cells, binds to soluble guanylate cyclase (sGC) and stimulates the production of cyclic guanylate monophosphate (cGMP) which will reduce intracellular Ca^{2+} and result in vasodilation.

activity resulting in the contraction of the smooth muscles that line the walls of the resistance vessels.

Amperometric determination of NO produced from ATP stimulated bovine pulmonary artery endothelial cells (bPAECs) that were cultured within a section of fused silica microbore tubing demonstrated that NO production was dependent on the concentration of ATP pumped through the tubing.[58] The cultured endothelium is a close mimic of the lining of the lumen found *in vivo* and it was also demonstrated that shear alone did not cause synthesis and release of NO into the effluent. Fluorescence-based determination of intracellular NO production has been demonstrated by our group both in non-flow[41] and flow-based experiments.[59,60] In the non-flow system, bPAECs were cultured in tissue culture flasks and the fluorescence intensity of intracellular NO production was monitored as increasing concentrations of ATP (10-100 μM) were introduced to the flask. The observed intensity was shown to be statistically different from the fluorescence intensity resulting from buffer alone and basal levels of intracellular NO production.

The resistance vessels found *in vivo* were better mimicked in the flow-based system where microfluidic devices were used to determine the concentration of NO production as various agonists, bradykinin and ATP, and L-nitroarginine methyl ester (L-NAME) were pumped through the channel and over the endothelium.[59] L-NAME inhibits the production of NO from the endothelial cell lining the vascular system within rabbit lungs, such that, there was an inhibited vasodilation when blood is perfused through this vasculature[61] and has also been shown clinically to result in increased hypertension.[54] In order to demonstrate the ability of RBC-mediated ATP to induce

endothelium NO *in vitro*, a microfluidic device that is discussed in detail here will be presented.[60] Collectively, the resulting effects of diabetes are thought to decrease blood flow in the microcirculation, inducing an increase is tissue hypoxia and possibly the mechanism for increased incidence of hypertension and cardiovascular disease.

1.2.6 GLUCOSE UPTAKE AND METABOLISM

Cellular metabolism, while essential for catabolic and anabolic reactions, also plays an important role in diabetic complications due to its involvement with blood glucose levels. While the RBC is absent of intracellular organelles and unable to perform protein or lipid synthesis, nor oxidative phosphorylation, there is still a requirement for energy production in order to maintain ATP dependent membrane pumps and osmotic stability. It was also suggested in the literature that the oxygenation state of Hb affects specifically RBC glucose metabolism.[21,62] It is thought that the oxygenation state of Hb directly affects the glucose metabolism through glycolysis or the pentose phosphate pathway (PPP) by affecting the interaction of band 3 proteins with either glycolytic enzymes (redirecting to PPP shunt) or deoxygenated Hb (metabolism through glycolysis) as illustrated in figure 1.5 from Messana *et al.* During periods of high oxidative stress with high levels of R-state oxygenated Hb, the RBC membrane shifts glucose metabolism through the PPP, increasing antioxidant ability of the cell via nicotinamide adenine dinucleotide phosphate (NADPH) and glutathione (GSH) production.

The two main processes for glucose metabolism in the RBC are glycolysis, and to a lesser extent, the PPP. It is through the latter that glucose is shunted, when the need for antioxidant production is required to protect the cell from oxidative stress, for which the

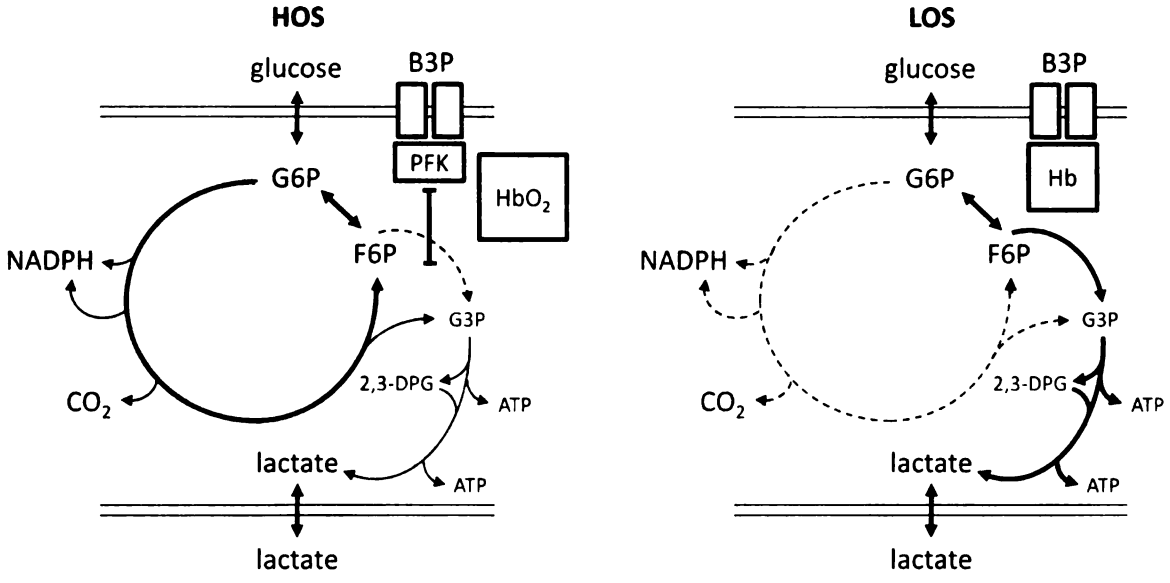

Figure 1.5 Illustration taken from Messana *et al* illustrating the integral role hemoglobin (Hb) plays in glucose metabolism to form either antioxidants via the pentose phosphate pathway in the case of high oxygen stress (HOS) or the production of ATP through glycolysis in the case of low oxygen stress (LOS).

RBC is largely susceptible to. Oxidative stress can compromise the vitality of the cell and inhibit the proper function of a number of enzymes and membrane proteins. In this instance, glucose metabolism is redirected to the PPP where glucose-6-phosphate dehydrogenase (G6PD) converts glucose-6-phosphate to 6-phosphogluconolactone (6GP), producing NADPH, which is a major proton donor for a number of other enzymatic processes including those of GSH as well as catalase, both of which are involved in peroxide detoxification. It has been reported that the normal amount of glucose metabolism through the PPP under normal conditions only operates at $1/60^{th}$ of its potential,[21] indicating the great reductive potential this system is capable of under high incidence of oxidative stress.

RBCs of diabetic patients have been shown to release a lower concentration of ATP under mechanical deformation when compared to RBCs of non-diabetic patients.[41] Vasodilation is dependent upon the amount of ATP released from RBCs within the circulation, which has been shown to be directly affected by the antioxidant system. It is speculated that the reduced release of ATP from RBCs of diabetic patients is linked to the reduced deformability of the cell membrane due to an increase in oxidative stress under hyperglycemic conditions.

Diabetes and the associated complications are subject for the research presented here, as it pertains to the ability of the RBC to mediate vasodilation of the vascular system. By employing a flow-based microfluidic device that incorporates microtitre plate technology, the relationship between glucose metabolism within the RBC and the resulting affect on cellular function is examined. Specifically, the antioxidant status of

the cell is determined by quantifying various intracellular glucose metabolites while simultaneously determining the affect on RBC-derived ATP release.

REFERENCES

1. Spence, D.M. Bioanalytical challenges for analytical chemists. *Analyst* **129**, 102-104 (2004).

2. Executive Summary: Standards of Medical Care in Diabetes - 2009. *Diabetes Care* **32**, S6-S12 (2009).

3. Nathan, D.M., Singer, D.E., Hurxthal, K. & Goodson, J.D. The clinical information value of the glycosylated hemoglobin assay. *N Engl J Med* **310**, 341-346 (1984).

4. CDC Centers for Disease Control and Prevention. National Diabetes Fact Sheet: General information and National Estimates on Diabetes in the United States, 2007. *US Department of Health and Human Services* (2008).

5. Anon Diagnosis and classification of diabetes mellitus. *Diabetes Care* **31**, S55-S60 (2008).

6. Castano, L. & Eisenbarth, G.S. Type-I Diabetes: A Chronic Autoimmune Disease of Human, Mouse, and Rat. *Annu Rev Immunol* **8**, 647 (1990).

7. Roep, B.O. Islet Autoreactive CD8 T-cells in Type 1 Diabetes. *Diabetes* **57**, 1156-1156 (2008).

8. Eisenbarth, G.S. Molecular aspects of the etiology of type I diabetes mellitus. *J Diabetes Complications* **7**, 142-150 (1993).

9. Filippi, C.M. & von Herrath, M.G. Viral trigger for type 1 diabetes: pros and cons. *Diabetes* **57**, 2863-2871 (2008).

10. Cudworth, A.G. Type I diabetes mellitus. *Diabetologia* **14**, 281-291 (1978).

11. von Herrath, M. Can we learn from viruses how to prevent type 1 diabetes? The role of viral infections in the pathogenesis of type 1 diabetes and the development of novel combination therapies. *Diabetes* **58**, 2-11 (2008).

12. Nathan, D.M. Initial Management of Glycemia in Type 2 Diabetes Mellitus. *N Engl J Med* **347**, 1342-1349 (2002).

13. Bonner-Weir, S. & O'Brien, T.D. Islets in type 2 diabetes: in honor of Dr. Robert C. Turner. *Diabetes* **57**, 2899-2904 (2008).

14. Hod, M. & Yogev, Y. Goals of metabolic management of gestational diabetes: is it all about the sugar? *Diabetes Care* **30**, S180-S187 (2007).

15. Kitzmiller, J.L., Dang-Kilduff, L. & Taslimi, M.M. Gestational diabetes after delivery: short-term management and long-term risks. *Diabetes Care* **30**, S225-S235 (2007).

16. Fong, D.S. et al. Diabetic retinopathy. *Diabetes Care* **26**, 226-229 (2003).

17. EDIC Intensive Diabetes Treatment and Cardiovascular Disease in Patients with Type 1 Diabetes. *N Engl J Med* **353**, 2643-2653 (2005).

18. Carpenter, M.W. Gestational diabetes, pregnancy hypertension, and late vascular disease. *Diabetes Care* **30**, S246-S250 (2007).

19. Stephens, J.W., Khanolkar, M.P. & Bain, S.C. The biological relevance and measurement of plasma markers of oxidative stress in diabetes and cardiovascular disease. *Atherosclerosis* **202**, 321-329 (2009).

20. DCCT The effect of intensive treatment of diabetes on the development and progression of long-term complications in insulin-dependent diabetes mellitus. The Diabetes Control and Complications Trial Research Group. *N Engl J Med* **329**, 977-986 (1993).

21. Bossi, D. & Giardina, B. Red cell physiology. *Mol Aspects Med* **17**, 117-128 (1996).

22. Fischer, T.M., Haest, C.W.M., Stoehr, M., Kamp, D. & Deuticke, B. Selective alteration of erythrocyte deformability by sulfhydryl reagents. Evidence for an involvement of spectrin in membrane shear elasticity. *Biochim Biophys Acta* **510**, 270-282 (1978).

23. MacRury, S.M., Small, M., Anderson, J., MacCuish, A.C. & Lowe, G.D. Evaluation of red cell deformability by a filtration method in type 1 and type 2 diabetes mellitus with and without vascular complications. *Diabetes Res* **13**, 61-65 (1990).

24. Delaunay, J. The molecular basis of hereditary red cell membrane disorders. *Blood Rev* **21**, 1-20 (2007).

25. Jain, S.K. Hyperglycemia can cause membrane lipid peroxidation and osmotic fragility in human red blood cells. *J Biol Chem* **264**, 21340-21345 (1989).

26. Schwartz, R.S., Madsen, J.W., Rybicki, A.C. & Nagel, R.L. Oxidation of spectrin and deformability defects in diabetic erythrocytes. *Diabetes* **40**, 701-708 (1991).

27. Straface, E. et al. Structural Changes of the Erythrocyte as a Marker of Non-Insulin-Dependent Diabetes: Protective Effects of N-Acetylcysteine. *Biochem. Biophys. Res. Commun.* **290**, 1393-1398 (2002).

28. Gaskin, R.S., Estwick, D. & Peddi, R. G6PD deficiency: its role in the high prevalence of hypertension and diabetes mellitus. *Ethn Dis* **11**, 749-754 (2001).

29. Fischer, D.J., Torrence, N.J. & Spence, D.M. Development of a biomimetic circulatory system using chips fabricated from PDMS. *Abstracts of Papers, 225th ACS National Meeting, New Orleans, LA, United States, March 23-27, 2003*, BIOT-099 (2003).

30. Ellsworth, M.L., Forrester, T., Ellis, C.G. & Dietrich, H.H. The erythrocyte as a regulator of vascular tone. *Am J Physiol Heart Circ Physiol* **269**, H2155-2161 (1995).

31. McCullough, W.T., Collins, D.M. & Ellsworth, M.L. Arteriolar responses to extracellular ATP in striated muscle. *Am J Physiol Heart Circ Physiol* **272**, H1886-H1891 (1997).

32. Collins, D.M., McCullough, W.T. & Ellsworth, M.L. Conducted vascular responses: communication across the capillary bed. *Microvasc Res* **56**, 43-53 (1998).

33. Dietrich, H.H., Ellsworth, M.L., Sprague, R.S. & Dacey, R.G., Jr. Red blood cell regulation of microvascular tone through adenosine triphosphate. *Am J Physiol Heart Circ Physiol* **278**, H1294-H1298 (2000).

34. Sprague, R.S., Ellsworth, M.L., Stephenson, A.H. & Lonigro, A.J. ATP: the red blood cell link to NO and local control of the pulmonary circulation. *Am J Physiol Heart Circ Physiol* **271**, H2717-H2722 (1996).

35. Sprung, R., Sprague, R. & Spence, D. Determination of ATP release from erythrocytes using microbore tubing as a model of resistance vessels in vivo. *Anal Chem* **74**, 2274-2278 (2002).

36. Sprague, R.S., Ellsworth, M.L., Stephenson, A.H., Kleinhenz, M.E. & Lonigro, A.J. Deformation-induced ATP release from red blood cells requires CFTR activity. *Am J Physiol Heart Circ Physiol* **275**, H1726-1732 (1998).

37. Sprague, R.S., Stephenson, A.H., Bowles, E.A., Stumpf, M.S. & Lonigro, A.J. Reduced expression of Gi in erythrocytes of humans with type 2 diabetes is associated with impairment of both cAMP generation and ATP release. *Diabetes* **55**, 3588-3593 (2006).

38. Olearczyk, J.J., Stephenson, A.H., Lonigro, A.J. & Sprague, R.S. Receptor-mediated activation of the heterotrimeric G-protein Gs results in ATP release from erythrocytes. *Med Sci Monit* **7**, 669-674 (2001).

39. Olearczyk, J.J., Stephenson, A.H., Lonigro, A.J. & Sprague, R.S. Heterotrimeric G protein Gi is involved in a signal transduction pathway for ATP release from erythrocytes. *Am J Physiol Heart Circ Physiol* **286**, H940-945 (2004).

40. Sprague, R.S., Stephenson, A.H. & Ellsworth, M.L. Red not dead: signaling in and from erythrocytes. *Trends Endocrinol Metab* **18**, 350-355 (2007).

41. Carroll, J. et al. An altered oxidant defense system in red blood cells affects their ability to release nitric oxide-stimulating ATP. *Mol Biosyst* **2**, 305-311 (2006).

42. Sprague, R.S., Stephenson, A.H., Ellsworth, M.L., Keller, C. & Lonigro, A.J. Impaired release of ATP from red blood cells of humans with primary pulmonary hypertension. *Exp Biol Med* **226**, 434-439 (2001).

43. Hashim, S., Liu, Y.Y., Wang, R. & Anand-Srivastava, M.B. Streptozotocin-induced diabetes impairs G-protein linked signal transduction in vascular smooth muscle. *Mol Cell Biochem* **240**, 57-65 (2002).

44. Matsuda, N. et al. Differential gene transcriptional regulation of Gi isoforms and Gs protein expression in diabetic rat hearts. *Naunyn Schmiedebergs Arch Pharmacol* **361**, 53-60 (2000).

45. Hashim, S., Li, Y., Nagakura, A., Takeo, S. & Anand-Srivastava, M.B. Modulation of G-protein expression and adenylyl cyclase signaling by high glucose in vascular smooth muscle. *Cardiovasc Res* **63**, 709-718 (2004).

46. Moxham, C.M. & Malbon, C.C. Insulin action impaired by deficiency of the G-protein subunit Gi[alpha]2. *Nature* **379**, 840-844 (1996).

47. Gawler, D., Milligan, G., Spiegel, A.M., Unson, C.G. & Houslay, M.D. Abolition of the expression of inhibitory guanine nucleotide regulatory protein Gi activity in diabetes. *Nature* **327**, 229-232 (1987).

48. Furchgott, R.F. & Zawadzki, J.V. The obligatory role of endothelial cells in the relaxation of arterial smooth muscle by acetylcholine. *Nature* **288**, 373-376 (1980).

49. Moncada, S., Palmer, R.M.J. & Higgs, E.A. Nitric oxide: physiology, pathophysiology, and pharmacology. *Pharmacol Rev* **43**, 109-142 (1991).

50. Moncada, S., Palmer, R. & Higgs, E. The discovery of nitric oxide as the endogenous nitrovasodilator. *Hypertension* **12**, 365-372 (1988).

51. Palmer, R.M.J., Ashton, D.S. & Moncada, S. Vascular endothelial cells synthesize nitric oxide from L-arginine. *Nature* **333**, 664-666 (1988).

52. Carroll, J.S., Ku, C.-J., Karunarathne, W. & Spence, D.M. Red Blood Cell Stimulation of Platelet Nitric Oxide Production Indicated by Quantitative Monitoring of the Communication between Cells in the Bloodstream. *Anal Chem* **79**, 5133-5138 (2007).

53. Ku, C.-J., Karunarathne, W., Kenyon, S., Root, P. & Spence, D. Fluorescence Determination of Nitric Oxide Production in Stimulated and Activated Platelets. *Anal Chem* **79**, 2421-2426 (2007).

54. Tuteja, N., Chandra, M., Tuteja, R. & Misra, M.K. Nitric oxide as a unique bioactive signaling messenger in physiology and pathophysiology. *J Biomed Biotechnol*, 227-237 (2004).

55. Murad, F. Discovery of some of the biological effects of nitric oxide and its role in cell signaling. *Biosci Rep* **24**, 452-474 (2004).

56. Sobey, C.G. Potassium channel function in vascular disease. *Arterioscler Thromb Vasc Biol* **21**, 28-38 (2001).

57. Webb, R.C. Smooth Muscle Contraction and Relaxation. *Advan. Physiol. Edu.* **27**, 201-206 (2003).

58. Kotsis, D.H. & Spence, D.M. Detection of ATP-induced nitric oxide in a biomimetic circulatory vessel containing an immobilized endothelium. *Anal Chem* **75**, 145-151 (2003).

59. Oblak, T.D.A., Root, P. & Spence, D.M. Fluorescence Monitoring of ATP-Stimulated, Endothelium-Derived Nitric Oxide Production in Channels of a Poly(dimethylsiloxane)-Based Microfluidic Device. *Anal Chem* **78**, 3193-3197 (2006).

60. Genes, L.I., Tolan, N.V., Hulvey, M.K., Martin, R.S. & Spence, D.M. Addressing a vascular endothelium array with blood components using underlying microfluidic channels. *Lab Chip* **7**, 1256-1259 (2007).

61. Sprague, R.S. et al. Effect of L-NAME on pressure-flow relationships in isolated rabbit lungs: role of red blood cells. *Am J Physiol Heart Circ Physiol* **269**, H1941-H1948 (1995).

62. Messana, I. et al. Human erythrocyte metabolism is modulated by the O2-linked transition of hemoglobin. *FEBS Letters* **390**, 25-28 (1996).

CHAPTER 2: MERGING FLOW INTO MICROTITRE TECHNOLOGY

2.1 MICROFLUIDIC DEVICES: GENERAL HISTORY AND APPLICATIONS

The main advantage associated with the miniaturization of analytical processes by employing microscale total analysis systems (μTAS)[1] is to be able to perform fast, accurate and inexpensive analyses in a high throughput manner. Ideally these systems integrate sample and reagent introduction, the ability to move these solutions on-chip, often times requiring mixing of liquids or gases, incorporating purification processes when chemical synthesis is employed, and finally the ability to detect various analytes on a single platform. These systems are highly dependent on the developments in the fabrication of microelectronics and microelectromechanical systems (MEMS), providing a means to easily integrate fluid flow into a similar silicon or glass device. [2-4] Microfluidics, as put best by Hansen and Quake,[5] integrates the high levels of wet laboratory functionality on a single chip by manipulating solutions in volumes ranging from nano- to femtoliters. The employment of μTAS is highly dependent on microfluidic technology, leading to advantages over standard systems that include the reduction of consumed sample and reagents, faster analysis times, increased sensitivity, disposability and portability.[2,3]

The first demonstration of microfluidic technology was the development of a gas chromatograph on a silicon wafer in 1979 at Stanford University by Terry *et al.*[6] Miniaturized analytical systems have been primarily employed since then using microfluidic technology in the areas of capillary electrophoresis (CE), gas chromatography (GC), liquid chromatography (LC), and mass spectrometry (MS) to

name a few of the earliest applications. Along with the MEMS platforms that were typically fabricated in silicon and glass, there were additional motivations for the development of microfluidics and the resulting μTAS that are employed today as reviewed by Whitesides.[7] First, molecular analysis was integrated into a miniaturized system to employ GC, high-performance liquid chromatography (HPLC) and CE, allowing for an increased sensitivity and resolution that was not obtained with standard bench top instrumentation. Secondly, there was motivation for the development of portable μTAS in order to combat chemical and biological weapons in the field, where they posed military and terrorist threats. Finally, the requirement for high throughput analysis, as well as increased sensitivity and resolution for DNA sequencing during the 1980s for genetic research, was enhanced with the employment of microfluidic systems.

Microfluidic technologies were developed in the four research labs of Manz, Harrison, Ramsey and Mathies. Manz has demonstrated the ability to perform free-flow electrophoresis and synchronized cyclic CE devices.[1,2,8,9] Harrison's group has developed the ability to integrate immunoassays and chemical reactions in organic solvents on-chip.[10-15] Ramsey and Jacobson are best known for incorporating various elements for on-chip sample pre- and post-treatments for CE, PCR, and DNA sequencing.[16] Additional work includes the ability to study enzyme kinetics, perform electrospray for subsequent mass spectrometry (MS), and carry out miniaturized open channel electrochromatography and micellar electrokinetic capillary chromatography, all in microfluidic devices.[17-22] Finally, Mathies developed the ability to perform DNA sequencing and restriction assays for genotyping, using multichannel analysis with the incorporation of multicolor detection.[23-27]

With advanced fabrication techniques and component integration, there are currently an expansive number of applications for microfluidic technology. Some of the most prominent include the integration in biochemical and chemical processes, analytical systems, biomedical devices and systems for fundamental research.[28,29] Biochemical applications have enabled on-chip cell growth, counting, and sorting, in order to detect various biological species and have also been employed in genomic studies. Additional applications include the time-resolved studies of protein folding and highly efficient protein crystal growth.[5] This is performed in a high throughput approach by monitoring the effect of various conditions such as pH, ionic strength, composition, and concentration of solvents on crystalline growth. By performing protein crystallization within microfluidics, subsequent damage through handling is reduced and electrokinetic manipulation, vesicle encapsulation and the incorporation of mechanical valves have been demonstrated.[30]

Systems biology, the integration of complex biological systems to understand cellular mechanisms, is strongly dependent on the ability to study both single cells and bulk cellular samples using microfluidic platforms.[31] The nature of microfluidics provides a means to mimic physiological conditions and apply specific experimental conditions for studying intra- and intercellular molecular interactions involved in cellular events.

2.1.1 MATERIAL ADVANTAGES AND DISADVANTAGES

Microfluidic devices have been fabricated in many substrates such as silicon, glass, and polymers like poly(methyl methacrylate) (PMMA) and poly(dimethylsiloxane)

(PDMS).[3,28,32,33] Silicon micromachining is typically utilized in mass production applications, especially for MEMS devices where the resulting features range from 1 μm into the millimeter range. Silicon is opaque in the ultraviolet and visible region (UV/VIS), rendering it incompatible with many optical detection techniques, and relatively expensive. Glass, while transparent in the UV/VIS region, is an amorphous material, making it difficult to etch vertical side walls.[28] Together, the major disadvantages associated with using silicon and glass for microfluidic devices are that the fabrication processes are slow and complicated, clean room facilities are required for each unit fabricated and the bonding techniques are time consuming. Also, the high temperatures that are required for bonding are not well tolerated by various surface chemistry modifications that may be desired.[4] The material properties of each, their fragility, cost, and incompatibility with various detection schemes, increased the need for new polymeric substrates.

Structures composed of silicon or glass are rigid, making moving parts such as valves difficult to integrate. By integrating valves, pumps, mixers, filters and necessary interconnects, μTAS systems are defined by the ability to convert large analytical devices to small miniaturized platforms that are often disposable. μTAS systems incorporate sample acquisition, pre- and post-treatment, separation, and detection all on a single device without external components for the analysis of liquid or gas samples.[3] Polymers are less expensive, more rugged, and their fabrication is faster and cheaper by employing the processes of casting, embossing and injection molding.[34]

Polymers have many advantages over both silicon and glass, a few of which are their ease of use, numerous fabrication and sealing techniques not requiring a clean room,

rapid fabrication in comparison, and economically advantageous both in the cost of material and reusability. Non-traditional materials such as hydrogels, plastics and elastomers allow for fast and economical, passive and active microfluidic devices.[5] As outlined in table 2.1, Becker *et al.*[34] compare various attributes of silicon, glass, technical thermoplastics, thermoset polymers and elastomers detailing how they each perform in various fabrication processes for microfluidic devices.

Technical thermoplastics, such as poly(methyl methacrylate) (PMMA), polycarbonate (PC), and polyetheretherketone (PEEK), become malleable at elevated temperatures and can be remolded by reheating. Although these materials were among the first employed for the fabrication of microfluidic devices, much attention is now being directed to cycloolefin polymers and copolymers for their optical properties. Thermoset polymers, on the other hand unlike technical thermoplastics, undergo a chemical reaction when cured at elevated temperatures. They represent duroplastic materials, such as the photoresists used in photolithography and polyimide, which is frequently used in the fabrication of microelectronics. These materials are often referred to as resins that cure at elevated temperatures forming a rigid, inflexible replica mold. Elastomers, as classically defined, exhibit at least 200% elastic elongation due to their composition of long entangled molecular chains. These materials, the most common of which is PDMS, are cured at relatively low temperatures and make up the bulk of materials currently used for the fabrication of microfluidic devices.

There are numerous advantages to fabricating microfluidic devices in PDMS including the properties associated with optical transparency (from 240 to 1100 nm), permeability to gases, non-toxic properties to mammalian cells, and the ability to

	Silicon	Glass	Technical thermoplastics (e.g. PMMA, PC, PEEK)	Thermoset polymers	Elastomers
Microfabrication	Easy-medium	Easy-medium	Easy	Medium	Easy
Structuring processes	Wet and dry etching	Wet etching, photostructuring	Injection molding, hot embossing, thermoforming, laser ablation	Casting, lithography, etching	Casting
Possible geometries	Limited, 2D	Limited, 2D	Many, 2D, 3D	Mostly 2D, 3D possible	Mostly 2D, 3D possible
Assembly	Easy	Medium	Easy	Medium	Easy
Interconnections	Difficut	Difficult	Easy	Easy	Easy-medium
Mechanical stability	High	High	Low-medium	High	Very low
Temperature stability	High	High	Low-medium	Medium	Low
Acid stability	High	High	High	High	High
Alkaline stability	Limited	High	High	High	High
Organic solvent stability	High	Medium-high	Low-medium	Medium-high	Low
Optical transparency	No	High	Mostly high	Partly	High
Material price	Medium	Medium-high	Low-medium	Medium	Low

Table 2.1 Table adapted from Becker *et al.* detailing the properties of silicon, glass, technical thermoplastics, thermoset polymers and elastomers as it pertains to their use in fabrication of microfluidic devices.

fabricate structures on the micro scale at relatively low temperatures.[28,29] These characteristics allow for UV/VIS absorption as well as fluorescence detection without interference from the substrate. The ability to incorporate multiple cellular components allows for the fabrication of an *in vitro* platform that can closely replicate the *in vivo* system.

2.1.2 FABRICATION METHODS IN PDMS

The fabrication method chosen to prepare a microfluidic device depends upon the material used, the complexity of the desired design, the compatibility between the solutions intended for use within the device, and the application for flexible academic or commercial mass production. The fabrication processes for PDMS-based devices are discussed here, focusing primarily on the techniques of photolithography and replica molding, or casting of PDMS.

Photolithography is a technique used to obtain microscale structures from thermoset polymer resins, which cross-link under exposure to light, on various substrates. Rapid prototyping, as first described by the Whitesides group,[3] is the fabrication of a master wafer using photolithography for subsequent replica molding in PDMS. A high-resolution commercial image setter is used to create a negative transparency of channels designed using a computer software program. This transparency, with approximately 20 μm resolution, can be used in contact photolithography to create a positive relief of photoresist on a silicon wafer, serving as a master for subsequent replica molding with polymeric materials. While the channel dimensions possible are much smaller (500 nm) using a chrome mask in contact photolithography, the transparencies are much more

economical, not only in cost, but also in the time required to obtain the mask, lending flexibility to the channel designs necessary for method development.[28]

The term soft lithography refers to any non-lithographic technique, such as PDMS casting, where the resolution of the resulting replica mold is dependent upon the resolution of the master wafer from which it is molded, not by the optical diffraction limit of the incident light. When fabricating microfluidic devices using PDMS and replica molding, there are many advantages associated with various aspects of design and sealing that are specific to the experimental methodology employed. Flexibility in the design of the microfluidic channels comes in the ability to design any arrangement of various dimensions through the high-resolution printing of transparency masks.

In order to direct flow throughout the device, the channels have to be sealed either reversibly or irreversibly to another substrate. Reversible sealing is possible due to hydrophobic conformal contact, displaying between a replica molded layer of PDMS and a second layer of glass, silicon, or another PDMS slab.[3] Due to the flexibility of the material, PDMS is able to seal to another layer despite minor imperfections. These sealing properties of PDMS make it a fast process and it occurs at room temperature. There is no residue left behind on the substrate, allowing for reusability of the device through repeated resealing events that are water tight, but don't withstand high pressures (>5 psi).[28] Due to the hydrophobic nature of the native PDMS, it is difficult to wet the channels fully with aqueous solutions, resulting in bubbles and adsorption of other hydrophobic moieties onto the surface of the device.

Irreversible sealing is possible with microfluidic devices fabricated in PDMS by employing plasma sealing. Plasma sealing involves the oxidation of two layers of PDMS

and has been developed as a means to irreversibly enclose the channels with a second layer of PDMS, oxidized polystyrene, glass, silicon or silicon oxide. Plasma, partially charged ionized gas that is composed of an equal number of independent positive and negative charges occupying the same space, results in the formation of silanol groups on the surface of the PDMS.[3] Once sealed, the device can withstand much higher pressures (30-50 psi) than a reversible seal and cannot be separated. This technique, while fast and strong, is a permanent, requiring precise alignment and an additional step in fabrication of the device. The PDMS surfaces become negatively charged, which is much more compatible with aqueous solutions, allowing for the integration of electroosmotic flow (EOF) and chemical separations using neutral or basic solutions.

EOF within a microfluidic device can be generated by applying an electrical potential across the length of the channel. Molecules can then be separated based on their electrophoretic mobilities towards the cathode.[35] Inducing flow in an ionic liquid will allow for the integration of pumping, mixing, and injection techniques without the need for any mechanical components. Jacobson *et al.* have reported on a technique for sample and reagent parallel and serial mixing within an EOF-based microfluidic device, where the voltage control is simplified.[22] A single voltage source is employed and by combining the termination reservoirs of various buffers, samples and analysis channels, the complex external hardware such as programmable power supplies is not needed to obtain desired voltage division. More recent work in Jacobson's lab has demonstrated the ability to create spatial and temporal gradients with varying slopes and offsets that are easily altered, changing gradient composition in both pressure and EOF systems.[36]

When employing EOF, the electrical double layer (EDL) becomes prominent within microfluidic systems, as compared to conventional systems, due to the high surface area to volume ratio in these miniaturized devices.[35] This allows for biological assays that are impracticable or impossible on the macroscale to benefit from the increasing interaction between the sample and the surface of the channel wall or sensing element. By employing EOF within the micrometer footprint of the channels, there is elimination of the parabolic-flow profile that is observed with pumping. This causes the sample to move throughout the channel in a plug, reducing the sample broadening, and results in the increased separation resolution observed within microfluidic devices.

Multilayer soft lithography allows for the integration of valves and pumps by employing a thin elastomer layer to separate planar channel structures. Specifically, mechanical elastomeric valves allow for precise fluid control where complete sealing of multiple layers allows for low actuation forces, small space requirements with negligible dead volumes and flow rates of approximately 3 nL/sec.[4,5] Implementation of these structures increases the sophistication of assays that can be employed where the sample solution within a specific portion of the device can be adjusted to sensitivity.

Various manipulations such as pneumatic valving[4], sample injection techniques[37], and sample separation[2] are all possible using such PDMS-based devices. Peristaltic and membrane pumps are possible by incorporating multilayer microfluidic fabrication with the use of elastomeric polymers.[29] In both techniques, actuation of pump channels in an adjacent layer can occur using a variety of materials such as water, air, the properties associated with the expansion of hydrogel, or magnetic field forces.

When studying the unique physics of fluid flow and mass transport on the microscale, when compared to those occurring within macroscale channels, many advantages are realized. First, there is an absence of turbulent flow, meaning that when solutions are pumped through microfluidic channels they adopt laminar flow.[7] This is due to the reduced Reynolds number (Re):

$$Re = \rho \upsilon L/\mu \quad (1)$$

where ρ = fluid density (g/cm^3), υ = characteristic velocity (cm/s), L = characteristic channel dimension (cm), and μ = viscosity (g/cm·sec) and is the ratio of the relative inertial forces to solution viscosity, which is minimized for the flow of water in microfluidic channels.[5]

In macroscopic fluids, Re is large, meaning that the inertia overpowers the effect of the solution viscosity resulting in turbulent flow. In contrast, within microscale systems, this number is reduced because here, the viscosity is the major contributing component. With laminar flow, two samples introduced into a single channel will flow adjacent to one another, only mixing by diffusion across the defined interface. Increased mass transport to the channel walls is exhibited, resulting in a parabolic-flow profile which gives advantageous fluid-flow properties in the case of separation science. However, it is a major obstacle to overcome when considering the need to combine and mix various solutions on-chip, which have been the motivation to integrate mixing components.

2.1.3 PHOTOLITHOGRAPHY: OBTAINING A SILICON WAFER MASTER

In order to obtain master wafers for soft lithography techniques and fabricate PDMS replica molds, photolithography was used as previously established,[3,28,29] and figure 2.1 highlights the key steps in the process. First, 4 mL (1 mL per inch substrate) of degassed SU8-50 negative photoresist (MicroChem, Newton, MA) is spin coated onto a 4" silicon wafer (Silicon Inc., Boise, Idaho) using a dual-step program to obtain a thickness of approximately 100 μm, corresponding to final channel depth. The spread cycle, ramped at 100 rpm/sec to 500 rpm and held for 10 sec is used to cover the entire substrate surface while the spin cycle, 300 rpm/sec to 1000 rpm for 30 sec will provide a uniform coating of the silicon wafer. In order to evaporate the solvent and densify the film, the coated wafer is then placed on a digital hot plate (VWR, West Chester, PA) at 95 °C for 15 min.

The desired channel widths and patterns are first created by specifying their exact dimensions using Freehand software, which is then printed on a negative transparency mask with 5080 dpi resolution (Pageworks, Cambridge, MA). This transparency mask, which is adhered to a piece of glass, is placed transparency-side down on top of the photoresist-coated silicon wafer. As illustrated in figure 2.2, a flood source (Newport, Irvine, CA) provides near ultraviolet light (with a wavelength range of 350 to 400 nm) which passes through the transparent regions of the mask, comprising the channel pattern, polymerizing the photoresist below. An energy dosage of 550 $J \cdot sec^{-1}$ is provided by exposing the substrate for 31.19 sec, leading to an optimal exposure and preventing uneven overexposure of the top of the photoresist layer, resulting in t-topping. A post exposure bake for 5 min at 95 °C is performed to cross-link only the exposed portions of the photoresist, which corresponds to the desired channel pattern. The unexposed

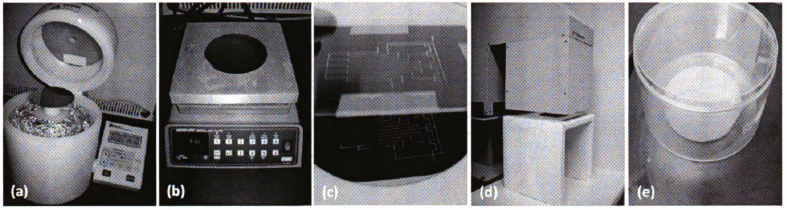

Figure 2.1 Photolithography technique employed, illustrating the steps of a) spin coating, b) pre- and post-baking, c) transparency mask alignment, d) UV exposure, and e) development of SU-8 50 negative photoresist, to fabricate a raised featured silicon wafer master for subsequent replica molding.

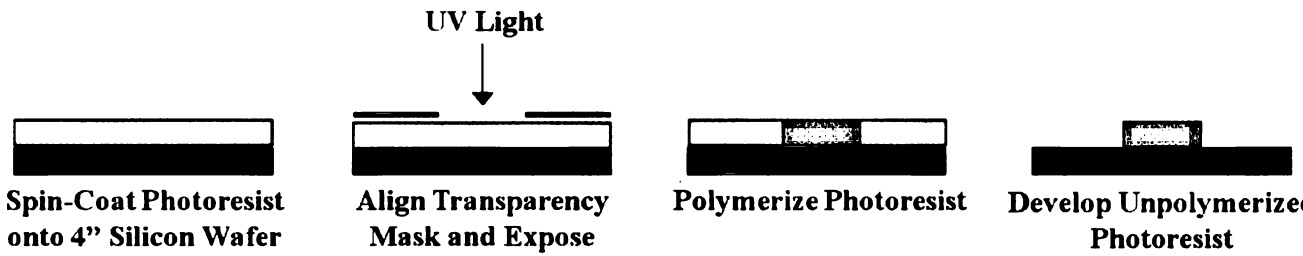

Figure 2.2 Illustration of process for master wafer production indicating the multiple steps required to obtain a raised feature master. Here, the spin-coating process results in approximately 100 μm thick photoresist coating on the 4" silicon wafer, which is then exposed to UV light through the negative transparency mask. After inducing polymerization of the photoresist below the transparent portions of the transparency mask, developer is used to remove the unpolymerized photoresist left remaining on the silicon substrate leaving only the desired raised-features.

photoresist is then developed away using propylene glycol monomethyl ether acetate as the silicon wafer is submerged with agitation for approximately 3 min or until only minor amounts of unpolymerized photoresist is remaining on the substrate. The wafer is then removed from the developer bath and rinsed with acetone, then isopropyl alcohol, and dried with a stream of compressed, clean, dry air. The master wafer obtained is then used for replica molding employing previously established soft-lithographic techniques.[28]

2.1.4 SOFT LITHOGRAPHIC TECHNIQUES TO OBTAIN REPLICA MOLDS

The microfluidic array (μFA) fabricated here is comprised of two individual layers of PDMS that are irreversibly sealed around a track-etched polycarbonate membrane (TEPC) membrane allowing underlying microfluidic channels to deliver solutions to a microtitre plate-like array of wells. A 12-channel master wafer, obtained using the photolithography techniques described above, was used in replica molding to obtain the bottom layer of the μFA. In this instance, a degassed mixture of 20:1 Sylgard 184 PDMS (DOW Corning, Midland, MI), where the ratio refers to the amount of elastomeric base to curing agent, is poured onto the silicon wafer and partially cured for 20 min at 75 °C. Once removed from the silicon wafer, the inlets for each channel were punched through this layer of PDMS using a 20 gauge luer stub adaptor (BD, Sparks, MD) while waste ports were generated using a 1/8" hollow punch (Fastenal, Winona, MN). A second master wafer, absent of any raised channel features, is used to obtain the top layer of the μFA in which subsequent array-like wells are punched through. This layer was produced by pouring a degassed mixture of 5:1 PDMS onto the blank master and as before, partially baking for 20 min at 75 °C. The array of wells was obtained in

the top layer by using the 1/8" hollow punch to produce various wells that are then aligned over the parallel channels once the membrane is placed in between the PDMS. The μFA is completed by further baking these layers together for 30 min at 75 °C. A displacement syringe pump is used to introduce samples from 500 μL gas-tight syringes (Hamilton, Reno, NV) through Tygon tubing (Saint-Gobain PPL, Courbevoie, France) that are fitted with 15 mm 23 gauge hypodermic steel tubing bent at 90 degrees (New England Small Tube, Litchfield, NH). This steel tubing is placed in each of the inlets created in fabrication in order to deliver solutions directly into the channels. Solutions can be flowed through the underlying channels for an optimized time allowing for diffusion through the polycarbonate membrane, where the time chosen is specific for the type of experimental methodology desired. Fluorescence microscopy is employed to monitor the fluorescence intensity observed in each well and the fluorescence images are analyzed for pixel intensities, which are dependent upon the concentrations of analytes of interest within the flowing solutions below. By including various fluorescence probes or cultured cells within the wells, this μFA serves as a precursor for future integration of a more realistic flow-based *in vitro* platform into the already available microtitre technologies, including automation, which is currently employed in drug research laboratories.

2.2 PDMS μFA

To better understand the metabolic processes of glucose that may lead to a decreased antioxidant system, a microfluidic device is used to address various glucose metabolism pathways of interest. Exploiting the benefits of soft lithography techniques

and the rapid replica molding associated with PDMS, the multi-dimensional μFA detailed in this research[38] is fabricated in a relatively short period of time. Moreover, the microscale dimensions of the channels of the μFA approximate resistance vessels *in vivo,* providing a more realistic mimic of the *in vivo* environment, while including an important semi-preparative sampling technique all on chip.

A microfluidic device, composed of two individual PDMS layers that are irreversibly sealed around a TEPC (GE Osmonics, Minnetonka, MN) is obtained by simply aligning the layers prior to full polymerization in the baking process.[39] Similar methods of thermocuring have been described[32,37,40,41] in comparison to traditional plasma sealing. The actual fabrication of this device depends upon the application, the top layer is composed of a variable number of 1/8" wells that contain either fluorescent reaction solutions or cultured bPAECs while the bottom layer includes individual channels (approximately 200 μm wide by 100 μm in depth) providing a means to deliver sample solutions and blood components under the wells above. The TEPC membrane pore inner diameters are selected to optimize the interaction of the analyte(s) flowing through the underlying microfluidic channels for the individual experiment of interest. The channel-containing PDMS layer is replica molded from a silicon wafer master that is obtained using standard photolithographic techniques.

2.3 IMPLEMENTING AUTOMATION TECHNIQUES

The automation and various technologies already available for micro-titre plates will allow for this μFA to handle simultaneous and variable sample volumes all while maintaining the currently accepted dimensions of micro-titre plates. Techniques for drug

development utilizing micro-titre plate technology have the advantage of incorporating commercial automation capabilities for high-throughput screening (HTS). Complex biological sample preparation, introduction of various sample volumes simultaneously, and integrating various instrumentation for sample separation, identification, and quantification are various tasks that can be performed with automated instruments. Due to the acceptance of a standard dimension for the micro-titre plate, numerous instruments have been developed on this scale leading to various advancements in the automation and detection methods for this technology. Houston and Banks[42] reviewed the transformations that were taking place in drug discovery in 1997 and discussed the implementation of automation for various HTS techniques, from dry compound storage and handling to solid and liquid combinatorial chemistry, for developing possible drug candidates. As noted, the requirements for integrating HTS automation into the drug research field requires homogeneous assays (devoid of separation) that use innovative assay designs, focusing on cellular and biochemical *in vitro* assays. The lead rationale is to construct potential drug targets, and hope that a candidate interacts with one of the more than 100 targets studied. Increased competition and exponentially increasing healthcare costs have led researches to now focus on changing the serendipity into certainty and this is where the μFA may be beneficial.

An evolutionary process has been implemented in current drug discovery techniques to increase assay density and miniaturize by converting automation techniques from the standard 96-well plate to 384-well plates and beyond. One possible reason why microfluidics hasn't been incorporated into drug discovery is because of the lack of application of these automation techniques due to varying dimensions. The advancement

in automation to include reliable small volume dispensing, effective mixing at such small volumes, and increased detection schemes and sensitivity suggests that the μFA holds great possibilities for high-throughput and automated clinical testing and research by combining all of the advantages listed for each system in table 2.2.

The development of a device that includes multiple cell types, coupled with the fluid flow forces that are found within the circulation, results in a tool that more closely mimics cell-to-cell communication that may exist in the bloodstream. For instance, overcoming hypertension through vasodilation (resulting from the communication between multiple cell types) can now be investigated more closely using this *in vitro* platform. Also, the current plate design limits the ability to incorporate both adherent and non-adherent cells such as those found within the vascular system (endothelial cells, white and red blood cells, platelets, etc.). This limits the ability to realistically mimic and monitor the toxicity of a drug candidate on a particular cell-type of interest while simultaneously monitoring the effect on non-targeted cell-types.

2.4 INTEGRATING FLUID FLOW: CIRCULATION SYSTEM MIMIC

Although automation of micro-titre plate technology can reduce the time required to perform redundant analyses, there are limitations of such systems when applied to drug discovery. For example, current micro-titre plate technology results in a static system that is unable to mimic the flow-based vascular system observed *in vivo*. Many of the advantages of microfluidic devices are associated with the ability to integrate a more lab-on-a-chip approach onto a single device such as the ability to perform on-chip cell culture, sample injection and separation, and incorporate gaseous interfaces and valving

	Microfluidic Technologies	Micro-titre Plate Technologies	Microfluidic Array
Flow-based System	✓		✓
μL to nL Volumes	✓		✓
Lab-on-a-Chip Integration	✓		✓
Eliminate Matrix Interferences	✓		✓
Multicellular Capabilities	✓		✓
Multiple Detection Schemes	✓	✓	✓
High Throughput Analysis		✓	✓
Simultaneous Detection		✓	✓
Current Clinical Diagnostic Tool		✓	✓
Automation Systems		✓	✓

Table 2.2 Comparison of various aspects associated with microfluidic and micro-titre plate technologies and the combination of these advantages associated with the microfluidic array.

techniques. The ability to better mimic the *in vivo* circulation by incorporating the flow of blood components, coupled with simultaneous detection and laboratory automation in place for micro-titre plates, suggests that the microfluidic array presented here will allow for improved mechanistic drug research studies.

By integrating the microfluidic channels and maintaining the dimensions of the standard micro-titre plate as illustrated in figure 2.3, clinical diagnosis, disease progression, drug research and efficacy studies could now include the very relevant aspect of blood flow. Here, the potential of such a device is demonstrated with two examples; an application to more individualized medicine, as well as the application of this device for determining drug efficacy and mechanisms of action. This device may improve the manner by which drugs are prescribed to patients by first providing a means to study personalized drug efficacy on various cell types. It is anticipated that the μFA may lead to higher success rates of prescribing the right drug for the right patient on the first attempt. Specifically, in order to prescribe the most effective drug and at an effective dosage, this device will allow clinicians to actually monitor the effect on various cell-types even before the drug is administered to the patient. For example, this device has used fluorescence microscopy to determine concentrations of multiple metabolites present within the RBC and here, its application towards using this device for personalized medicine is presented.

Separately, this device has demonstrated its improved *in vitro* measurement capabilities involving iloprost, a pharmaceutical drug reported to improve blood flow,[43] and how its mechanism of action is determined by incorporating multiple cell types onto a single device. This device is employed to detect multiple components from various

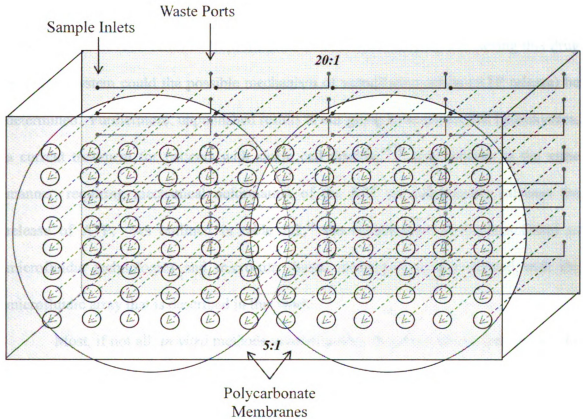

Figure 2.3 Flow-based microfluidic 96-well plate fabricated using the standard dimensions from two individual PDMS layers thermocured around a polycarbonate membrane. Here, sample inlets and waste ports are introduced through the bottom layer of PDMS, comprising the network of microfluidic channels, each addressing in parallel a series of triplicate array-like wells that are contained in the top layer of PDMS.

RBC samples in less than 20 minutes and will enable improved *in vitro* experimentation. By integrating flow into a high throughput and automated platform, drug efficacy that is dependent upon shear-induced deformation (such as pentoxyfilline, with brand name Trental) can now be accurately analyzed using a controlled *in vitro* platform. Our group previously determined[44] that the ability of Trental to increase the ATP release from a RBC sample was dependent upon the RBC being subjected to flow-induced deformation. In the absence of flow, it was established that Trental did not significantly increase the concentration of ATP released from the RBCs. Therefore, only by monitoring this drug in a flow system could the possible mechanism of vasodilation action (ATP release) be determined. Furthermore, unpublished results in our group have shown that hydroxyurea, a current treatment for patients with sickle cell disease,[45,46] also behaves in the same manner, requiring mechanical deformation of the RBC to substantially increase the release of ATP. As outlined in table 2.2,[38] the combination of features found in microfluidic technologies and micro-titre based measurements are utilized with the microfluidic array that is described in this work.

Most, if not all, *in vitro* methods involving drug discovery do not incorporate the flow of blood that is found *in vivo*. Recently, the role of microfluidics in drug discovery has been discussed[47] and focuses on each individual step involved, including compound generation through chemical synthesis, target identification, as well as lead identification and optimization, using HTS and cell sorting techniques, as illustrated in figure 2.4. Here, the numerous advantages microfluidic technologies have over conventional liquid handling techniques are outlined and the implementation of miniaturized robotic systems, including the introduction of high-density micro-titre plates as well as nanoliter

	Target Identification	Compound Generation	Lead Identification	Lead Optimization
Microfluidic Methods	cell culture, single cell studies	2D & 3D micromixers, microreactors	microctometry, cell sorting, small volume liquid handling and generation	cell and tissue studies
Applications	metabolomics, proteomics	organic synthesis, combinatorial chemistry	drug discovery, protein crystallization, molecular evolution, compound library screening	drug efficacy, pharmacological profiling, toxicity testing, chemotaxis

Figure 2.4 Illustration of possible integrations of microfluidics into drug discovery processes as discussed by Dittrich *et al.* highlighting the individual applications in generation of target investigational new drugs through chemical synthesis on-chip, as well as lead identification and optimization utilizing HTS and cell sorting techniques.

dispensing systems. The μFA presented here is expected to play an important role in the *in vitro* testing period of drug development prior to entering clinical trials.

2.5 ADMET: DRUG TESTING APPLICATION

Collectively, the advantages associated with microfluidic technologies and micro-titre plate automation may enable advancements in biotechnology associated with improved mimics of *in vivo* processes. For example, this device is an initial step toward incorporating the flow-based systems of microfluidics with already available micro-titre plate technology to monitor the properties of absorption, distribution, metabolism, excretion, and toxicity (ADMET) on a more realistic *in vitro* platform.[31,47,48] The Food and Drug Administration's Center for Drug Evaluation and Research has reported that it requires anywhere from 0.8 to 1.7 billion dollars for one drug candidate to reach the market[49]. Recently, it was estimated that the costs associated with bringing a new drug to market were due to poorly designed clinical trials.[50] In addition, recent reports of hidden marketing campaigns have made the clinical trial phase of drug discovery inefficient, resulting in trivial information that doesn't address relevant concerns. It was reported[51] that an estimate of 46% of investigational new drugs (INDs) fail in clinical and pre-clinical development due to insufficient efficacy and an additional 40% of INDs fail due to safety reasons. It has been speculated by the FDA[52] that the recent pipeline problem, resulting in a progressive slow down in innovative medical therapies, could be circumvented by employing new knowledge-based biomedical research. Kola and Landis[53] describe that one of the most effective ways for drug development companies to reduce attrition rates is to pursue more applicable models that provide strong evidence for

proof of mechanisms, targeting specifically, efficacy and toxicity properties. It was also considered by Hood *et. al* in 2004, that the reason for the overall decrease in pharmaceutical research and development and the decade-long decrease in INDs in late-stage clinical trials was due to the inability for current drug research to fully incorporate the complexity of biological systems. Integrating systems biology into drug discovery, or approaching analytically the complexities involved in a biological system, the overall understanding of predisposition to disease, its diagnosis, and prevention, would lead to earlier diagnoses with overall disease comprehension for individualized drug therapy ultimately resulting in preventative drugs.[54] Many aspects of the drug discovery process, including the mechanism of action of certain drugs, solubility of the drug candidate, and toxicity studies could be examined using the described μFA, a multicellular system that involves actual blood flow, prior to the drug candidate entering into the clinical trial phase of development. This would allow researchers to discover any unforeseen complications earlier in the drug development stage, thereby reducing the number of drugs that reach clinical trials only to fail and add to the cost associated with testing unpromising drug candidates.

2.6 DIABETES AND PRE-DIABETES SCREENING

In continuance with the complications linked with diabetes, we have recently reported that the ability of RBCs obtained from people with type 2 diabetes to release ATP is decreased in comparison to control subjects and that this decrease is associated with oxidant stress in the RBC.[55,56] As a stimulus of NO production in the endothelium, RBC-derived ATP has been implicated as a possible determinant in the control of blood

flow *in vivo*. Another report[57] has also shown a decrease in ATP release from the RBCs of people with diabetes that may be correlated with an increase in the glycation of proteins involved in the ATP release pathway. Finally, it has also been shown that RBCs in the absence of metal-activated C-peptide, also release less ATP than those RBCs in the presence of the peptide.[58] Summarily, the various ATP release pathways suggest that multiple factors or metabolic processes may affect ATP release from the RBC and some of these processes are described here in detail.

While studies are still ongoing in our labs and others to identify those factors affecting such cellular phenomena as ATP release from RBCs, until recently[59] there was no device available to perform an assessment of metabolic status and cellular function, simultaneously. Such a device, as illustrated in figure 2.5, has been beneficial because it not only enables the detection of possible biomarkers for a particular disease (e.g., low ATP release from the RBCs of people with diabetes), but also provides information towards a therapeutic intervention and the root cause of the decreased ATP as it pertains to glucose metabolism in RBCs from diabetic patients. Unfortunately, there are challenges associated with measuring multiple analytes and cell function simultaneously because the measurement of the analytes typically requires cell lysis while cell function would be better studied on the intact cell. The current approach to solving this problem is to compartmentalize the required measurements to different areas on a device, thus facilitating the measurements while at the same time enabling the potential for high throughput analyses. By monitoring both intracellular components of the RBC while simultaneously evaluating cell function, the μFA presented here has applications for determining diabetes as well as the earlier stages, pre-diabetes. This device is described

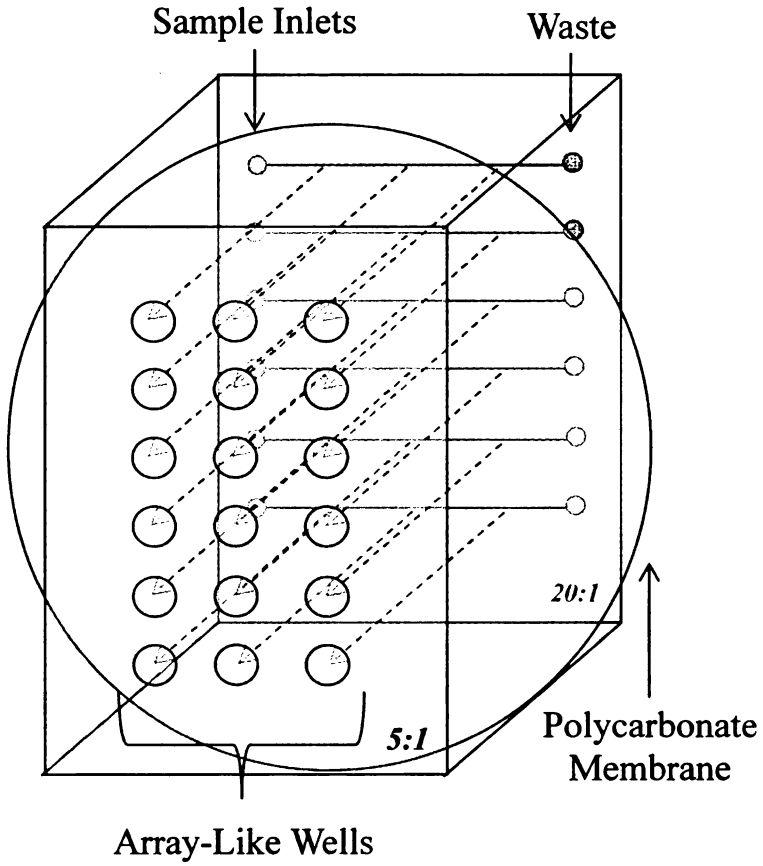

Figure 2.5 Schematic drawing of the μFA used for the determination of intracellular RBC metabolites and separately, for determining ATP-stimulated intracellular NO production within cultured bPAECs. Here, two layers of PDMS, containing parallel microfluidic channels and array-like wells, are sealed around a track-etched polycarbonate (TEPC) membrane.

to not only determine the level of shear-induced ATP release from RBCs, as cell function, but also, the ability to simultaneously determine intracellular components that may indicate a metabolic disorder.

REFERENCES

1. Manz, A., Graber, N. & Widmer, H.M. Miniaturized total chemical analysis systems: A novel concept for chemical sensing. *Sens Actuators B Chem* **1**, 244-248 (1990).

2. Manz, A. et al. Planar chips technology for miniaturization and integration of separation techniques into monitoring systems. Capillary electrophoresis on a chip. *J Chromatogr* **593**, 253-258 (1992).

3. Duffy, D.C., McDonald, J.C., Schueller, O.J.A. & Whitesides, G.M. Rapid Prototyping of Microfluidic Systems in Poly(dimethylsiloxane). *Anal Chem* **70**, 4974-4984 (1998).

4. Quake, S.R. & Scherer, A. From micro- to nanofabrication with soft materials. *Science* **290**, 1536-1540 (2000).

5. Hansen, C. & Quake, S.R. Microfluidics in structural biology: smaller, faster... better. *Curr Opin Struct Biol* **13**, 538-544 (2003).

6. Terry, S.C., Jerman, J.H. & Angell, J.B. A gas chromatographic air analyzer fabricated on a silicon wafer. IEEE Trans *Electron Devices* **26**, 1880-1886 (1979).

7. Whitesides, G.M. The origins and the future of microfluidics. *Nature* **442**, 368-373 (2006).

8. Seiler, K., Harrison, D.J. & Manz, A. Planar glass chips for capillary electrophoresis: repetitive sample injection, quantitation, and separation efficiency. *Anal Chem* **65**, 1481-1488 (1993).

9. Kopp, M.U., De Mello, A.J. & Manz, A. Chemical amplification: continuous-flow PCR on a chip. *Science* **280**, 1046-1048 (1998).

10. Fluri, K., Fitzpatrick, G., Chiem, N. & Harrison, D.J. Integrated Capillary Electrophoresis Devices with an Efficient Postcolumn Reactor in Planar Quartz and Glass Chips. *Anal Chem* **68**, 4285-4290 (1996).

11. Salimi-Moosavi, H., Tang, T. & Harrison, D.J. Electroosmotic Pumping of Organic Solvents and Reagents in Microfabricated Reactor Chips. *J Am Chem Soc* **119**, 8716-8717 (1997).

12. Harrison, D.J. et al. Micromachining a miniaturized capillary electrophoresis-based chemical analysis system on a chip. *Science* **261**, 895-897 (1993).

13. Liang, Z. et al. Microfabrication of a Planar Absorbance and Fluorescence Cell for Integrated Capillary Electrophoresis Devices. *Anal Chem* **68**, 1040-1046 (1996).

14. Chiem, N. & Harrison, D.J. Microchip-based capillary electrophoresis for immunoassays: analysis of monoclonal antibodies and theophylline. *Anal Chem* **69**, 373-378 (1997).

15. Li, P.C.H. & Harrison, D.J. Transport, Manipulation, and Reaction of Biological Cells On-Chip Using Electrokinetic Effects. *Anal Chem* **69**, 1564-1568 (1997).

16. Waters, L.C. et al. Multiple Sample PCR Amplification and Electrophoretic Analysis on a Microchip. *Anal Chem* **70**, 5172-5176 (1998).

17. Hadd, A.G., Raymond, D.E., Halliwell, J.W., Jacobson, S.C. & Ramsey, J.M. Microchip device for performing enzyme assays. *Anal Chem* **69**, 3407-3412 (1997).

18. Ermakov, S.V., Jacobson, S.C. & Ramsey, J.M. Computer simulations of electrokinetic transport in microfabricated channel structures. *Anal Chem* **70**, 4494-4504 (1998).

19. Kutter, J.P., Jacobson, S.C., Matsubara, N. & Ramsey, J.M. Solvent-Programmed Microchip Open-Channel Electrochromatography. *Anal Chem* **70**, 3291-3297 (1998).

20. Jacobson, S.C., Culbertson, C.T., Daler, J.E. & Ramsey, J.M. Microchip Structures for Submillisecond Electrophoresis. *Anal Chem* **70**, 3476-3480 (1998).

21. Khandurina, J., Jacobson, S.C., Waters, L.C., Foote, R.S. & Ramsey, J.M. Microfabricated Porous Membrane Structure for Sample Concentration and Electrophoretic Analysis. *Anal Chem* **71**, 1815-1819 (1999).

22. Jacobson, S.C., McKnight, T.E. & Ramsey, J.M. Microfluidic Devices for Electrokinetically Driven Parallel and Serial Mixing. *Anal Chem* **71**, 4455-4459 (1999).

23. Woolley, A.T. & Mathies, R.A. Ultra-high-speed DNA sequencing using capillary electrophoresis chips. *Anal Chem* **67**, 3676-3680 (1995).

24. Woolley, A.T., Lao, K., Glazer, A.N. & Mathies, R.A. Capillary electrophoresis chips with integrated electrochemical detection. *Anal Chem* **70**, 684-688 (1998).

25. Simpson, P.C. et al. High-throughput genetic analysis using microfabricated 96-sample capillary array electrophoresis microplates. *Proc Natl Acad Sci U S A* **95**, 2256-2261 (1998).

26. Liu, S., Shi, Y., Ja, W.W. & Mathies, R.A. Optimization of High-Speed DNA Sequencing on Microfabricated Capillary Electrophoresis Channels. *Anal Chem* **71**, 566-573 (1999).

27. Paegel, B.M., Grover, W.H., Skelley, A.M., Mathies, R.A. & Joyce, G.F. Microfluidic Serial Dilution Circuit. *Anal Chem* **78**, 7522-7527 (2006).

28. McDonald, J.C. et al. Fabrication of microfluidic systems in poly(dimethylsiloxane). *Electrophoresis* **21**, 27-40 (2000).

29. McDonald, J.C. & Whitesides, G.M. Poly(dimethylsiloxane) as a Material for Fabricating Microfluidic Devices. *Acc Chem Res* **35**, 491-499 (2002).

30. Hong, J.W. & Quake, S.R. Integrated nanoliter systems. *Nat Biotech* **21**, 1179-1183 (2003).

31. Breslauer, D.N.L., P. J.; Lee, L. P. Microfluidics-based systems biology. *Mol BioSyst* **2**, 97–112 (2006).

32. Becker, H.G.C. Polymer microfabrication methods for microfluidic analytical applications. *Electrophoresis* **21**, 12-26 (2000).

33. Dolnik, V.L., S.; Jovanovich S. Capillary electrophoresis on microship. *Electrophoresis* **21**, 41-54 (2000).

34. Becker, H. & Gärtner, C. Polymer microfabrication technologies for microfluidic systems. *Anal Bioanal Chem* **390**, 89-111 (2008).

35. Barz, D.P.J. & Ehrhard, P. Model and verification of electrokinetic flow and transport in a micro-electrophoresis device. *Lab Chip* **5**, 949-958 (2005).

36. Amarie, D., Glazier, J.A. & Jacobson, S.C. Compact Microfluidic Structures for Generating Spatial and Temporal Gradients. *Anal Chem* **79**, 9471-9477 (2007).

37. Li, M.W., Huynh, B.H., Hulvey, M.K., Lunte, S.M. & Martin, R.S. Design and Characterization of Poly(dimethylsiloxane)-Based Valves for Interfacing Continuous-Flow Sampling to Microchip Electrophoresis. *Anal Chem* **78**, 1042-1051 (2006).

38. Tolan, N.V., Genes, L.I. & Spence, D.M. Merging Microfluidics with Microtitre Technology for More Efficient Drug Discovery. *JALA* **13**, 275-279 (2008).

39. Genes, L.I., Tolan, N.V., Hulvey, M.K., Martin, R.S. & Spence, D.M. Addressing a vascular endothelium array with blood components using underlying microfluidic channels. *Lab Chip* **7**, 1256-1259 (2007).

40. Wu, H., Huang, B. & Zare, R.N. Construction of microfluidic chips using polydimethylsiloxane for adhesive bonding. *Lab Chip* **5**, 1393-1398 (2005).

41. Unger, M.A., Chou, H.-P., Thorsen, T., Scherer, A. & Quake, S.R. Monolithic microfabricated valves and pumps by multilayer soft lithography. *Science* **288**, 113-116 (2000).

42. Houston, J.G. & Banks, M. The chemical-biological interface: developments in automated and miniaturised screening technology. *Curr Opin Biotechnol* **8**, 734-740 (1997).

43. Schillinger, E., Krais, T., Lehmann, M. & Stock, G. Iloprost. *Am J Cardiovasc Drugs* 209-231 (1986).

44. Carroll, J.S., Ku, C.-J., Karunarathne, W. & Spence, D.M. Red Blood Cell Stimulation of Platelet Nitric Oxide Production Indicated by Quantitative Monitoring of the Communication between Cells in the Bloodstream. *Anal Chem* **79**, 5133-5138 (2007).

45. Ballas, S.K., Dover, G.J. & Charache, S. Effect of hydroxyurea on the rheological properties of sickle erythrocytes in vivo. *Am J Hematol* **32**, 104-111 (1989).

46. Athanassiou, G., Moutzouri, A., Kourakli, A. & Zoumbos, N. Effect of hydroxyurea on the deformability of the red blood cell membrane in patients with sickle cell anemia. *Clin Hemorheol Microcirc* **35**, 291-295 (2006).

47. Dittrich, P.S. & Manz, A. Lab-on-a-chip: microfluidics in drug discovery. *Nat Rev Drug Discov* **5**, 210-218 (2006).

48. Cohen, C.M. A path to improved pharmaceutical productivity. *Nat Rev Drug Discov* **2**, 751-753 (2003).

49. Galson, S. in Piper Jaffray 17th Annual Healthcare Conference (FDA Center for Drug Evaluation and Research, New York, NY; 2005).

50. Malakoff, D. Spiraling Costs Threaten Gridlock. *Science* **322**, 210-213 (2008).

51. Varma Manthena, V.S. et al. Biopharmaceutic classification system: a scientific framework for pharmacokinetic optimization in drug research. *Curr Drug Metab* **5**, 375-388 (2004).

52. FDA (U.S. Department of Health and Human Serives Food and Drug Administration, 2004).

53. Kola, I. & Landis, J. Opinion: Can the pharmaceutical industry reduce attrition rates? *Nat Rev Drug Discov* **3**, 711-716 (2004).

54. Hood, L. & Perlmutter, R.M. The impact of systems approaches on biological problems in drug discovery. *Nat Biotechnol* **22**, 1215-1217 (2004).

55. Carroll, J. et al. An altered oxidant defense system in red blood cells affects their ability to release nitric oxide-stimulating ATP. *Mol Biosyst* **2**, 305-311 (2006).

56. Subasinghe, W. & Spence, D.M. Simultaneous determination of cell aging and ATP release from erythrocytes and its implications in type 2 diabetes. *Anal Chim Acta* **618**, 227-233 (2008).

57. Sprague, R.S., Stephenson, A.H., Bowles, E.A., Stumpf, M.S. & Lonigro, A.J. Reduced expression of Gi in erythrocytes of humans with type 2 diabetes is associated with impairment of both cAMP generation and ATP release. *Diabetes* **55**, 3588-3593 (2006).

58. Meyer, J.A., Froelich, J.M., Reid, G.E., Karunarathne, W.K.A. & Spence, D.M. Metal-activated C-peptide facilitates glucose clearance and the release of a nitric oxide stimulus via the GLUT1 transporter. *Diabetologia* **51**, 175-182 (2008).

59. Tolan, N.V., Genes, L.I., Subasinghe, W., Raththagala, M. & Spence, D.M. Personalized Metabolic Assessment of Erythrocytes Using Microfluidic Delivery to an Array of Luminescent Wells. *Anal Chem* **81**, 3102-3108 (2009).

CHAPTER 3: PERSONALIZED METABOLIC ASSESSMENT

3.1 METABOLIC SYNDROME: COMPETING PATHWAYS IN DIABETES

Metabolic syndrome (MetS) is generally accepted, as the presence of, first and foremost, insulin resistance, central adiposity or obesity, dyslipidemia in the form of elevated triglycerides and decreased high-density lipoprotein (HDL) cholesterol, as well as hypertension. Increased risk of cardiovascular disease and developing diabetes has been reported to be anywhere from 2-5 times more likely with the diagnosis of MetS and it has been shown to be a statistical determinant of micro- and macrovascular complications.[1] These vascular complications, retinopathy, neuropathy, nephropathy and cardiovascular disease are also risks associated with diabetes, [2-5] further exemplifying the strong link with MetS.

Various therapies include the modification of lifestyle, as it pertains to healthy dietary restrictions as well as the increase in daily activity. Pharmotherapies have concentrated on treating these conditions by the administration of insulin, metformin, α-glucosidase inhibitors, glucagon-like peptides (GLP-1), receptor agonists and dipeptidyl-peptidase IV (PPP-IV) enzyme inhibitors.[6] There is generally an observed weight gain associated with these treatment options, which is also associated with worsening insulin resistance. Clinical studies have demonstrated the physical toll MetS plays on the vascular system, specifically, the increased vascular thickness in the arterial wall and also wall stiffness,[7] resulting in an increased risk of cardiovascular complications.

By employing the μFA that is first introduced in chapter 2, this research focuses on the use of the flow-based system, providing a high throughput platform, to better

understand the relationship of the associated risk factors of MetS, specifically as it pertains to oxidant stress and hypertension. This device allows for the simultaneous determination of intracellular glucose metabolites within a RBC sample, while also monitoring the resulting affects on cell function, as expressed by the ability to release ATP. Furthermore, this work is an extension of the research performed in our group[8-10] to link the intracellular antioxidants produced through glucose metabolism in a dynamic measurement scheme that is important for measuring the effect of oxidant stress on cellular function. In this work, the relationship between the pentose phosphate and the polyol pathways for glucose metabolism are investigated, as it pertains to the complications exhibited by diabetic patients by using this *in vitro* model.

The most relevant application for this μFA is in pharmaceutical drug discovery, as previously discussed in chapter 2, specifically monitoring the properties of absorption, distribution, metabolism, excretion and toxicity (ADMET)[11-13] and the implementation of already available microtitre plate technology. Development of the ability to efficiently screen multiple samples for various metabolic functions will allow for a more specialized treatment of individual diabetic patients.

3.2 PPP: PRODUCTION OF GSH

Illustrated in figure 3.1, as glucose metabolism is shifted to the pentose phosphate pathway (PPP) to provide antioxidant defense for the cell, it is first phosphorylated by hexokinase (HK) to produce glucose-6-phosphate (G6P). Glucose-6-phosphate dehydrogenase (G6PD) will then oxidize G6P, forming 6-phosphogluconolactone (6GP) upon the reduction of $NADP^+$ to NADPH. NADPH is consumed in the production of

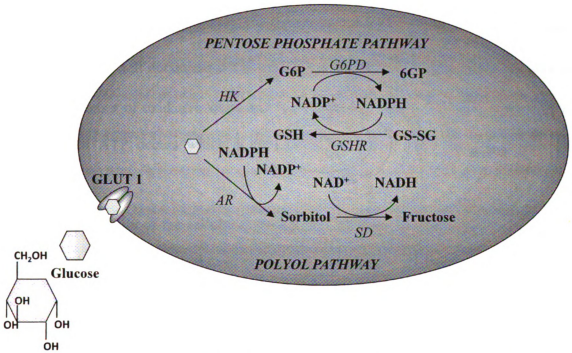

Figure 3.1 Illustration of the pentose phosphate and polyol pathways available for the metabolism of glucose within the red blood cell. Glucose is normally metabolized through the pentose phosphate pathway where glucose is phosphorylated by hexokinase (HK) to form glucose-6-phosphate (G6P) which is then oxidized to 6-phosphogluconoδ-lactone (6GP) upon the reduction of $NADP^+$ to NADPH. NADPH is an essential cofactor for the production of reduced glutathione (GSH) from its disulfide form (GS-SG), but it is also consumed in the polyol pathway where aldose reductase (AR) converts glucose to sorbitol. Upon the oxidation of sorbitol to form fructose by sorbitol dehydrogenase (SD), NAD^+ is reduced to form NADH.

reduced GSH, the most abundant non-enzymatic antioxidant, by way of glutathione reductase (GSHR).[14-17] Reduced GSH is formed from oxidized glutathione (GSSG), which contains a disulfide bond between two GSH molecules, while NADPH is oxidized back to $NADP^+$.

The enzyme activity of G6PD has been shown to be lower in patients with diabetes, leading to a reduced conversion of G6P to 6GP in the PPP.[18] Likewise, there is a reduction in the concentration of NADPH that is coproduced, leading to a reduced concentration in GSH and antioxidant ability within the RBCs obtained from diabetic patients, which is well documented throughout the literature.[19-23] Our group has shown that with the onset of oxidative stress and with decreased levels of GSH, a reduction in the release of ATP occurs which is thought to be due to a decrease in membrane flexibility.[8]

The flexibility of the cellular membrane is restricted when insulted with oxidant stressors such as peroxides, superoxides, and free radicals that oxidize spectrin instead of the biological alternative GSH.[16,18,19,24] Without sufficient GSH available, oxidant stressors will oxidize spectrin, introducing disulfide bonds and ultimately stiffen the cell membrane.[25-27] Importantly, our group and others have shown that RBCs from diabetic patients release less ATP in comparison to RBCs from healthy, non-diabetic controls, when these cells are subjected to mechanical deformation.[8] This is thought to be due, in part, to a reduction in the ability of the cells to fight off oxidant insults, resulting in decreased membrane flexibility when subjected to oxidant stressors. Further work in our lab has shown that the reduced level in RBC-derived ATP release coincides with a

decrease of intracellular NADPH concentrations[10] as well as reduced levels of GSH within RBCs from diabetics.[28]

Together, these results indicate that RBCs obtained from diabetic patients have reduced intracellular NADPH, the necessary precursor for GSH production, rendering the cell susceptible to oxidant stress. This oxidant stress has been shown to decrease the RBC-derived ATP release, which is a major contributor for endothelium-derived NO production and vasodilation action. This decrease in NO is thought to result in reduced vasodilation and, ultimately, increased hypertension and prevalence of the observed complications associated with diabetes.

3.3 POLYOL PATHWAY: SORB FORMATION AND DIABETIC COMPLICATIONS

In the case of chronic hyperglycemia when blood glucose levels are elevated, aldolase reductase (AR), which typically has a low affinity for glucose, initiates the polyol pathway and converts excess glucose to sorbitol (SORB). This process requires the oxidation of NADPH to form $NADP^+$ which reduces the substrate available for GSH production in the competing PPP. SORB is then metabolized to fructose upon the reduction of NAD^+ to NADH with the coenzyme sorbitol dehydrogenase (SD). The buildup of SORB within the nerve and lens tissues, due to its reduced permeability through the cell membrane, results in osmotic stress on the cell as the body tries to equilibrate the concentration gradient over the membrane. This results in structure and function abnormalities that is thought to be the cause for neuropathy and retinopathy complications exhibited by patients with diabetes.[29-31]

The research presented here attempts to demonstrate that increased metabolism of glucose through the polyol pathway may lead to a decrease in antioxidant ability of the RBC, resulting in reduced deformability upon oxidant attack. This may play an important role in the observed complications associated with diabetes, because a reduced deformability of the RBC has been well established to result in decreased shear-induced ATP release. ATP is a known stimulus for the production of endothelium-derived NO, which plays an important role in determining vascular caliber.[32-36] It is speculated that a reduced NO production from the endothelial lining of the vascular system could result in reduced vasodilation, which may decrease the ability of RBCs to deliver O_2 to the tissues surrounding the microvascular system.

3.4 GLUCOSE METABOLISM AND AFFECT ON ATP RELEASE

It has been speculated that reduced flexibility in the RBC membrane is due to the malfunction of the PPP, namely reduced G6PD activity.[8,10] However, a re-examination is necessary because of the complex involvement of both the pentose phosphate and polyol pathways in glucose metabolism, specifically, the intersection of the shared coenzyme, NADPH. The most recently reported method[8,10] of determining G6PD activity by quantifying the intracellular NADPH concentration, also simultaneously accounts for the activity of AR, which oxidizes NADPH to form SORB. The proposed reduction of G6PD activity in RBCs from diabetic patients[8] may actually be due to an increase in the polyol pathway and AR activity. The quantification of NADPH concentration cannot distinguish the enzyme activities of AR and G6PD individually;

however it can effectively measure the amount of NADPH available for the reduction of GSSG to GSH.

The more recent "redox hypothesis" focuses on the competing pentose phosphate and polyol pathways, specifically their intersection of the required NADPH substrate.[37-41] Research is needed to determine if the previously found reduction of G6PD activity is the foundation for the occurrence of diabetic complications or if the increased flux of glucose metabolism through the polyol pathway plays a vital role.

3.5 EXPERIMENTAL

Previous experiments[8,9] have utilized fluorescence detection of NADPH and GSH by employing non-flow fluorometer. Here, these same reactions will be monitored using fluorescence microscopy within a flow system, specifically the μFA, as diffusion of cellular components through the track-etched polycarbonate (TEPC) membrane react with isolated fluorescence probe solutions within the array of wells above. RBC samples and standard solutions are delivered to each row of wells that are loaded with the corresponding fluorescence probes for the analytes of interest, namely NADPH, GSH, SORB and ATP. In order to effectively measure the enzyme activities of G6PD, GSHR, AR and SD, concentrations of NADPH, GSH, SORB and ATP are quantified in individual wells by fluorescence and chemiluminescence detection. RBC samples are flowed at an optimized flow rate and time through the underlying microfluidic channels such as to maximize the sensitivity of the assay.

Using a fluorescence microscope, the fluorescence intensities are measured by analyzing each fluorescence image for average pixel intensities. The fluorescence

intensities are proportional to the concentrations of each metabolite present in the solutions other than ATP, which will utilize microscopy to image the chemiluminescence intensity produced without employing the excitation source. The experimental set up for the determination of intracellular metabolites and the simultaneous detection of ATP release is illustrated in figure 3.2. The entire μFA can be imaged by taking advantage of the low magnification capabilities of the Olympus MVX fluorescence steromicroscope (Center Valley, PA). The MVX microscope utilizes a mercury-arc lamp fitted with a carousel of various filter cubes allowing for fast and instantaneous wavelength selection.

The microfluidic delivery of the samples to the wells is important both analytically and physiologically, because the ATP release from the RBCs is stimulated by flow-induced shear stress. By incorporating microfluidic delivery of the intact cells to the wells, a portion of the cellular oxidant status and cellular function can be monitored simultaneously. Moreover, calibration and measurement of the analytes are performed in the presence and absence of various inhibitors on a single device. Furthermore, simultaneous imaging of the wells that are addressed by the underlying channels represent a starting point for attempts to merge microfluidic and microtitre-plate technology.

3.5.1 OBTAINING ISOLATED RBCS

All reagents were from Sigma Chemical (St. Louis, MO) unless otherwise noted. The RBCs used in these studies were obtained from male New Zealand White rabbits following the protocols approved by the Animal Investigation Committee at Michigan State University. As previously described,[42-46] rabbits (2.0-2.5 kg) were anesthetized

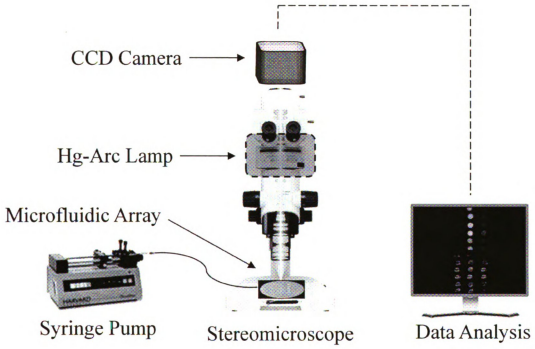

Figure 3.2 Experimental set up used to simultaneously monitor intracellular metabolites as well as the extracellular deformation-induced ATP release from RBC samples. Here, a displacement syringe pump is used to deliver solutions through the underlying microfluidic channels of the μFA while the steromicroscope images both fluorescence intensities and chemiluminescence produced in the determination of NADPH, GSH, SORB and ATP.

using ketamine (8 mL/kg, i.m.) and xylazine (1 mg/kg i.m.) followed by pentobarbital sodium (15 mg/kg i.v.). Rabbits are then ventilated with room air, at a rate of 20 breaths/min using a tidal volume of 20 mL/kg, by placing a cannula in the trachea. A catheter is then placed into the carotid artery for the administration of heparin (500 units, i.v.) prior to the exsanguination and collection of approximately 80 mL whole blood, which is obtained through the same catheter.

Whole blood is then centrifuged at 500 x *g* at 25 °C for 10 min at which time, the platelet-rich plasma and buffy coat were collected for other experimentation, as illustrated in figure 3.3. Here, the illustration shows the separation of the platelet-rich plasma and buffy coat, containing platelets and leukocytes, from the RBCs. The remaining RBCs were resuspended and washed three times in a physiological salt solution (PSS) (containing in mM, 4.7 KCl, 2.0 $CaCl_2$, 140.5 NaCl, 12 $MgSO_4$, 21.0 tris(hydroxymethyl)aminomethane, 5.6 glucose with 5% bovine serum albumin at a final pH of 7.4). All samples were prepared, the final solution's hematocrit is determined for subsequent dilutions, and experiments were performed within 8 hrs of RBC collection.

3.5.2 STANDARD MEASUREMENTS OF NADPH, GSH, SORB AND ATP

A single fluorescence image can be used to simultaneously provide the information necessary to construct a standard calibration curve as well as quantify the concentration of NADPH, GSH, and SORB contained in, as well as the concentration of ATP released from a single RBC sample. The microfluidic array employed here significantly reduces the time required to make multiple measurements when compared to a single measurement detection method. Sample preparation and fabrication of the

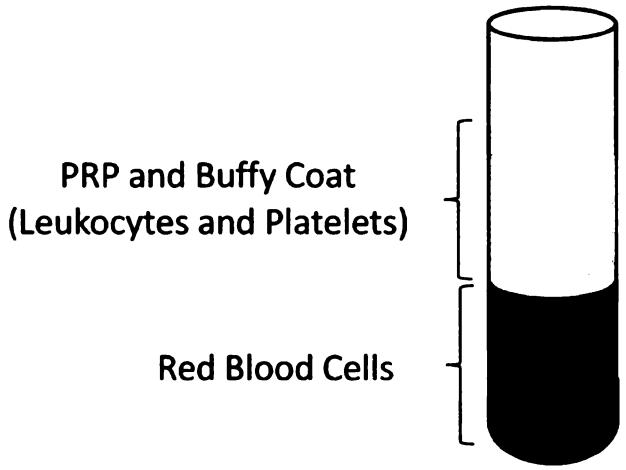

Figure 3.3 Illustration of centrifuged whole blood where the red blood cells are separated from the platelet-rich plasma (PRP) and buffy coat that contain the leukocytes and platelets.

microfluidic array aside, the actual time required for the entire analysis including the incubation required for the analytes in the channels to react with the luminescent probes immobilized within each well, is approximately 20 minutes.

As previously reported[8], the activity of G6PD was monitored by measuring the fluorescence intensity of red-fluorescent resorufin that was produced when NADPH, found within lysed RBC samples, was incubated with a resazurin reaction mixture containing diaphorase (Vybrant Cytotoxicity Assay Kit, Invitrogen Corp., Carlsbad, CA). This reaction mechanism is illustrated in figure 3.4, and although the concentration of NADPH is not exclusive to G6PD as previously discussed, it can however, be directly linked to the concentration available for the production of GSH for antioxidant defense.

Standard solutions of NADPH in phosphate buffered saline (PBS) solution (containing in g/L, 0.144 KH_2PO_4, 9.00 NaCl, 0.795 Na_2PO_4 (anhydrous), with a final pH of 7.4 ± 0.1) ranging from 12.5 to 200 μM and a single 0.7% lysed RBC sample solution, as illustrated in figure 3.5, were pumped through the underlying microfluidic channels for 20 min at a flow rate of 1.0 μL/min. These standard solutions were prepared from a 1.0 mM stock solution (8.3 mg dissolved and diluted with PBS to 10 mL). The RBC sample flowed through channel 6, was prepared by diluting the washed RBCs to a 0.7% hematocrit in deionized and distilled water (DDW, 18.1 MΩ resistivity) which results in complete lysis, thus enabling the intracellular concentrations of the NADPH and GSH to be determined. The resazurin fluorescence probe (30 μM) was pipetted into each of the 18 individual wells of the μFA, which was reduced by NADPH to produce the fluorescent resorufin product having excitation and emission wavelengths of 563 and 587 nm respectively. Fluorescence images were obtained using the Olympus MVX macro

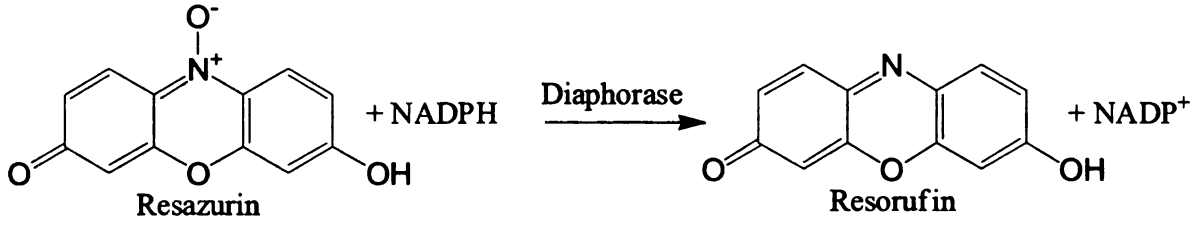

Figure 3.4 Illustration of the reaction used to determine the concentration of NADPH in various standard and sample solutions employing the μFA. Here resazurin, in the presence of diaphorase, is oxidized to the red-fluorescent resorufin as NADPH is reduced to $NADP^+$. Resorufin has excitation and emission wavelengths of 563 and 587 nm respectively.

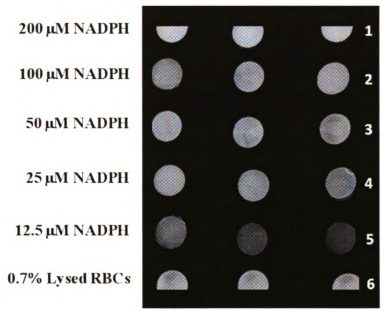

Figure 3.5 Fluorescence image of the 6-channel μFA used to determine the concentration of NADPH found within a 0.7% lysed RBC solution by simultaneously monitoring the fluorescence intensities from five NADPH standards ranging in concentration from 12.5 to 200 μM. Here, each standard and the single RBC sample solutions are flowed through the underlying microfluidic channels for 20 min while the resazurin contained within the wells above is reduced to the red-fluorescent resorufin product as NADPH is oxidized to form $NADP^+$.

zoom fluorescence microscope fitted with a resorufin filter cube that has maximum excitation and emission wavelengths of 570 nm and 585 nm respectively. The images were then analyzed for average pixel intensities, averaging each of the three wells thus enabling triplicate measurements, and plotted versus the known concentration of NADPH within each standard solution.

The methodology developed in our group to determine the concentration of GSH within a RBC sample[9] was modified slightly, however the enzymatic process is the same as illustrated in figure 3.6, only that the semi-preparative properties of the membrane within the μFA omitted the need to perform standard addition. The fluorescence probe mixture of 500 μM monochlorobimane and 8 U/mL glutathione-S-transferase (from equine liver, Sigma G6511) (MCB-GST) were pipetted into the 18 array-like wells and upon reaction, the fluorescence intensity of the GSH-MCB product with excitation and emission wavelengths of 370 nm and 478 nm respectively was determined. Here, the GST was added to aid in the binding of GSH to the MCB probe, significantly reducing the time required for analysis.[9] Figure 3.7 illustrates the fluorescence image obtained as standard solutions of GSH in PBS ranging from 2.5 to 40 μM and a single 0.7% lysed RBC sample solution were pumped through the underlying microfluidic channels for 20 min at a flow rate of 1.0 μL/min. These standard solutions were prepared from a 10 mM stock solution (0.0307 g in 10 mL PBS). The microscope was fitted with a 4',6'-diamidino-2-phenylindole (DAPI) filter cube having excitation and emission wavelengths of 372 nm and 456 nm respectively. The images were analyzed for fluorescence intensity, averaging the three wells for each channel, and plotted against the known GSH concentrations within solution to obtain the standard working curve.

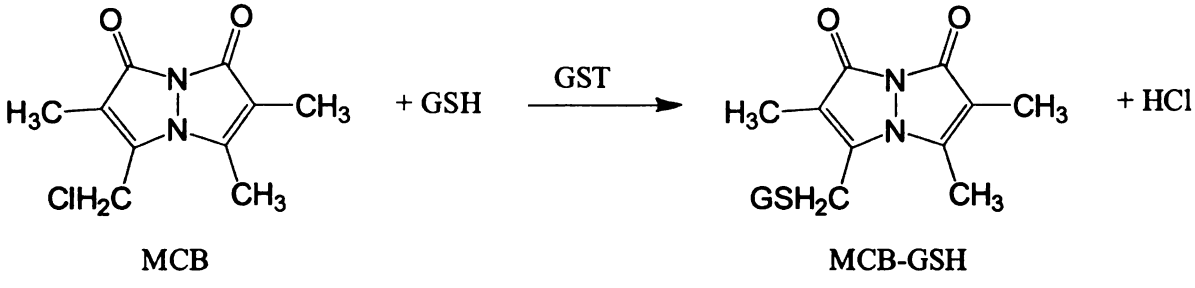

MCB MCB-GSH

Figure 3.6 Reaction mechanism for the determination of GSH in various standard and sample solutions where MCB and GSH form a fluorescent product (MCB-GSH) with excitation and emission wavelengths of 370 nm and 478 nm in the presence of glutathione-S-transferase (GST).

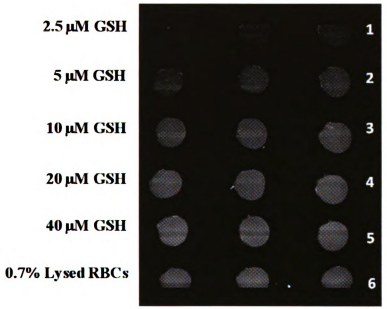

Figure 3.7 Fluorescence image of the 6-channel μFA used to determine the concentration of GSH found within a 0.7% lysed RBC solution by simultaneously monitoring the fluorescence intensities from five GSH standards ranging in concentration from 2.5 to 40 μM. As with the NADPH determination, each standard and the single RBC sample solutions are flowed through the underlying microfluidic channels for 20 min while the monochlorobimane and glutathione-S-transferase (MCB-GST) contained within the wells above forms the fluorescent MCB-GSH product.

Using the luciferin/luciferase enzyme-based reaction, detailed in figure 3.8 and as previously employed using microbore tubing,[10,43-45,47-49] an ATP calibration curve was constructed by monitoring the chemiluminescence produced, which is directly proportional to the concentration of ATP within each standard solution. To prepare the luciferin/luciferase mixture used to measure the ATP by chemiluminescence, 5 mL of DDW were added to a vial containing luciferase and luciferin (FLE-50, Sigma). In order to enhance the sensitivity of the assay, 2 mg of luciferin were added to the vial.

This assay was used to determine the ATP concentration released from 7% RBC sample solutions with and without the addition of diamide, a known cell-membrane stiffener.[24,50] As illustrated in figure 3.9, ATP standard solutions ranging from 0.25-1.0 μM in PSS and the RBC samples are flowed through the microfluidic channels, reacting with the luciferin/luciferase solution contained in each of the 18 wells that comprise the μFA. The ATP standard solutions were prepared from a 100 μM stock solution (27.6 mg in 500 mL DDW) in PSS. In addition, two 7% RBC samples were prepared by diluting the washed RBCs to 7% in PSS; however, one of these RBC samples is incubated in PSS containing 20 μM diamide. The diamide incubation occurred for 15 min prior to starting flow within the array in order to maximize the effect of the diamide solution and because the RBCs are able to recover from the oxidant attack and regain membrane flexibility to near initial levels within 30 to 40 min.[8] The excitation lamp was not employed for the chemiluminescence determination of ATP and the images were obtained without a wavelength selection filter cube. Images were obtained with a 5 sec exposure time in order to maximize the chemiluminescence intensity from each well. The pixel intensities

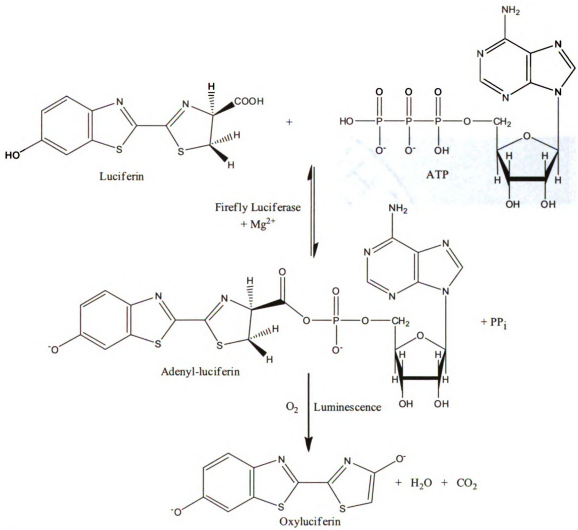

Figure 3.8 Reaction mechanism of the luciferin-catalyzed chemiluminescent reaction employed here for the determination of mechanical deformation induced-ATP release.

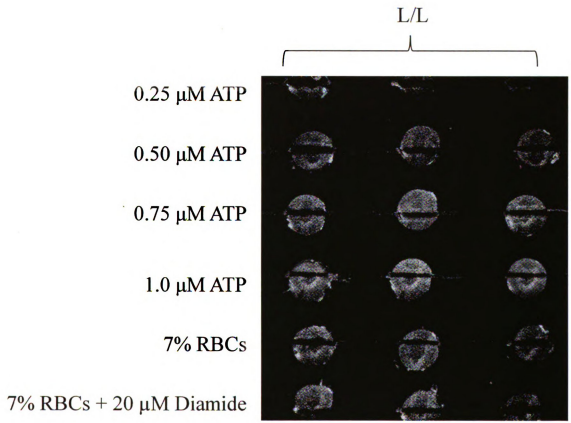

Figure 3.9 Chemiluminescence image, without the excitation source employed, for the determination of ATP within standard solutions as well as from the mechanical deformation of a 7% RBC sample with and without the incubation of diamide, a known cell-membrane stiffener. Here the luciferin and luciferase (L/L) solutions are pipetted into the 18 wells that comprise the μFA while the solutions are flowed through the microfluidic channels below.

for the standard solutions were used for linear regression analysis in order to determine the concentration of ATP release from the two non-lysed RBC samples.

The calibration curves for both NADPH and GSH were performed simultaneously by combining NADPH standards ranging from 25 to 200 μM and GSH standards ranging from 5 to 40 μM together into four individual standard solutions. Combining NADPH and GSH in the same standard solutions, while monitoring the fluorescence intensities produced in the two separate columns of wells, allowed for the construction of two separate calibration curves and only required three channels. Each metabolite was effectively measured in the presence of the other within each standard solution and from the same RBC sample. Here, the standard preparation was identical to that described above; however, the incremental standard solutions of NADPH and GSH were prepared in the same volumetric flask.

As illustrated in figure 3.10, the first 6 channels of the 12-channel array contain the resazurin probe solution which was only loaded in the first column of wells, while the MCB-GST probe solution was loaded into the second column of wells. The NADPH and GSH present in each standard solution reacts with their respective fluorescent probe immobilized within wells above, allowing for the determination of both NADPH and GSH within each solution pumped through the underlying microfluidic channels. Here, the standard samples and a 0.7% lysed RBC sample were pumped through the underlying channels for 20 min at which point, the average pixel intensities were used to construct a calibration curve to determine the concentration of both NADPH and GSH within the same RBC sample.

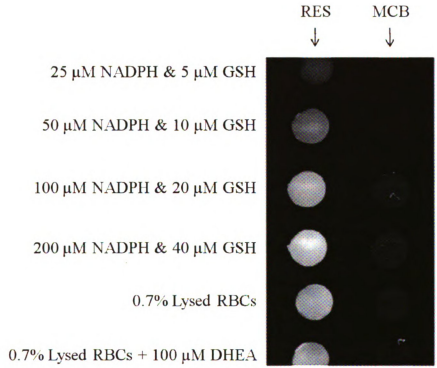

Figure 3.10 Fluorescence image of the simultaneous detection of both NADPH and GSH within standard sample solutions as well as within a 0.7% lysed RBC solution with and without the inhibition of G6PD by dehydroepandroesterone (DHEA). As before, solutions were flowed through the underlying microfluidic channels and both the resazurin (RES) and monochlorobimane and glutathione-S-transferase (MCB-GST) were pipetted into only one column in order to detect both analytes from within the same solution. Images were obtained as before except that the resorufin and DAPI filter cubes were employed to select the appropriate wavelengths for each analyte, NADPH and GSH, respectively.

On a single 12-channel μFA the determination of intracellular metabolites (NADPH and GSH) were performed while simultaneously monitoring the cellular function (as ATP release) from the same RBC sample. Figure 3.11 shows the fluorescence image obtained for the determination of NADPH and GSH from within two lysed RBC samples while simultaneously monitoring the concentration of ATP release from two non-lysed RBC solutions, each incorporating calibration standards.

The standard samples containing NADPH (25-200 μM) and GSH (5-40 μM) were prepared as detailed above and flowed through the first four channels of the μFA. Two 0.7% lysed RBC solutions with and without the incubation (prior to lysis) with dehydroepandroesterone (DHEA), a known G6PD inhibitor, were flowed through channels five and six. A 1 mM stock solution of DHEA was prepared by dissolving 0.0043 g in 10 mL of PSS which was subsequently diluted to obtain a solution containing 100 μM DHEA and 7% RBCs. This solution was incubated for 30 min in order to inhibit G6PD and effectively lower the GSH and NADPH concentrations within the cell, simulating RBCs obtained from a patient with diabetes.[51-54] A control sample was also prepared, containing 7% RBC in PSS without DHEA. After the 30 min incubation, both cell solutions were diluted to 0.7% and lysed by adding 200 μL of the 7% RBC solutions to 1.8 mL DDW, individually.

The standard and sample solutions were pumped through the underlying microfluidic channels for 20 min at a flow rate of 1.0 μL/min at which time, the fluorescence images were obtained using both the resorufin and DAPI filter cubes. The fluorescence intensities observed in each well are directly proportional to the concentration of each NADPH and GSH within the solutions, allowing for simultaneous

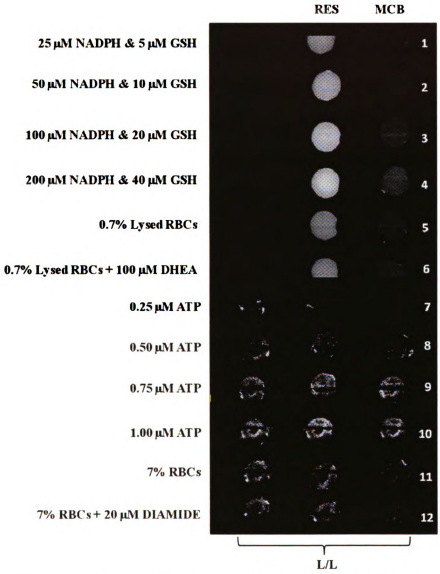

Figure 3.11 Images for the determination of intracellular NADPH and GSH as well as for the mechanical deformation-induced ATP release from RBC samples. The first six channels, employ fluorescence spectroscopy where two columns of wells contain RES and MCB fluorescence probes while the last six channels, employ chemiluminescence where all three columns contain the L/L reaction mixture.

detection of both metabolites by simply changing the excitation and emission wavelengths.

The ATP assay that was described above was carried out on the last six channels of the same μFA (figure 3.11). This assay monitored cell function, requiring non-lysed solutions, making it was necessary to carry out the ATP determination in separate channels from those used to monitor NADPH and GSH. ATP standard solutions ranging in concentration from 0.25-1.0 μM were pumped through channels seven through ten, while two 7% non-lysed RBC samples in the presence and absence of 20 μM diamide, a known cell stiffener, were pumped through the last two channels. The pixel intensities for the standard solutions were used for linear regression analysis in order to determine the concentration of ATP release from the two non-lysed RBC samples.

3.5.3 THE AFFECT OF G6PD AND AR INHIBITION

The complications exhibited by patients with diabetes have been reduced with continued treatment of aldose reductase inhibitors (ARIs).[29,55-63] However, clinical trials have revealed that pharmaceutical drugs developed for the inhibition of AR, in order to promote the PPP for glucose metabolism and increase the intracellular level of GSH, have serious side affects.[62] These negative side effects, including hypersensitivity reactions and liver damage, result when administering ARIs such as Fidarestat, Aldos, Sorbinil, Tolrestat, and Statinil.

Recent studies have indicated that these side effects can be eliminated by the use of ascorbic acid (AA), or vitamin C for the inhibition of AR.[64-66] It was concluded that administration of approximately 1,000 mg of AA per day, results in a significant decrease

in the concentration of sorbitol found within RBCs as well as the previously reported diabetic complications (such as neuropathy and retinopathy). It is suspected that this is due to an increase in intracellular metabolites of the PPP and antioxidant status, preventing the stiffening of the cellular membrane when insulted with oxidant stress and increasing ATP release by maintaining RBC deformability.

The inhibition of G6PD will allow for the quantification of NADPH found within RBCs due to the polyol pathway and indirectly measure the activity of AR. Here, quantification of NADPH and GSH with alternating inhibition of AR and G6PD, will allow for the determination of enzyme activities of each and for further conclusions to be made regarding any enzyme deficiency of diabetic patients. It has been shown that the inhibition of AR and the polyol pathway will redirect the metabolism of glucose though the pentose phosphate pathway, decreasing the concentration of sorbitol and increasing the concentration of GSH found within various cell types.[56,61] Preliminary research has shown that the incubation of RBCs with AA will increase the release of ATP once treated with DHEA, a known G6PD inhibitor, compared to a control RBC sample not incubated with AA prior to introduction of DHEA.

The concentration of RBC-derived ATP was determined using the chemiluminescence reaction with the luciferin/luciferase assay solution by implementing the flow-based system illustrated in figure 3.12. A single syringe pump was used to flow ATP standards and various RBC samples, as well as the luciferin/luciferase solution through microbore tubing, with an internal diameter of 50 μm. The samples were flowed at a rate of 6.7 μL/min and combined in a T-junction (Upchurch Scientific, Oak Harbor, WA) allowing for the solutions to mix before combining into another 50 cm section of

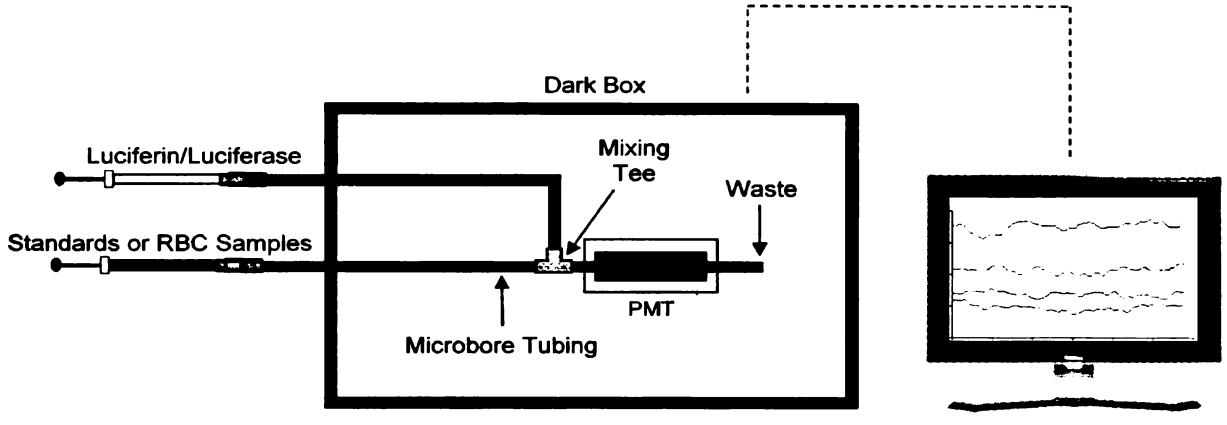

Figure 3.12 Schematic drawing of the experimental setup used to determine RBC-derived ATP release in a continuous flow system employing 75 μm internal diameter tubing. Here the luciferin and luciferase enzymatic assay was employed, monitoring the chemiluminescence produced that is directly proportional to the concentration of ATP released from various samples.

tubing with the polyimide coating removed allowing for the chemiluminescence produced to be detected by the PMT housed within a light excluding box. The current collected by the PMT from the chemiluminescence produced, is converted to voltage, measured in real time, and plotted at a rate of 10 measurements per second for 30 seconds onto a computer using LabView software (National Instruments, Austin, TX) with a program that was written in-house.

Figure 3.13 illustrates that the concentration of ATP released from RBCs incubated with a 1.0 mM AA solution prior to a 100 μM DHEA solution, was greater than that from RBCs treated with a 100 μM DHEA solution alone. A 10 mM AA stock solution was prepared by dissolving 0.0176 g in 10 mL PSS, prior to the combination with a second PSS solution to obtain a 1 mM AA and 20% RBC solution. This solution was incubated for 30 min prior to combining with a final PSS solution to obtain 7% RBCs and 100 μM DHEA which was incubated for an additional 30 min prior to determining the ATP release. The results indicate that the incubation of RBCs with AA prior to DHEA will increase ATP release, however, further studies are necessary to conclude that the incubation of RBCs with AA inhibits AR and promotes the pentose phosphate pathway and the production of GSH.

Finally, recent work has been performed to include both AA and DHEA along with various glycemic environments for the fluorescence determination of SORB[67-69] along with NADPH, GSH and ATP onto the μFA. As described above, the fluorescence probe solution was pipetted into the array like wells of a single column, where here the solution comprised of 2 U/mL SDH and 3.0 mM NAD^+. The SDH within the fluorescence probe solution converts SORB to fructose while NAD^+ is reduced to NADH

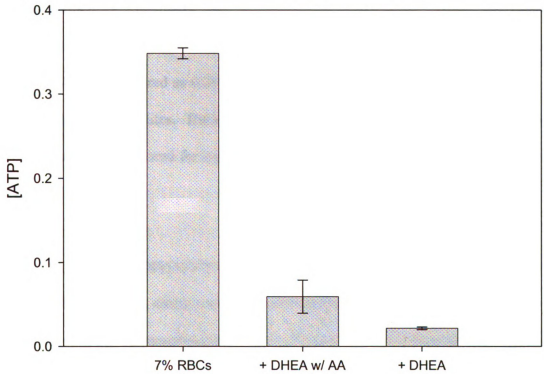

Figure 3.13 ATP release from 7% RBCs with the inhibition of G6PD using DHEA, resulting in a decrease in the concentration of deformation-induced ATP release in 50 μm diameter microbore tubing. Upon the pre-incubation of RBC with a 5 mM solution of ascorbic acid (AA), a known aldose reductase inhibitor, the reduction in ATP release due to the inhibition of G6PD with DHEA is somewhat opposed ($p < 0.05$). The mean concentrations of ATP released are reported where the error is represented as the SEM.

which is fluorescently active (excitation and emission wavelengths of 340 nm and 460 nm respectively). As illustrated in figure 3.14, the concentration of each NADPH, GSH, and SORB were monitored within the first six channels of the μFA as RBC incubated within various glucose environments, as well as, with DHEA and AA, flowed through the underlying microfluidic channels. Here, the samples were prepared as detailed above, for the preparation of RBCs with 1 mM AA and 100 μM DHEA separately, and combined. Additionally, RBC samples were prepared in PSS containing various concentrations of glucose, which were incubated for 6 hrs before they were pumped through the underlying microfluidic channels for 20 min. Each of samples flowed through the first six channels of the μFA were prepared as 0.7% RBCs in DDW, lysing the cells for the determination of intracellular metabolites. The samples flowed through the last six channels were intact RBCs that were monitored for cell function by way of mechanical deformation-induced ATP release.

3.6 RESULTS AND DISCUSSION

When NADPH, GSH, and ATP were optimized on separate microfluidic devices by monitoring the fluorescence intensities of the three wells for each underlying channel, the averages were used for the linear regression analysis. This effectively represented the variation associated with the consecutive sample analysis along the channel length and indicated that the reproducibility of each standard fluorescence intensity was appropriate for concentration determination of the analytes within the RBC samples. The flow rate of 1.0 μL/min was chosen along with the internal pore diameter of the TEPC membrane (0.1

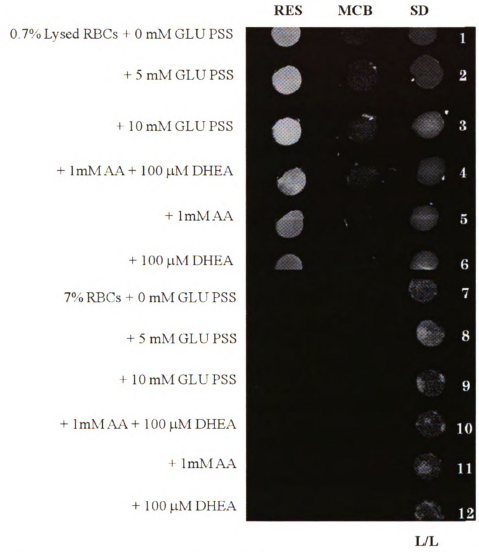

Figure 3.14 Images for the determination of intracellular NADPH and GSH as well as for the mechanical deformation-induced ATP release from RBC samples. The first six channels, employ fluorescence spectroscopy where two columns of wells contain RES and MCB fluorescence probes while the last six channels, employ chemiluminescence where all three columns contain the L/L reaction mixture.

μm) to minimize the bulk fluid flow through the membrane, preventing dilution of the fluorescence probe solution located in the wells.

For each sample analysis, background subtraction was performed and standard solutions were incorporated onto each device in order to reproducibly and accurately determine analyte concentrations with the RBC samples. The experimentation was performed intentionally to allow for only a single dependant variable, the analyte concentration, eliminating any inconsistencies within the set up, including but not limited to, variable excitation and emission intensities resulting from the wavelength selection filter cubes, any possible cross-talk between wavelengths, and heterogeneity of channel-well interface surface area. Here, standard and sample solutions were analyzed approximately 30 min after preparation in order to keep analyte degradation within solution minimal and consistent. More specifically, each solution was pumped through the underlying channels in a manner that would take into account the reaction kinetics between the analytes and the fluorescent probe solutions and the incubation time was determined by the commencement of fluid flow.

3.6.1 QUANTITATIVE DETERMINATION WITHIN THE RBC

As shown in figure 3.15a, the 0.7% RBC sample was determined to contain on average 31.06 ± 4.12 μM NADPH and 22.55 ± 2.47 μM GSH, which upon G6PD inhibition using DHEA, was reduced to 22.99 ± 4.63 μM NADPH and 14.60 ± 3.14 μM GSH, where the variance is reported as the standard error of the mean. The concentrations of NADPH and GSH for the 0.7% lysed RBC sample without DHEA

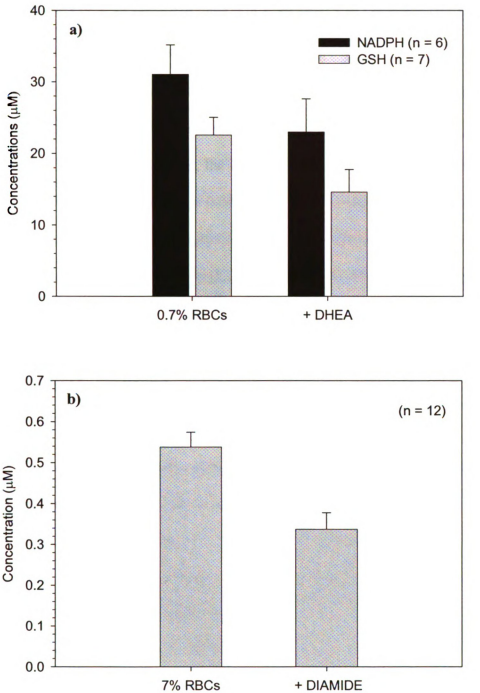

Figure 3.15 Concentrations of (a) NADPH, GSH, and (b) ATP determined for lysed and nonlysed RBC samples. Data representing figure 3.10, the concentrations of NADPH and GSH for 0.7% RBC samples were determined to be 31.06 ± 4.12 and 22.5 ± 2.47 μM, respectively; the concentrations decreased for each upon the incubation of DHEA to 22.9 ± 4.63 and 14.6 ± 3.1 μM, respectively. The concentration of ATP release within the flow-based μFA was determined to be 0.54 ± 0.04 μM for a 7% RBC sample which was reduced to 0.34 ± 0.04 μM when incubated with diamide. Error bars represent the SEM for the number of rabbits indicated in the figures.

incubation are 377 ± 50 amol/RBC and 274 ± 30 amol/RBC respectively, falling within the range reported elsewhere using various methods.[9,16,19-21,70]

Figure 3.15b illustrates the results for the quantitative determination of ATP release and is given as average micromolar amounts where the variance is expressed as standard error of the mean. Here, the concentration of ATP released from a 7% RBC sample was determined to be 0.54 ± 0.04 μM which was reduced to 0.34 ± 0.04 μM when incubated with diamide prior to analysis. ATP release, indicative of the shear forces that are exerted on the RBCs, is specific to the channel dimensions of this particular microfluidic device as well as the flow rate of the samples through the underlying channels. Here, the flow rate for this device is approximately three-fold greater than that found within 50 μm i.d. microbore tubing, indicating ATP release that is notably equivalent to previous reports.[8]

By incubating 7% RBC solutions in various glucose concentrations as well as with 1 mM AA and 100 μM DHEA separately and combined, figure 3.16a represents the preliminary data obtained from the 12-channel μFA for the determination of NADPH, GSH, SORB and ATP release. Here, as the concentration of glucose in the PSS solution increases there is a notable increase in the fluorescence intensity observed which is relative to the concentrations of NADPH and SORB. This is suspected to be due to an increase in glucose metabolism through both the pentose phosphate and polyol pathways. The incubation of RBCs with AA prior to the inhibition of G6PD, with DHEA, shows that there is an increase in the concentration of NADPH within the RBC, returning it to a value consistent with untreated 0.7% RBCs.

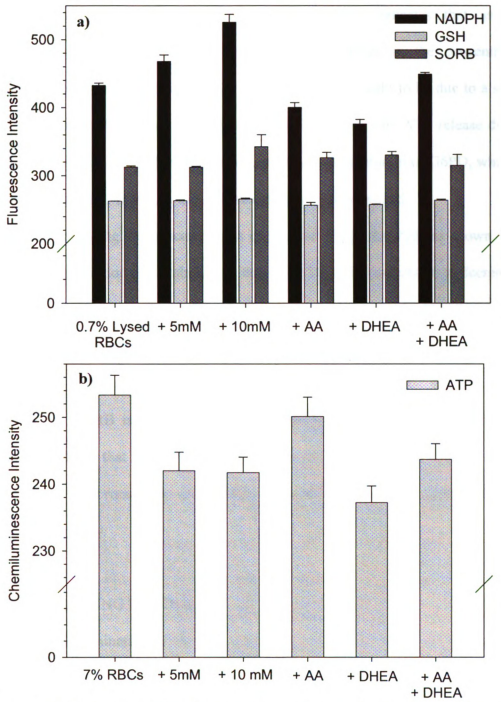

Figure 3.16 Data representing the intracellular a) metabolites and b) resulting affect on cellular function as expressed though mechanical deformation-induced RBC-derived ATP release. The fluorescence intensity for the metabolites (NADPH, GSH, SORB) and the chemiluminescence produced for monitoring the cellular function (ATP release) are reported as average intensities of three areas sampled within each well for RBCs in various glucose PSS solutions (0-10 mM) as well as with the incubation of ascorbic acid (AA) and dihydroxyepiandrosterone (DHEA) where the error reported represents the SEM.

The ATP release, as shown in figure 3.16b, indicates that as glucose concentrations increase there is a corresponding decrease in the concentration of mechanical deformation-induced ATP release, which is thought to be due to a stiffening of the RBC as oxidant attack and glycosylation increases. The ATP release due to the incubation with DHEA is shown to be reduced upon the inhibition of G6PD, which when pre-incubated with 1 mM AA, the ATP release is slightly regained.

By expanding the concentrations of glucose within the PSS, as shown in figure 3.17, the concentration of metabolites within the 0.7% RBCs are shown to decrease when incubated in hyperglycemic conditions (15-25 mM). In this range, there is a substantial decrease in the intracellular concentration of NADPH and GSH. At elevated glucose concentrations, it is suspected that as the glucose is metabolized through the polyol pathway, the SORB is more rapidly metabolized to fructose resulting in the gradual decrease in SORB that is shown. Future studies should include a SD inhibitor in order to prevent fructose formation to more effectively monitor the glucose metabolism through the polyol pathway.

3.6.2 EVALUATING THE DIABETIC-SIMULATED RBC

The determination of the concentrations of NADPH, GSH and ATP from RBC samples treated to reflect the state of RBCs obtained from patients with diabetes is demonstrated here. It is anticipated that this methodology will allow for the differentiation of RBCs obtained from diabetic patients, compared to those obtained from healthy non-diabetic controls. This μFA allows for multiple optical detection methods (fluorescence and chemiluminescence) to be used simultaneously, while also

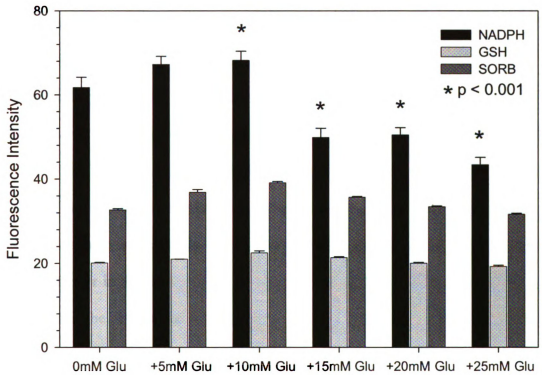

Figure 3.17 Data representing the fluorescence intensities for monitoring the intracellular concentrations of each metabolite, NADPH, GSH and SORB when incubated in various glucose (GLU) containing PSS solutions (0-25 mM). The fluorescence intensities are reported as the average of three sampled areas within each well and the error is reported as the SEM.

incorporating a flow-based system without the need for sample preparation due to the separation of the wells from the channels by a TEPC membrane. Here, simultaneous analysis performed on a single platform may serve as a diagnostic tool for determining the cause for hypertension complications as it relates to diabetes.[71] This research illustrates the ability to profile various analytes from within a lysed RBC solution, as well as analytes released from intact RBCs.

Monitoring the concentrations of NADPH, GSH and ATP on a single device is an initial attempt at merging metabolic profiling with cell function assays simultaneously. For example, people with cystic fibrosis have RBCs that release very little ATP due to a reduced activity of the CFTR.[72] However, as mentioned above, people with diabetes have similar ATP release patterns. Collectively, if a blood (or RBC) sample was to be screened for ATP release and the release was found to be lower than normal, it would be premature to conclude the subject has cystic fibrosis unless more quantitative information about the sample was obtained. A glycosylated hemoglobin value (A1C), which is generally higher in the poorly controlled diabetic but often normal in people with cystic fibrosis, could be obtained to learn more about the initial screen. Therefore, coupling a quantitative determination of ATP with another measured parameter would be useful, if not necessary.

REFERENCES

1. The Metabolic Syndrome Is a Risk Indicator of Microvascular and Macrovascular Complications in Diabetes. *Diabetes Care* **29**, 2701-2707 (2006).

2. Fong, D.S. et al. Diabetic retinopathy. *Diabetes Care* **26**, 226-229 (2003).

3. EDIC Intensive Diabetes Treatment and Cardiovascular Disease in Patients with Type 1 Diabetes. *N Engl J Med* **353**, 2643-2653 (2005).

4. CDC Centers for Disease Control and Prevention. National Diabetes Fact Sheet: General information and National Estimates on Diabetes in the United States, 2007. *US Department of Health and Human Services* (2008).

5. Stephens, J.W., Khanolkar, M.P. & Bain, S.C. The biological relevance and measurement of plasma markers of oxidative stress in diabetes and cardiovascular disease. *Atherosclerosis* **202**, 321-329 (2009).

6. Joffe, D. & Yanagisawa, R.T. Metabolic syndrome and type 2 diabetes: can we stop the weight gain with diabetes? *Med. Clin. North Am.* **91**, 1107-1123 (2007).

7. Scuteri, A. et al. Metabolic syndrome amplifies the age-associated increases in vascular thickness and stiffness. *J Am Coll Cardiol* **43**, 1388-1395 (2004).

8. Carroll, J. et al. An altered oxidant defense system in red blood cells affects their ability to release nitric oxide-stimulating ATP. *Mol Biosyst* **2**, 305-311 (2006).

9. Raththagala, M., Root, P.D. & Spence, D.M. Dynamic Monitoring of Glutathione in Erythrocytes, without a Separation Step, in the Presence of an Oxidant Insult. *Anal Chem* **78**, 8556-8560 (2006).

10. Subasinghe, W. & Spence, D.M. Simultaneous determination of cell aging and ATP release from erythrocytes and its implications in type 2 diabetes. *Anal Chim Acta* **618**, 227-233 (2008).

11. Dittrich, P.S. & Manz, A. Lab-on-a-chip: microfluidics in drug discovery. *Nat Rev Drug Discov* **5**, 210-218 (2006).

12. Breslauer, D.N.L., P. J.; Lee, L. P. Microfluidics-based systems biology. *Mol BioSyst* **2**, 97–112 (2006).

13. Cohen, C.M. A path to improved pharmaceutical productivity. *Nat Rev Drug Discov* **2**, 751-753 (2003).

14. Meldrum, N.U. & Tarr, H.L.A. The reduction of glutathione by the Warburg-Christian system. *Biochem J* **29**, 108-115 (1935).

15. Dumaswala, U.J., Zhuo, L., Jacobsen, D.W., Jain, S.K. & Sukalski, K.A. Protein and lipid oxidation of banked human erythrocytes: role of glutathione. *Free Radic Biol Med* **27**, 1041-1049 (1999).

16. Aaseth, J. & Stoa-Birketvedt, G. Glutathione in overweight patients with poorly controlled type 2 diabetes. *Journal of Trace Elements in Experimental Medicine* **13**, 105-111 (2000).

17. Di Mascio, P., Dewez, B. & Garcia, C.R.S. Ghost protein damage by peroxynitrite and its protection by melatonin. *Braz J Med Biol Res* **33**, 11-17 (2000).

18. Beard, K.M., Shangari, N., Wu, B. & O'Brien, P.J. Metabolism, not autoxidation, plays a role in a-oxoaldehyde- and reducing sugar-induced erythrocyte GSH depletion: Relevance for diabetes mellitus. *Mol Cell Biochem* **252**, 331-338 (2003).

19. Costagliola, C. Oxidative state of glutathione in red blood cells and plasma of diabetic patients: in vivo and in vitro study. *Clin Physiol Biochem* **8**, 204-210 (1990).

20. De Mattia, G. et al. Influence of reduced glutathione infusion on glucose metabolism in patients with non-insulin-dependent diabetes mellitus. *Metabolism* **47**, 993-997 (1998).

21. Dincer, Y., Akcay, T., Alademir, Z. & Ilkova, H. Effect of oxidative stress on glutathione pathway in red blood cells from patients with insulin-dependent diabetes mellitus. *Metabolism* **51**, 1360-1362 (2002).

22. Constantin, A., Constantinescu, E., Dumitrescu, M., Calin, A. & Popov, D. Effects of ageing on carbonyl stress and antioxidant defense in RBCs of obese type 2 diabetic patients. *J Cell Mol Med* **9**, 683-691 (2005).

23. Nwose, E.U., Jelinek, H.F., Richards, R.S. & Kerr, P.G. in Redox Report, Vol. 11 99-104 (Maney Publishing, 2006).

24. Ghigo, D. et al. Changes in erythrocyte deformability resulting from alterations of redox metabolism in diabetes mellitus. *Ric Clin Lab* **13**, 375-381 (1983).

25. Fischer, T.M., Haest, C.W.M., Stoehr, M., Kamp, D. & Deuticke, B. Selective alteration of erythrocyte deformability by sulfhydryl reagents. Evidence for an involvement of spectrin in membrane shear elasticity. *Biochim Biophys Acta* **510**, 270-282 (1978).

26. Schwartz, R.S., Madsen, J.W., Rybicki, A.C. & Nagel, R.L. Oxidation of spectrin and deformability defects in diabetic erythrocytes. *Diabetes* **40**, 701-708 (1991).

27. Cicha, I., Tateishi, N., Suzuki, Y. & Maeda, N. Rheological changes in human red blood cells under oxidative stress: effects of thiol-containing antioxidants. *Pathophysiology* **6**, 121-128 (1999).

28. D'Amico Oblak, T., Meyer, J.A. & Spence, D.M. A microfluidic technique for monitoring bloodstream analytes indicative of C-peptide resistance in type 2 diabetes. *Analyst* **134**, 188-193 (2008).

29. Bravi, M.C. et al. Polyol pathway activation and glutathione redox status in non-insulin-dependent diabetic patients. *Metabolism* **46**, 1194-1198 (1997).

30. Gabbay, K.H. Role of sorbitol pathway in neuropathy. *Advances in Metabolic Disorders, Supplement* **2**, 417-424 (1973).

31. Chylack, L.T., Jr. & Kinoshita, J.H. A biochemical evaluation of a cataract induced in a high-glucose medium. *Invest Ophthalmol* **8**, 401-412 (1969).

32. Ellsworth, M.L., Forrester, T., Ellis, C.G. & Dietrich, H.H. The erythrocyte as a regulator of vascular tone. *Am J Physiol Heart Circ Physiol* **269**, H2155-2161 (1995).

33. McCullough, W.T., Collins, D.M. & Ellsworth, M.L. Arteriolar responses to extracellular ATP in striated muscle. *Am J Physiol Heart Circ Physiol* **272**, H1886-H1891 (1997).

34. Collins, D.M., McCullough, W.T. & Ellsworth, M.L. Conducted vascular responses: communication across the capillary bed. *Microvasc Res* **56**, 43-53 (1998).

35. Dietrich, H.H., Ellsworth, M.L., Sprague, R.S. & Dacey, R.G., Jr. Red blood cell regulation of microvascular tone through adenosine triphosphate. *Am J Physiol Heart Circ Physiol* **278**, H1294-H1298 (2000).

36. Sprague, R.S., Ellsworth, M.L., Stephenson, A.H. & Lonigro, A.J. ATP: the red blood cell link to NO and local control of the pulmonary circulation. *Am J Physiol Heart Circ Physiol* **271**, H2717-H2722 (1996).

37. Varma, S.D.K., J. H. Sorbitol pathway in diabetic and galactosemic rat lens. *Biochim Biophys Acta*632-640 (1974).

38. Morrison, A.D., Clements, R.S. & Travis, S.B. Glucose utilization by the polyol pathway in human erythrocytes. *Biochem Biophys Res Commun* 199-205 (1970).

39. Travis, S.F., D., M.A. & Clements, R.S. Metabolic alterations in the human erythrocytes produced by increases in glucose concentrations. *J Clin Invest* 2104-2112 (1971).

40. Williamson, J.R. et al. Hyperglycemic pseudohypoxia and diabetic complications. *Diabetes* **42**, 801-813 (1993).

41. Barnett, P.A.G., R. G.; Chylack L. T. The effects of oxidation on sorbitol pathway kinetics. *Diabetes*, 426-432 (1986).

42. Sprague, R.S. et al. Effect of L-NAME on pressure-flow relationships in isolated rabbit lungs: role of red blood cells. *Am J Physiol Heart Circ Physiol* **269**, H1941-H1948 (1995).

43. Edwards, J., Sprung, R., Spence, D. & Sprague, R. Chemiluminescence detection of ATP release from red blood cells upon passage through microbore tubing. *Analyst* **126**, 1257-1260 (2001).

44. Sprung, R., Sprague, R. & Spence, D. Determination of ATP release from erythrocytes using microbore tubing as a model of resistance vessels in vivo. *Anal Chem* **74**, 2274-2278 (2002).

45. Fischer, D.J., Torrence, N.J., Sprung, R.J. & Spence, D.M. Determination of erythrocyte deformability and its correlation to cellular ATP release using microbore tubing with diameters that approximate resistance vessels in vivo. *Analyst* **128**, 1163-1168 (2003).

46. Oblak, T.D.A., Root, P. & Spence, D.M. Fluorescence Monitoring of ATP-Stimulated, Endothelium-Derived Nitric Oxide Production in Channels of a Poly(dimethylsiloxane)-Based Microfluidic Device. *Anal Chem* **78**, 3193-3197 (2006).

47. Carroll, J.S., Ku, C.-J., Karunarathne, W. & Spence, D.M. Red Blood Cell Stimulation of Platelet Nitric Oxide Production Indicated by Quantitative Monitoring of the Communication between Cells in the Bloodstream. *Anal Chem* **79**, 5133-5138 (2007).

48. Faris, A. & Spence, D.M. Measuring the simultaneous effects of hypoxia and deformation on ATP release from erythrocytes. *Analyst* **133**, 678-682 (2008).

49. Meyer, J.A., Froelich, J.M., Reid, G.E., Karunarathne, W.K.A. & Spence, D.M. Metal-activated C-peptide facilitates glucose clearance and the release of a nitric oxide stimulus via the GLUT1 transporter. *Diabetologia* **51**, 175-182 (2008).

50. Kosower, N.S., Kosower, E.M., Wertheim, B. & Correa, W.S. Diamide, a new reagent for the intracellular oxidation of glutathione to the disulfide. *Biochem Biophys Res Commun* **37**, 593-596 (1969).

51. Shantz, L.M., Talalay, P. & Gordon, G.B. Mechanism of inhibition of growth of 3T3-L1 fibroblasts and their differentiation to adipocytes by dehydroepiandrosterone and related steroids: role of glucose-6-phosphate dehydrogenase. *Proc Natl Acad Sci U S A* **86**, 3852-3856 (1989).

52. Gupte, S.A. et al. Pentose phosphate pathway coordinates multiple redox-controlled relaxing mechanisms in bovine coronary arteries. *Am J Physiol Heart Circ Physiol* **285**, H2316-H2326 (2003).

53. Leopold, J.A., Cap, A., Scribner, A.W., Stanton, R.C. & Loscalzo, J. Glucose-6-phosphate dehydrogenase deficiency promotes endothelial oxidant stress and decreases endothelial nitric oxide bioavailability. *FASEB Journal* **15**, 1771-1773 (2001).

54. Yang, N.C., Jeng, K.C., Ho, W.M., Chou, S.J. & Hu, M.L. DHEA inhibits cell growth and induces apoptosis in BV-2 cells and the effects are inversely associated with glucose concentration in the medium. *J Steroid Biochem Mol Biol* **75**, 159-166 (2000).

55. Tomlinson, D.R., Willars, G.B. & Carrington, A.L. Aldose reductase inhibitors and diabetic complications. *Pharmacol Ther* **54**, 151-194 (1992).

56. Nakamura, J. et al. Polyol pathway, 2,3-diphosphoglycerate in erythrocytes and diabetic neuropathy in rats. *Eur J Pharmacol* **294**, 207-214 (1995).

57. Eaton, R.P. et al. A commentary on 10 years of aldose reductase inhibition for limited joint mobility in diabetes. *J Diabetes Complications* **12**, 34-38 (1998).

58. Parry, G.J. Management of diabetic neuropathy. *Am J Med* **107**, 27S-33S (1999).

59. Suzuki, T. et al. Characterization of polyol pathway in Schwann cells isolated from adult rat sciatic nerves. *J Neurosci Res* **57**, 495-503 (1999).

60. Cameron, N.E., Cotter, M.A., Basso, M. & Hohman, T.C. Comparison of the effects of inhibitors of aldose reductase and sorbitol dehydrogenase on neurovascular function, nerve conduction, and tissue polyol pathway metabolites in streptozotocin-diabetic rats. *Diabetologia* **40**, 271-281 (1997).

61. Asano, T., Saito, Y., Kawakami, M. & Yamada, N. Fidarestat (SNK-860), a potent aldose reductase inhibitor, normalizes the elevated sorbitol accumulation in erythrocytes of diabetic patients. *J Diabetes Complications* **16**, 133-138 (2002).

62. Hamada, Y.N., Jiro Clinical Potential of Aldose Reductase Inhibitors in Diabetic Neuropathy. *Treat Endocrinol* **3**, 245-255 (2004).

63. Rakowitz, D., Gmeiner, A. & Matuszczak, B. Discovery of Novel Aldose Reductase Inhibitors Characterized by an Alkoxy-Substituted Phenylacetic Acid Core. *Archiv der Pharmazie* **339**, 559-563 (2006).

64. Vinson, J.A., Staretz, M.E., Bose, P., Kassm, H.M. & Basalyga, B.S. In vitro and in vivo reduction of erythrocyte sorbitol by ascorbic acid. *Diabetes* **38**, 1036-1041 (1989).

65. Wang, H., Zhang, Z.-b., Wen, R.-r. & Chen, J.-w. Experimental and clinical studies on the reduction of erythrocyte sorbitol-glucose ratios by ascorbic acid in diabetes mellitus. *Diabetes Res Clin Pract* **28**, 1-8 (1995).

66. Vincent, T.E., Mendiratta, S. & May, J.M. Inhibition of aldose reductase in human erythrocytes by vitamin C. *Diabetes Res Clin Pract* **43**, 1-8 (1999).

67. Anaja, H.P. Diagnostic performance of red cell sorbitol assay in a Nigerian teaching hospital. *Clinica Chimica Acta* **262**, 1-11 (1997).

68. Shinohara, R., Ohta, Y., Yamauchi, M. & Ishiguro, I. Improved fluorometric enzymatic sorbitol assay in human blood. *Clinica Chimica Acta* **273**, 171-184 (1998).

69. Umeda, M. et al. Determination of D-sorbitol in human erythrocytes by an enzymatic fluorometric method with an improved deproteinization procedure. *Ann Clin Biochem* **38**, 701-707 (2001).

70. Cereser, C. et al. Quantitation of reduced and total glutathione at the femtomole level by high-performance liquid chromatography with fluorescence detection: application to red blood cells and cultured fibroblasts. *J Chromatogr B Biomed Sci Appl* **752**, 123-132 (2001).

71. Hood, L. & Perlmutter, R.M. The impact of systems approaches on biological problems in drug discovery. *Nat Biotechnol* **22**, 1215-1217 (2004).

72. Sprague, R.S., Ellsworth, M.L., Stephenson, A.H., Kleinhenz, M.E. & Lonigro, A.J. Deformation-induced ATP release from red blood cells requires CFTR activity. *Am J Physiol Heart Circ Physiol* **275**, H1726-1732 (1998).

CHAPTER 4: ADDRESSING ENDOTHELIUM WITH BLOOD COMPONENTS

4.1 MULTIPLE CELL TYPES WITH THE μFA: CELL-CELL INTERACTIONS

The μFA has been employed as an *in vitro* model of the *in vivo* circulation system by addressing an array of cultured bovine pulmonary artery endothelial cells (bPAECs) with underlying microfluidic channels containing various RBC samples.[1] This device has been used to demonstrate the ability to monitor cellular communication between multiple cell types to help better understand the various mechanisms of vasodilation.

Many technologies, such as those designed to perform ADMET screening, are beginning to emerge as significant tools in drug discovery[2] and systems biology[3] and motivation for continued advancements in this area is high.[4] As discussed in detail in chapter 2, the most logical way to improve the drug discovery process at the preclinical stage is to create technologies that incorporate controlled, *in vitro* designs that mimic the *in vivo* environment, allowing for the determination of molecular-mediated communication between different cell types. Importantly, there is a necessity to incorporate components of the circulation, specifically the aspect of flow-induced shear stress, to accurately mimic the system as it exists *in vivo*.

There have been many reports involving microfluidics or lab-on-a-chip technology to create *in vivo* mimics using controlled, *in vitro* platforms and many of these devices incorporate cellular components.[5-8] *In vitro* platforms have integrated various cell types including a dopaminergic cell model (PC12 cells),[9] endothelial cells,[10] and islets[11] contained within microfluidic devices. Although previous reports have described the successful direct immobilization of endothelial cells in the channels of a

microfluidic device,[10,12] the μFA first described in chapter 2, incorporates a track-etched polycarbonate (TEPC) membrane to separate the flow of RBCs from the bPAECs as illustrated in figure 4.1. The integration of the membrane allows for easily accessible wells for the culture of an endothelial cell layer with a future prospect of integrating other cell types (such as PC12 cells) as well. Thus, creating a working mimic of the blood brain barrier in a three dimensional device, enabling the communication between the circulation (in particular, RBCs) and the nervous system. In this construct, our device enables communication among tissues, not just cells.

This μFA serves as a precursor for the implementation of a microfluidic flow-based system, with already available microtitre plate technologies, to elucidate the communication between RBCs and bPAECs. The channels were fabricated such that the internal diameter closely approximates those of resistance vessels *in vivo* as RBCs were pumped through these channels. Moreover, this device was used to monitor ATP release from RBCs that were incubated in the presence or absence of iloprost (a substrate known to stimulate ATP release via a G-protein coupled receptor mechanism).[13]

4.2 ILOPROST: PROSTACYCLIN RECEPTOR-MEDIATED ATP RELEASE

The mechanism by which iloprost induces ATP release from RBCs was first proposed by Olearczyk *et al.*[14] and has been adapted for figure 4.2. Here, the binding of iloprost to the prostacyclin (PGI_2) receptor (IPR)[15-18] leads to the cascade of intracellular events within the proposed signal transduction pathway,[19-21] as also observed in the mechanical deformation-induced ATP release from RBCs, by way of G_s activation.

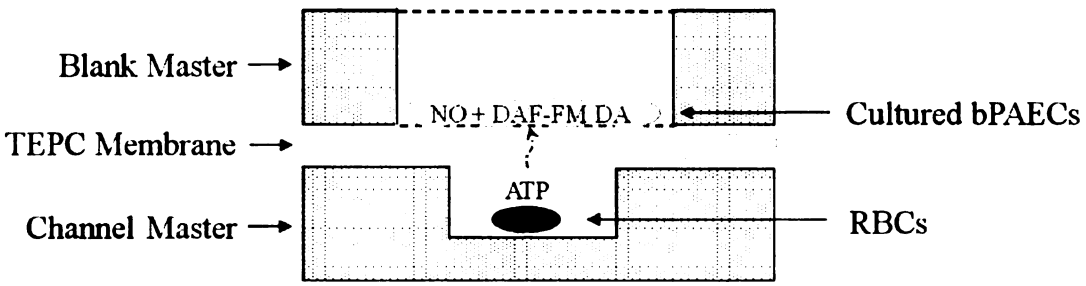

Figure 4.1 Cross-sectional illustration of the μFA used to monitor the cellular communication between RBCs transversing through the underlying microfluidic channels with the cultured bPAECs within the array-like wells. Here, RBC-derived ATP release is able to diffuse to the bPAECs though the TEPC membrane, stimulating the production of intracellular NO which is imaged using the fluorescence probe DAF-FM DA.

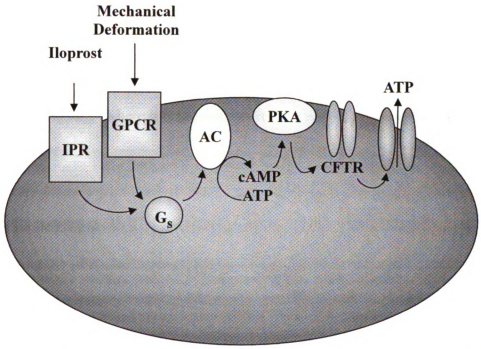

Figure 4.2 Illustration of the mechanism by which iloprost stimulates the release of ATP from the RBC through the signal transduction pathway first proposed by Olearczyk *et al.* by binding to the prostacyclin receptor (IPR) which activates the g-protein (G_s) cascading events.

Iloprost is a therapeutic agent prescribed to increase vasodilation and reduce hypertension, as a treatment for cardiovascular and circulatory disorders.[22] It is a second generation structural analog of PGI_2[23,24] that is more chemically stable and demonstrates oral effectiveness for the decrease of peripheral resistance and pulmonary arterial pressure. Our group has previously shown that incubation of a RBC sample with a 1 μM solution of iloprost for approximately 30 min will increase the amount of RBC-derived ATP release in both a flow and non-flow based system (this significance will be discussed later in detail).[25] Previously, the ATP release from RBCs was measured utilizing microbore tubing placed over a photomultiplier tube (PMT) housed within a light excluding box. More recently, as presented here, a microfluidic system has replaced the microbore tubing,[1] where it is used to mimic the resistance vessels and allow for on-chip mixing.

4.3 EXPERIMENTAL

Using the μFA, and incorporating multiple cell types, the additional ATP release from RBCs in the presence of iloprost and its subsequent effect on cultured bPAECs is demonstrated, as it pertains to the mechanism of vasodilation that occurs *in vivo*. Specifically, RBCs incubated with and without iloprost were pumped through the underlying microfluidic channels of the μFA in order to allow for the cellular communication between these RBCs and cultured bPAECs within the array-like wells *via* ATP, stimulating the intracellular production of NO. Using fluorescence spectroscopy, the intracellular NO production within the bPAECs contained in individual wells is determined.

4.3.1 DETERMINING ILOPROST-STIMULATED ATP RELEASE

In order to correctly monitor and determine the cellular communication between the RBCs and bPAECs within the μFA, and demonstrate that the intracellular endothelium-derived NO production is, in fact, due to an increased amount of pharmaceutically-induced ATP release from RBCs, the system must first be used to quantify ATP release. Illustrated in figure 4.3, a t-channel microfluidic device was used to validate that an increase in ATP release from RBCs occurs when these cells are incubated with iloprost.

Similar to the fabrication of the μFA, two layers of PDMS were used to fabricate this t-channel microfluidic device. One layer, comprised of 5:1 (elastomer base to curing agent), was obtained using a t-channel master wafer, and the other, comprised of 20:1, was a blank PDMS slab without any features. Each layer of PDMS was obtained in the same fashion as for the μFA, mixing PDMS base and curing agent, degassing the monomer, and partially baking at 75 °C for 20 min. The channel layer had inlet holes punctured through the chip using a 20 gauge luer stub adapter. A single waste port was also created using a 1/8" hollow punch. The device was completed by baking the two layers together at 75 °C for an additional 30 min, resulting in an irreversible seal between each layer.

To determine the concentration of ATP released from the RBC samples, a syringe pump is connected to the device *via* hypodermic stainless steel tubing for the introduction of flow into each inlet of the t-channel microfluidic device. The syringes deliver ATP standards ranging from 0.25-1.0 μM as well as various RBCs samples, in the presence

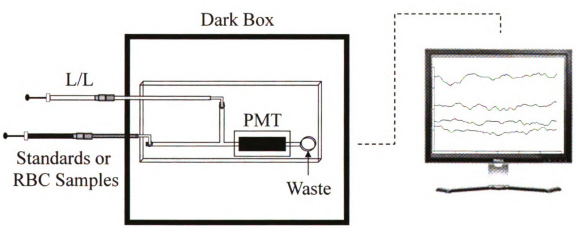

Figure 4.3 Schematic drawing of the experimental setup used, incorporating a t-channel microfluidic device with the methodology first employed by our group, to determine RBC-derived ATP release in a continuous flow system. Here the luciferin and luciferase enzymatic assay was employed, monitoring the chemiluminescence produced that is directly proportional to the concentration of ATP released from various samples.

and absence of an ATP release stimulus (iloprost) or an ATP release inhibitor (glybenclamide), through the underlying microfluidic channels. Glybenclamide is specific for inhibiting CFTR, which is involved in the signal transduction pathway responsible for the release of ATP from RBCs.[25] The ATP standard solutions were prepared from a 100 μM stock solution (27.6 mg in 500 mL DDW) in PSS. The luciferin/luciferase mixture used to measure chemiluminescence produced as a function of the ATP within the solutions was prepared by adding 5 mL of DDW to a vial containing luciferase and luciferin (FLE-50, Sigma). In order to enhance the sensitivity of the assay, 2 mg of luciferin were added to the vial.

The ATP standard solutions and the various RBC sample solutions are each pumped through one inlet, intersecting with the luciferin/luciferase that is pumped through the second inlet of the t-channel microfluidic device. The entire device was placed over a photo multiplier tube (PMT) to detect the chemiluminescence emission[26] that is produced downstream from the t-channel intersection. The current collected by the PMT from the chemiluminescence produced, is converted to voltage, measured in real time, and plotted at a rate of 10 measurements per second for 30 seconds onto a computer using LabView software (National Instruments, Austin, TX) with a program that was written in-house.

4.3.2 ENDOTHELIUM CULTURE ON THE μFA

In order to monitor the cellular communication between RBCs flowing through the microfluidic channels and the bPAECs cultured onto the membrane within the array like wells, a bPAEC cell suspension solution must first be prepared. Here, traditional cell

culture techniques are used to obtain a confluent monolayer within tissue culture flasks from which cells are harvested to prepare a cell suspension that can be pipetted into each of the wells within the μFA. As shown in figure 4.4 this cell solution is obtained by first washing a T-75 cell culture flask with 7 mL HEPES (4-(2-hydroxyethyl)-1-piperazineethanesulfonic acid, pH 7.4) to add buffering capacity to protect cell receptors during harvesting. This solution is aspirated off prior to the addition of 5 mL trypsin/EDTA solution (containing 0.5 g/L of trypsin (1:250) and 0.2 g/L of EDTA•4Na in Hanks' Balanced Salt Solution), which will cleave the peptide chains that are involved in cell attachment to the flask. The trypsin is allowed to sit on the cells for approximately 3 min, followed by the addition of 9 mL of trypsin neutralizing solution (sterile, phosphate-buffered saline solution (1x) containing calf serum as a trypsin inhibitor) is added to the flasks, halting the action of the trypsin.

Vigorous pipetting of the solution within the flask (trypsin and the neutralizing solution) is used to ensure the cells have become detached from the flask and are suspended in the solution. This suspension is centrifuged at 2200 rpm for 5 min at 25 °C, the supernatant is aspirated off and the remaining pellet of cells is resuspended in 1 mL endothelial growth media, (Clonetics® EGM® MV Microvascular Endothelial Cell Growth Medium with 5% fetal bovine serum) that has been equilibrated at 37°C and 5% CO_2, with repeated pipetting to ensure a homogeneous cell solution. This cell solution has been determined to contain on average approximately 1.0×10^8 cells/mL.

Prior to the introduction of the suspended cell solution into the wells of the μFA, 10 μL of a 100 μg/mL fibronectin solution is pipetted into each well, providing a fibronectin coating to promote cell adhesion to the membrane. The fibronectin solution is

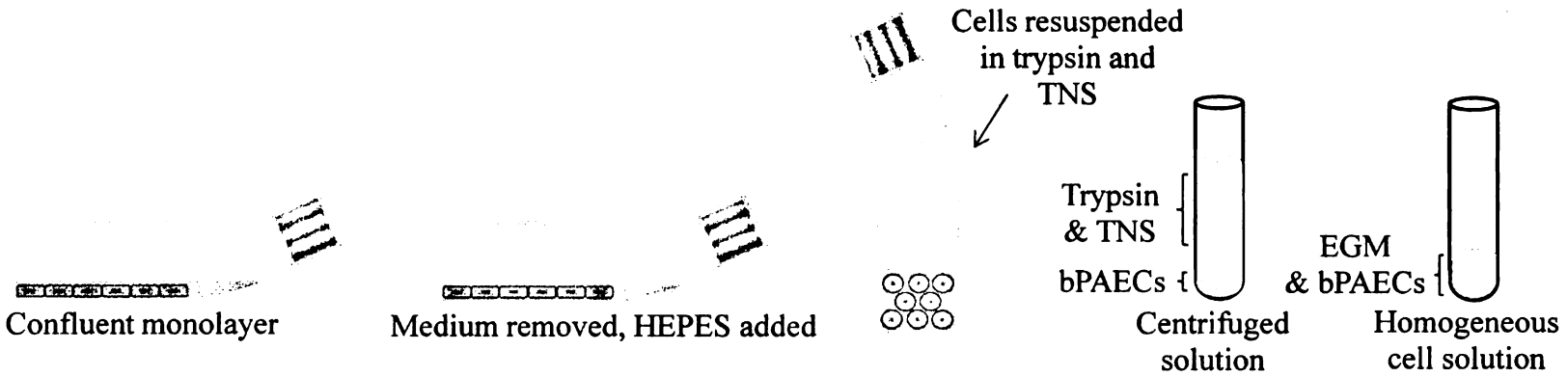

Figure 4.4 Schematic illustration of the method employed to prepare a cell suspension for the culture of bPACEs within the μFA. Here key steps are highlighted: removal of the endothelial growth medium, replaced with HEPES (4-(2-hydroxyethyl)-1-piperazineethanesulfonic acid) for the added buffering capacity during cell culture. The cells are removed from the flask by incubation with trypsin/EDTA solution followed by trypsin neutralizing solution (TNS) with vigorous pipetting. This solution is centrifuged at 2200 rpm for 5 min at 25 °C, upon the removal of the supernatant, the bPAEC pellet is resuspended in equilibrated media with repeated pipetting to obtain a homogenous cell solution.

prepared from a 5 mg vial of lyophilized powder that is diluted to obtain a 1000 μg/mL stock solution in DDW. This stock solution is stored as individual aliquots prior to diluting to the working solution in phosphate buffered saline (PBS). The PBS (within the fibronectin solution that is contained within each well) is evaporated by placing the device in a standard cell culture hood, providing increase air flow over the device. Subsequent serilization is performed by exposure to UV light for 15 min within the same cell culture hood.

The cell suspension described above is then pipetted into each well and allowed to incubate for one hour in a cell incubator at 37°C and 5% CO_2 to promote the adhesion of the cells to the surface. At which point, the media is changed by pipetting off the solution of each well and replacing it with media that has equilibrated to 37°C and 5% CO_2, taking care not to disturb the adhered cells. The cells are returned to the incubator for an additional two hrs, allowing the cells time to become confluent on the membrane.

4.3.3 FLUORESCENCE DETERMINATION OF INTRACELLULAR NO

Once the cells have become confluent within the wells of the μFA, they are then ready to be used for the determination of intracellular NO production as various stimuli are delivered through the underlying microfluidic channels. First, to ensure that the cells have sufficient substrate for the production of NO by NOS (i.e., that there is no limiting reactant), an equilibrated solution of 5 mM L-arginine (0.0044 g in 5 mL Hank's Balanced Salt Solution (containing in mM, 1.26 $CaCl_2$, 0.493 $MgCl_2 \cdot 6H_2O$, 0.407 $MgSO_4 \cdot 7H_2O$, 5.33 KCl, 0.441 KH_2PO_4, 4.17 $NaHCO_3$, 137.93 NaCl, 0.338 Na_2HPO_4, and 0.556 Dextrose with a final pH of 7.4)) is first incubated within each well at 37°C

and 5% CO_2 for 30 min. The solution is then removed and replaced with 100 μM DAF-FM DA (4-amino-5-methylamino-2',7'-difluorofluoroescein diacetate), an intracellular fluorescence probe for NO with excitation and emission wavelengths of 495 nm and 515 nm, respectively. DAF-FM DA, as illustrated in figure 4.5 is able to permeate the cell, after which diacetate groups are cleaved by an esterase, trapping the charged DAF-FM fluorescence probe within the cell. Upon reaction with NO, the DAF-FM forms the benzotriazole derivative that is highly fluorescent. The DAF-FM DA was prepared as a 5 mM stock by dissolving 1 mg within 20 μL anhydrous DMSO and making a subsequent dilution to 100 μM in HBSS, which was equilibrated to 37°C before incubation with the bPAECs within each well. The μFA was placed in the incubator at 37°C and 5% CO_2 for 30 min, at which point the DAF-FM DA is subsequently removed from the wells and replaced with equilibrated HBSS prior to fluorescence imaging.

This device is then used to monitor the production of intracellular NO within the bPAECs cultured in the wells above, as ATP diffuses from various RBC solutions that are pumped through the underlying microfluidic channels for 30 min. An Olympus IX71 inverted fluorescence microscope (Center Valley, PA) fitted with a mercury-arc lamp and a fluorescein isothiocyanate (FITC) filter cube (providing excitation and emission wavelengths of 470 nm and 525 nm, respectively) was used to image each well. The images were obtained at 20x magnification and shown in figure 4.6. After capturing the fluorescence images of the array, the pixel intensities were measured for each individual well, which is directly dependant on the concentration of NO produced within the bPAECs of each well.

c

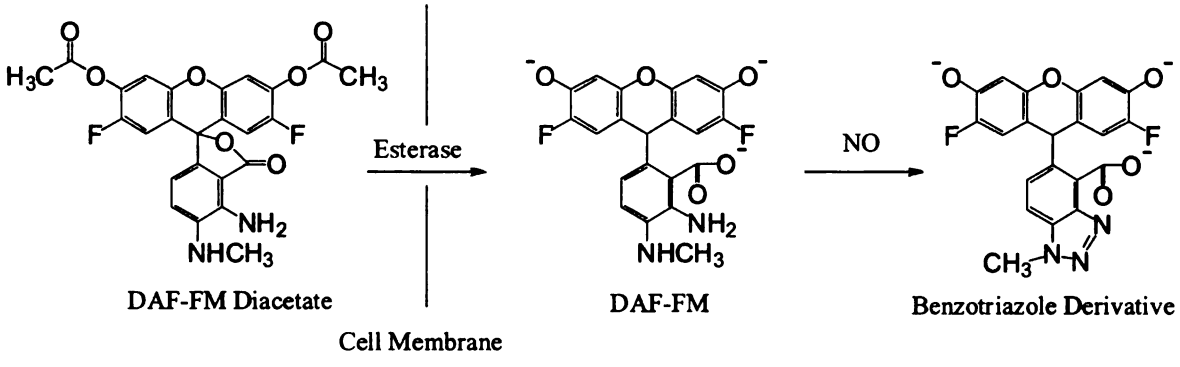

Figure 4.5 Mechanism detailing the process by which 4-amino-5-methylamino-2'7'-difluorofluoroescein (DAF-FM) diacetate enters the cell, whereby allowing for the intracellular detection of NO production. Here, the cleavage of the diacetate groups from DAF-FM DA occurs by an esterase as the molecule enters the cell, further reaction of DAF-FM with NO forms the fluorescent benzotriazole derivate with excitation and emission wavelengths of 495 nm and 515 nm, respectively.

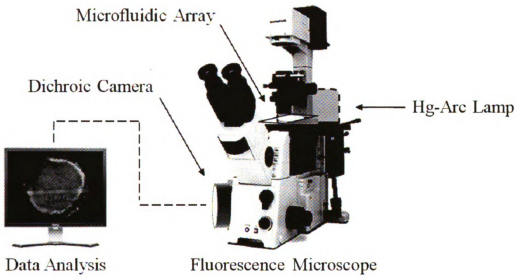

Figure 4.6 Fluorescence microscopy experimental setup used to monitor the intracellular production of NO within cultured bPAECs contained within the wells of the μFA as a result from ATP released from the RBCs transvering through the underlying microfluidic channels in this flow-based system. Here, the mercury arc (Hg-Arc) lamp provides the light that is selectively filtered by a FITC filter cube for the excitation of the benzotrazole derivative of DAF-FM and NO which is then imaged using a dichroic camera and Microsuite computer software.

To demonstrate the potential of such a multicellular device to mimic *in vivo* stimulation of NO by RBC-derived ATP, RBCs were incubated in the presence and absence of iloprost. A 100 μM iloprost solution was prepared by diluting 36.1 μL of the 13.87 mM stock solution (Cayman Chemical, Ann Arbor, MI) to 5 mL in PBS which is then diluted to a 1 μM working solution in PBS. Here, as illustrated in figure 4.7, two RBC samples are prepared with and without iloprost to determine the fluorescence intensity increase within the cultured bPAECs, as a function of NO production, due to an increased RBC-derived ATP release. Both RBC samples were prepared from the washed RBCs as 7% hematocrit solutions, in one of these samples, a final concentration of 1 μM iloprost was present in the PSS prior to the addition of RBCs. These samples were allowed to incubate at room temperature for 30 min prior to pumping through the underlying microfluidic channels of the μFA that contained bPAECs.

In order to effectively demonstrate that the increase in intracellular NO is in fact due to the increased ATP release from the RBCs flowed through the underlying microfluidic channels, and not due to cell lysis or the action of iloprost on the bPAECs themselves, various RBC samples and controls were pumped through the underlying channels. These solutions, as illustrated in figure 4.8 consisted of RBCs at 7% hematocrit (row 3), RBCs incubated with 1 μM iloprost (row 4), RBCs incubated with 1 mM glybenclamide (row 5), RBCs incubated with 1 mM glybenclamide and 1 μM iloprost (row 6), and two controls (buffer (row 1) and 1 μM iloprost (row 2)) were pumped through the underlying microfluidic channels. The 10 mM glybenclamide stock solution was prepared by combining 0.049 g with 2 mL 0.1 M NaOH, and 7.94 mL dextrose solution (1 g dextrose in 20 mL DDW) and heating to 52 °C until dissolved with

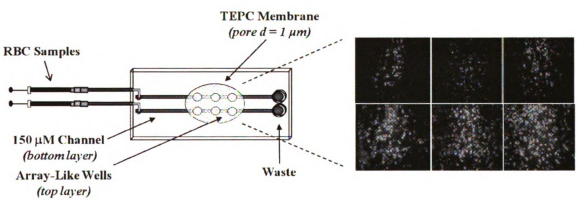

Figure 4.7 Initial microfluidic array used to monitor the fluorescence intensity corresponding to the intracellular production of NO as RBCs with and without the incubation of 1 μM iloprost are pumped through the underlying microfluidic channels.

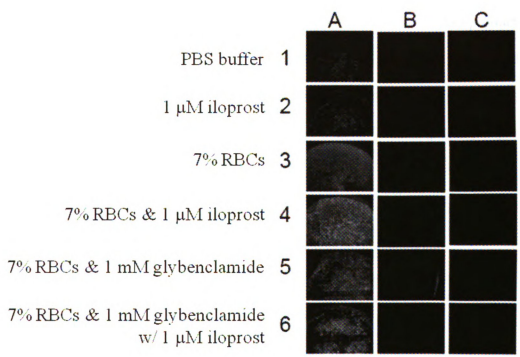

Figure 4.8 Fluorescence images of the six channel μFA used for the determination of intracellular NO resulting from the ATP released from various RBC and control samples. Specifically, columns A and B contain cultured bPAECs with and without the presence of intracellular DAF-FM DA, respectively, while column C contains cell-free wells.

stirring. This solution was added to the PSS to create the 7% RBC solutions flowed through channels five and six.

The 18 wells that comprised the device were prepared in the absence (column C) and presence (columns A and B) of bPAECs, where only the cells in column A were incubated with the DAF-FM DA probe for the intracellular fluorescence determination of NO production. After flowing the control and RBC samples through the underlying microfluidic channels of the μFA for 30 min, the fluorescence images corresponding to each well were taken and the increase in intensity (corresponding to the NO production by bPAECs) were analyzed. The wells in column B did not contain the DAF-FM DA fluorescence probe in order to eliminate the possibility of any type of fluorescence signal that might be due to the cells alone. Additionally, the wells comprising column C were absent of cells in order to demonstrate that no fluorescence was observed from the membrane alone.

4.4 RESULTS AND DISCUSSION: MULTICELLULAR COMMUNICATION

Initially, iloprost was shown to increase the RBC-derived ATP release using a flow-based microfluidic device and the luciferin/luciferase chemiluminescence detection method. Figure 4.9 shows the raw data that was collected for the real-time determination of ATP within a control 1 μM iloprost solution, and 7% RBC solution with and without the addition of 1 μM iloprost and 250 nM glybenclamide. Iloprost alone flowing through the microfluidic device resulted in an emission signal that is equilivent to that of buffer alone mixing with the luciferin/luciferase mixture. In the presence of a 7% hematocrit of RBCs, the measured ATP value was 0.27 ± 0.04 μM. However, as expected, RBCs

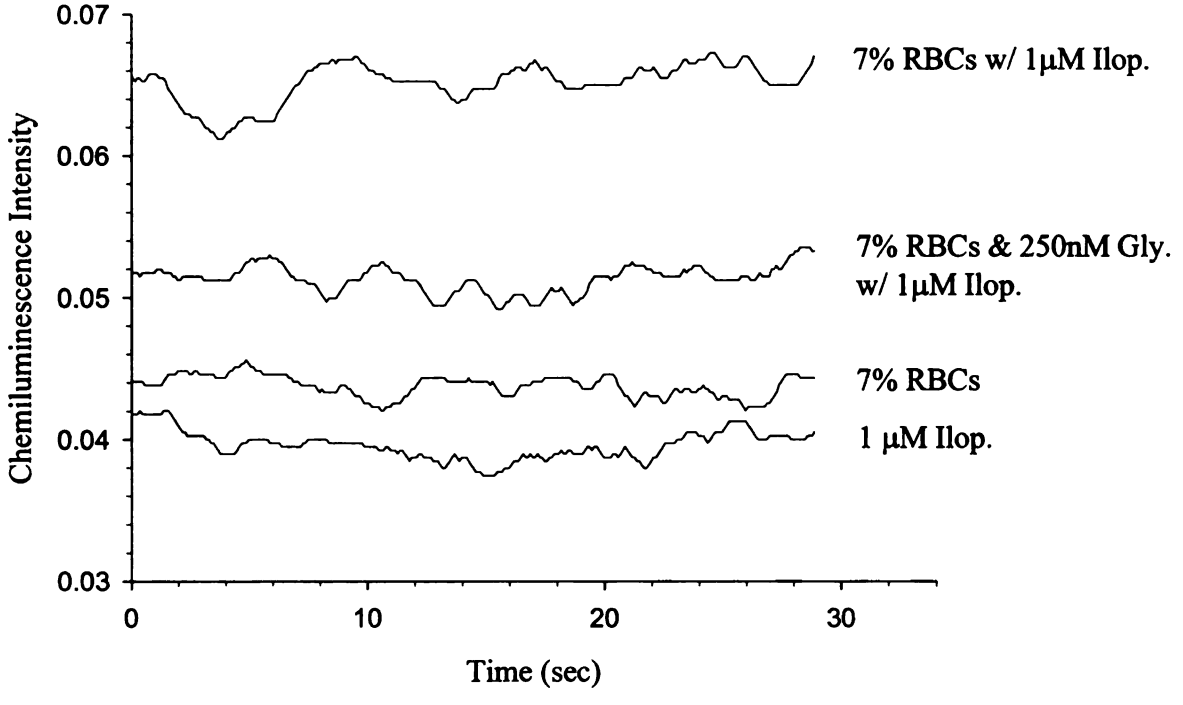

Figure 4.9 Raw data obtained for the real-time analysis of the chemiluminesence produced as a function of ATP concentration from 1 μM iloprost, 7% RBCs, 7% RBCs with 250 nM glybenclamide and 1 μM iloprost, and 7% RBCs with 1 μM iloprost by placing the microfluidic t-channel chip on a PMT housed within a dark box.

incubated in 1 μM iloprost released ATP at a concentration of 0.95 ± 0.18 μM, a value that dropped to 0.29 ± 0.14 μM in the presence of a sample containing 250 nm glybenclamide, an inhibitor of ATP release from RBCs. As illustrated in figure 4.10, if the signal was due to cellular lysis upon the addition of iloprost, glybenclamide would not be able to reduce the RBC-derived ATP chemiluminescence produced.

Figure 4.11 represents the fluorescence intensity resulting from the intracellular NO production in response to pumping a 7% RBC sample, in the presence and absence of 1 μM iloprost, through the underlying channels for 30 min. The increases in fluorescence intensity due to endothelium-derived NO production were determined to be 23.0 ± 3.5 and 16.5 ± 1.0 where the values reported are the average intensity and standard deviation (n = 3 wells for each sample). The difference in fluorescence intensities between samples is statistically different ($p < 0.005$).

The data for the final demonstration of iloprost-induced RBC-derived ATP release resulting in NO production within the cultured bPAECs are shown in figure 4.12. The results for column A for each of the six channels containing PBS buffer, 1 μM iloprost, 7% RBCs, RBCs with 1 μM iloprost, RBCs with 1 mM glybenclamide, and RBCs with both 1 mM glybenclamide and 1 μM iloprost are compiled. The fluorescence intensities are presented as the average pixel intensity of the five integrated areas of each acquired image. Note the significant increase in fluorescence intensity due to endothelium-derived NO in the presence of the RBCs (A3) and the RBCs incubated with iloprost (A4). The difference in fluorescence intensity between samples containing the RBCs in the absence (A3) and presence (A4) of iloprost are statistically different from the other rows. There is also a difference in the intensities of rows 3 and 4 ($p = 0.005$).

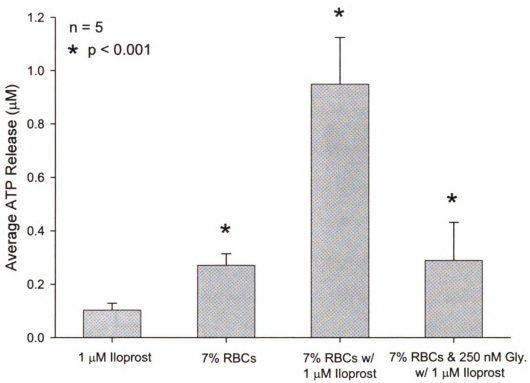

Figure 4.10 Data representation for the quantitative determination of ATP released from 7% RBCs in the presence and absence of 1 μM iloprost and 250 nM glybenclamide using the t-channel microfluidic chip and the luciferin and luciferase based enzymatic assay. A control sample of 1 μM iloprost alone without the presence of RBCs is also plotted, demonstrating the background chemiluminescence. Average concentrations of ATP in micromolar amounts are reported where the error is represented by the SEM. The reduction in ATP release due to the addition of glybenclamide (Gly.) is statistically

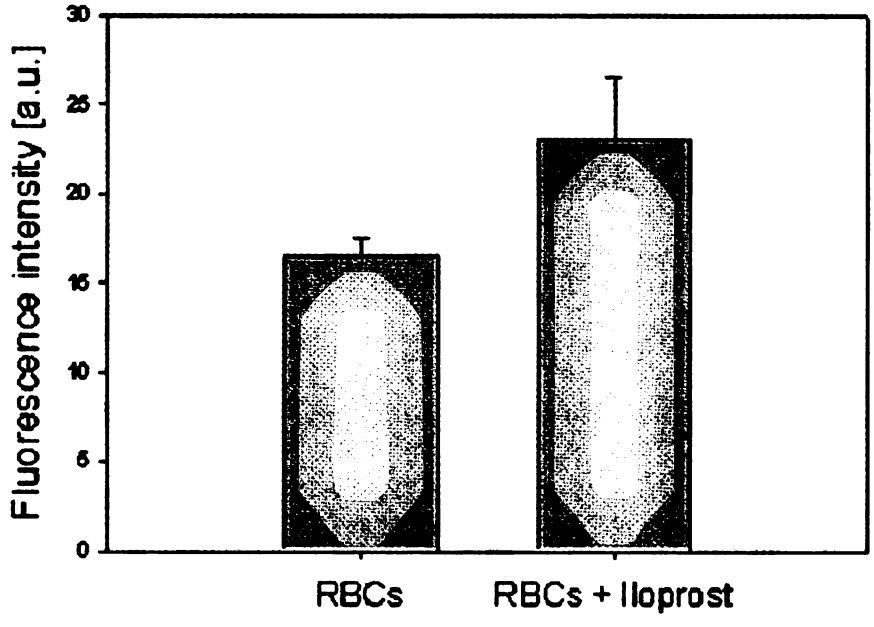

Figure 4.11 Representative data for the initial determination of intracellular NO production within bPAECs that are cultured within the wells of a two channel μFA through which a 7% RBC sample with and without the incubation of a 1 μM iloprost solution were flowed. The values reported are the average intensity and SEM (n = 3 wells for each sample). The difference in fluorescence intensity between samples incubated in the presence and absence of iloprost are statistically different ($p < 0.005$)

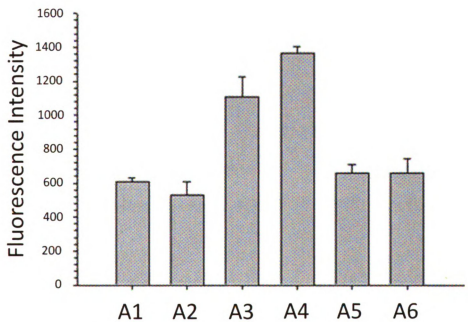

Figure 4.12 Data representing the intracellular NO production within bPAECs cultured in the wells of a six channel μFA, here samples were flowed through the underlying microfluidic channels for 30 min prior to obtaining fluorescence images. The samples included PBS buffer, 1 μM iloprost, 7% RBCs, RBCs with 1 μM iloprost, RBCs with 1 mM glybenclamide, and RBCs with both 1 mM glybenclamide and 1 μM iloprost (A1-A6 respectively). The difference in fluorescence intensity between samples containing the RBCs in the absence (A3) and presence (A4) of iloprost are statistically different from the other rows. There is also a difference in the intensities of rows 3 and 4 ($p = 0.005$).

These data suggest that the efficacy of iloprost occurs only through the interaction with the RBCs.

Such data would not have been found in classic *in vitro* studies containing only the iloprost and endothelial cells alone, as the mechanism of action is RBC mediated,[14,27] thus verifying the potential usefulness of the device containing underlying microfluidic channels that incorporate blood flow. Importantly, the device wells are addressable by a continuous flow of RBCs so that assays for drug action, drug inhibition, and control studies can be performed simultaneously using the same RBC source. In the future, the throughput of this approach could be increased by employing a device having a larger array of wells that are measured using a plate reader. As described in chapter 2, it is anticipated that the advances developed with this three dimensional device will successfully bridge results obtained with traditional *in vitro* studies to those in the *in vivo* state of drug discovery, thereby reducing the number of trials that fail at the later stage of clinical trials.

REFERENCES

1. Genes, L.I., Tolan, N.V., Hulvey, M.K., Martin, R.S. & Spence, D.M. Addressing a vascular endothelium array with blood components using underlying microfluidic channels. *Lab Chip* **7**, 1256-1259 (2007).

2. Dittrich, P.S. & Manz, A. Lab-on-a-chip: microfluidics in drug discovery. *Nat Rev Drug Discov* **5**, 210-218 (2006).

3. Breslauer, D.N.L., P. J.; Lee, L. P. Microfluidics-based systems biology. *Mol BioSyst* **2**, 97–112 (2006).

4. Cohen, C.M. A path to improved pharmaceutical productivity. *Nat Rev Drug Discov* **2**, 751-753 (2003).

5. Khademhosseini, A. et al. Cell docking inside microwells within reversibly sealed microfluidic channels for fabricating multiphenotype cell arrays. *Lab Chip* **5**, 1380-1386 (2005).

6. Shin, M. et al. Endothelialized Networks with a Vascular Geometry in Microfabricated Poly(dimethyl siloxane). *Biomed Microdevices* **6**, 269-278 (2004).

7. Takayama, S. et al. Laminar flows: Subcellular positioning of small molecules. *Nature* **411**, 1016-1016 (2001).

8. Aaron Sin et al. The Design and Fabrication of Three-Chamber Microscale Cell Culture Analog Devices with Integrated Dissolved Oxygen Sensors. *Biotechnol Prog* **20**, 338-345 (2004).

9. Li, M.W., Spence, D.M. & Martin, R.S. A microchip-based system for immobilizing PC 12 cells and amperometrically detecting catecholamines released after stimulation with calcium. *Electroanalysis* **17**, 1171-1180 (2005).

10. Spence, D.M., Torrence, N.J., Kovarik, M.L. & Martin, R.S. Amperometric determination of nitric oxide derived from pulmonary artery endothelial cells immobilized in a microchip channel. *Analyst* **129**, 995-1000 (2004).

11. Roper, M.G., Shackman, J.G., Dahlgren, G.M. & Kennedy, R.T. Microfluidic Chip for Continuous Monitoring of Hormone Secretion from Live Cells Using an Electrophoresis-Based Immunoassay. *Anal Chem* **75**, 4711-4717 (2003).

12. Oblak, T.D.A., Root, P. & Spence, D.M. Fluorescence Monitoring of ATP-Stimulated, Endothelium-Derived Nitric Oxide Production in Channels of a Poly(dimethylsiloxane)-Based Microfluidic Device. *Anal Chem* **78**, 3193-3197 (2006).

13. Olearczyk, J.J., Ellsworth, M.L., Stephenson, A.H., Lonigro, A.J. & Sprague, R.S. Nitric Oxide Inhibits ATP Release from Erythrocytes. *J Pharmacol Exp Ther* **309**, 1079-1084 (2004).

14. Olearczyk, J.J., Stephenson, A.H., Lonigro, A.J. & Sprague, R.S. Receptor-mediated activation of the heterotrimeric G-protein Gs results in ATP release from erythrocytes. *Med Sci Monit* **7**, 669-674 (2001).

15. Charles Willems, Herbert V. Stel, Willem G. van Aken & Jan A. van Mourik Binding and inactivation of prostacyclin (PGI₂) by human erythrocytes. *Br J Haematol* **54**, 43-52 (1983).

16. Dutta-Roy, A.K. & Sinha, A.K. Binding of prostaglandin E1 to human erythrocyte membrane. *Biochim. Biophys. Acta, Biomembr.* **812**, 671-678 (1985).

17. Sprague, R.S. et al. Prostacyclin Analogs Stimulate Receptor-Mediated cAMP Synthesis and ATP Release from Rabbit and Human Erythrocytes. *Microcirculation* **15**, 461 - 471 (2008).

18. Adderley, S.P. et al. Iloprost- and isoproterenol-induced increases in cAMP are regulated by different phosphodiesterases in erythrocytes of both rabbits and humans. *Am J Physiol Heart Circ Physiol* **296**, H1617-1624 (2009).

19. Davies, P.F. Flow-mediated endothelial mechanotransduction. *Physiol Rev* **75**, 519-560 (1995).

20. Sprague, R.S., Stephenson, A.H., Bowles, E.A., Stumpf, M.S. & Lonigro, A.J. Reduced expression of Gi in erythrocytes of humans with type 2 diabetes is associated with impairment of both cAMP generation and ATP release. *Diabetes* **55**, 3588-3593 (2006).

21. Sprague, R.S., Stephenson, A.H. & Ellsworth, M.L. Red not dead: signaling in and from erythrocytes. *Trends Endocrinol Metab* **18**, 350-355 (2007).

22. Skuballa, W. & Vorbrueggen, H. Synthesis of ciloprost (ZK 36 374): a chemically stable and biologically potent prostacyclin analog. *Adv Prostaglandin Thromboxane Leukot Res* **11**, 299-305 (1983).

23. Stoll, F. et al. Pharmacophore definition and three-dimensional quantitative structure-activity relationship study on structurally diverse prostacyclin receptor agonists. *Mol Pharmacol* **62**, 1103-1111 (2002).

24. Ruan, K.-H. & Dogne, J.-M. Implications of the molecular basis of prostacyclin biosynthesis and signaling in pharmaceutical designs. *Curr Pharm Des* **12**, 925-941 (2006).

25. Carroll, J.S., Ku, C.-J., Karunarathne, W. & Spence, D.M. Red Blood Cell Stimulation of Platelet Nitric Oxide Production Indicated by Quantitative Monitoring of the Communication between Cells in the Bloodstream. *Anal Chem* **79**, 5133-5138 (2007).

26. Price, A.K., Fischer, D.J., Martin, R.S. & Spence, D.M. Deformation-Induced Release of ATP from Erythrocytes in a Poly(dimethylsiloxane)-Based Microchip with Channels That Mimic Resistance Vessels. *Anal Chem* **76**, 4849-4855 (2004).

27. Olearczyk, J.J., Stephenson, A.H., Lonigro, A.J. & Sprague, R.S. Heterotrimeric G protein Gi is involved in a signal transduction pathway for ATP release from erythrocytes. *Am J Physiol Heart Circ Physiol* **286**, H940-945 (2004).

CHAPTER 5: FUTURE DIRECTION AND APPLICATIONS

5.1 μFA: FUTURE APPLICATIONS

Another objective of this work was to demonstrate that hypoxia-induced release of ATP was capable of stimulating endothelium-derived NO using this μFA. Recent studies in our group have demonstrated that hypoxia results in, what presents itself as, mechanical deformation-induced ATP release from RBCs.[1] Hemoglobin, a metalloprotein, is attached to the cellular membrane of the RBC and upon conformational change from oxygenated (R-state) to dexoygenated (T-state) will elicit ATP release in both a flow and non-flow system. Hypoxia-induced ATP release from the RBC can be inhibited with prior stiffening of the cell membrane by incubation with diamide, a known cell stiffener[2] as well as with the incubation of glybenclamide, which has been shown to inhibit CFTR.[3] This suggests that the mechanism by which hypoxia induces RBC-derived ATP release must be of a similar mechanism involving the mechanical deformation-induced signal transduction pathway previously discussed.[4-12]

Separately, previous studies in our group have found that there is an increase in the concentration of ATP release from RBCs of both diabetics and, to a greater extent, healthy controls, when incubated with metal activated C-peptide. [13] For years C-peptide was presumed to have little to no biological activity[14] which has been thought to be due to the lack of metal activation. Thus, the ability of metal-activated C-peptide to restore the ATP release from RBCs obtained from type 2 diabetics, to the normal levels associated with RBC from healthy controls, demonstrates the physiologically-relevant prospect of improving blood flow and reducing the complications associated with

diabetes. Here, it was also demonstrated that C-peptide will also increase the glucose uptake into RBCs through GLUT1, the primary glucose transporter in the cell, and is thought to enhance glycolysis which is the primary route of ATP production.

One of the main advantages to incorporating flow into microtitre plate technology is the ability to more realistically mimic the circulation system found *in vivo* and simulate the shear-forces that RBCs are subjected to. Demonstration of the ability of hypoxia- and C-peptide-induced RBC-derived ATP release to stimulate the intracellular production of NO within the bPAECs cultured within the array-like wells of the μFA is presented here. As previously discussed, this NO production plays a physiologically-relevant role in the process of vasodilation of the smooth muscle surrounding the vascular system,[4,10,11,15-22] and ultimately, the ability of the circulation system to deliver O_2 to deprived tissue.

Another application for this μFA is the ability to monitor the mechanism by which pentoxyfilline or trental, in contrast to iloprost, requires the shear aspect of flow to elicit RBC-derived ATP release.[3] Trental has been demonstrated to reduce the complications associated with nephropathy in diabetic patients and is thought to serve as an anti-inflammatory agent[23-26] by either suppressing oxygen radial formation, preventing lipid peroxidation, or scavenging radicals that are formed. The combination of trental and iloprost on the effect of RBC-derived ATP release in a non-flow system is demonstrated, lending to future work possible in the evaluation of the multicellular effect of stimulating endothelium NO and ultimately vasodilation.

5.2 EXPERIMENTAL

Three different applications of the μFA, specifically the application for cellular communication between RBCs and bPAECs cultured within the array-like wells by monitoring ATP-derived intracellular production as it pertains to vasodilation is presented. Also, preliminary work illustrating the ability to determine the mechanisms of action of two therapeutics, trental and iloprost are also discussed demonstrating that without employing accurate *in vitro* technologies trental could be mistakenly determined ineffective.

5.2.1 HYPOXIA-INDUCED ATP RELEASE: EFFECT ON NO

Employing the μFA, the effect of hypoxia-induced RBC-derived ATP release on the intracellular production of NO within the bPAECs cultured in the array-like wells is determined using fluorescence microscopy. The samples investigated include 3.5% RBCs, RBC incubated in hypoxic buffer, and RBCs initially incubated with 100 and 200 μM diamide and 20 and 40 μM diamide separately, prior to incubation in the hypoxic buffer. In order to demonstrate that the RBC-derived ATP release in response to hypoxia is dependent upon the signal transduction pathway previously detailed here, RBCs are incubated with diamide, a known cell stiffener, and niflumic acid, previously demonstrated to inhibit CFTR.[5] These solutions are increased from 100 to 200 μM for diamide and from 20 to 40 μM for niflumic acid to further illustrate the ability to inhibit the RBC-derived ATP release that is responsible for the intracellular NO production within the bPAECs of each well.

The RBCs were first prepared in PSS that contained the various concentrations of either diamide or niflumic acid. The niflumic acid was allowed to incubate with the cells

for 30 min, where as the diamide was only incubated for 10 min prior to centrifuging, at 500 x g at 4 °C for 3 min, for the following resuspension in hypoxic buffer. These times were chosen to maximize the effect of ATP inhibition, as previously reported, the RBC is able to begin to recover from the stiffening of the cell due to diamide within approximately 30 min at which point the concentration of ATP release begins to return to normal.[10] In order to introduce the RBCs in a hypoxic environment Oxyrase® was used to enzymatically remove the O_2 from the PSS and here 5 mL of PSS with 1.5 mL of Oxyrase® was added to each of the centrifuged RBCs.

The μFA was prepared as previously discussed in chapter 4, briefly, bPAECs were cultured within the array of wells which were then subsequently incubated with a 5 mM L-arginine solution prior to the incubation with 100 μM DAF-FM DA, a fluorescence probe for intracellular NO production, which was removed and replaced with HBSS prior to fluorescence imaging. Figure 5.1 illustrates the fluorescence image taken of the entire six channel device as various samples are flowed through the underlying microfluidic channels for 30 min at a flow rate of 1.0 μL/min. The Olympus MVX stereomicroscope (Center Valley, PA) fitted with a mercury-arc lamp and FITC filter cube, allowing for excitation and emission wavelengths of 470 nm and 525 nm was employed to obtain fluorescence image of the array of 18 wells. As before, the fluorescence intensities were imaged using Microsuite software and the pixel intensities were averaged for each of the three wells addressed by a single channel.

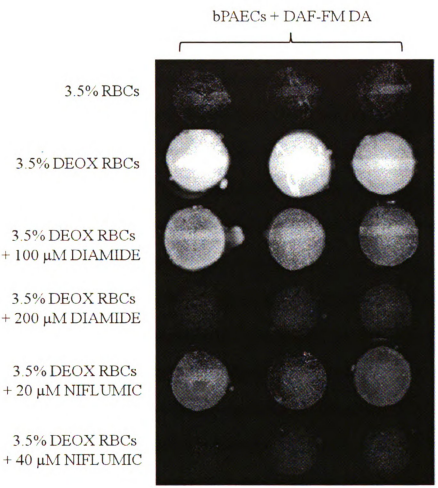

Figure 5.1 Fluorescence image of the six-channel μFA for the determination of intracellular NO production within the bPACEs as a result of hypoxia. Here, the RBC-derived ATP release from each sample stimulates the production of NO which is detected using DAF-FM DA and the Olympus MVX stereomicroscope fitted with a mercury-arc lamp for excitation and a FITC filter cube with excitation and emission wavelengths of 470 nm and 525 nm respectively.

5.2.2 C-PEPTIDE: RBC-MEDIATED NO PRODUCTION

The same μFA for the determination of intracellular NO production within bPAECs cultured within the array-like wells is used to demonstrate that an additional RBC-derived ATP release due to metal-activated C-peptide may play a vital role in increasing vasodilation *in vivo*. The samples examined were comprised of 7% RBCs, RBCs incubated with metal-activated C-peptide, with C-peptide alone and metal alone, with 1 mM glybenclamide, and finally, with 1 mM glybenclamide and metal-activated C-peptide. The solution containing 1 mM glybenclamide was prepared first, providing inhibition of CFTR prior to the incubation with metal-activated C-peptide. As discussed in chapter 4, the 10 mM glybenclamide stock solution was prepared by combining 0.049 g with 2 mL 0.1 M NaOH, and 7.94 mL dextrose solution (1 g dextrose in 20 mL DDW) and heating to 52 °C until dissolved with stirring. This solution was added to the PSS that was used to create the 7% RBC solution for subsequent incubation with metal-activated C-peptide.

Recent work in our lab has shown that the relevant metal for the activation of C-peptide resulting in an increased ATP release, is Zn^{2+} and its preparation allowing for non-competitive interaction with the peptide is necessary. An 80 μM stock solution of Zn^{2+} is prepared by dissolving 0.0055 g in 500 mL DDW. In order to obtain an 83 μM stock solution of C-peptide, 0.25 g of human C-peptide (American Peptide, Sunnyvale, CA, USA) is dissolved in 100 mL DDW which is then used to make subsequent dilutions within RBCs. To prevent competitive binding events between the peptide and other metals or ions, the Zn^{2+} and C-peptide are first combined in DDW before combining with PSS and RBCs. The final concentrations of each Zn^{2+} and C-peptide are 10 nM in PSS

which is incubated with 7% RBCs for 6 hrs prior to pumping through the underlying microfluidic channels of the μFA.

The fluorescence image, figure 5.2, was obtained by imaging the entire six channel device after each of the solutions were flowed through the underlying microfluidic channels for 30 min at a flow rate of 1.0 μL/min. The same Olympus MVX stereomicroscope (Center Valley, PA) fitted with a mercury-arc lamp and FITC filter cube, allowing for excitation and emission wavelengths of 470 nm and 525 nm was employed. As before, the fluorescence intensities were imaged using Microsuite software and the pixel intensities were averaged for each of the three wells addressed by a single channel.

5.2.3 REQUIRED ASPECT OF SHEAR: TRENTAL VS. ILOPROST

Our group has previously examined the necessity of a flow system as it applies to drug efficacy and mechanisms of action; specifically demonstrating the required aspect of shear-induced deformation for trental to increase RBC-derived ATP release.[3] Four samples consisting of 3.5% hematocrit RBCs alone, RBCs incubated with 5 μM trental, 1 μM iloprost and the combined incubation with both 5 μM trental and 1 μM iloprost. The trental stock solution is prepared as a 100 μM solution where 0.0028 g are dissolved in 10 mL PSS which is subsequently diluted to a 10 μM solution prior to the addition to the washed RBCs with a final concentration of 5 μM in PSS which is allowed to incubate for 30 min. The iloprost solution is prepared as previously described in chapter 4, where a 100 μM stock solution in PBS is diluted to 1 μM with 3.5% RBCs in PSS which is allowed to incubate for 30 min. For the solution containing both trental and iloprost, a

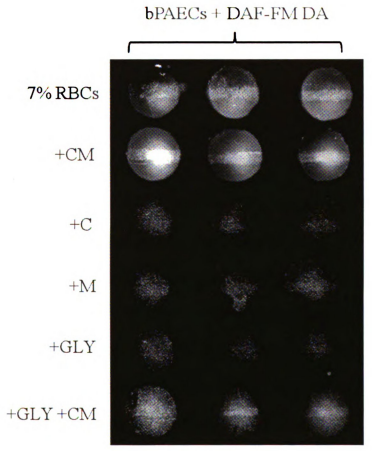

Figure 5.2 Fluorescence image of the six-channel μFA used to monitor the intracellular production of NO within the bPACEs cultured within the wells of the device due to the incubation of RBCs with C-peptide. Here, the RBC-derived ATP release from each sample stimulates the production of NO which is detected using DAF-FM DA and the Olympus MVX stereomicroscope fitted with a mercury-arc lamp for excitation and a FITC filter cube with excitation and emission wavelengths of 470 nm and 525 nm respectively.

solution containing 5 μM trental and 3.5% RBCs are incubated for 30 min to which the volume required for a final concentration of 1 μM iloprost solution is incubated for an additional 30 min, thus, allowing trental to act on the RBCs prior to the addition of iloprost.

Each of these solutions (100 μL) is combined with the luciferin/luciferase solution (100 μL) in a cuvette and placed over a PMT housed within a dark box, as illustrated in figure 5.3. A 100 μM stock solution of ATP was prepared by adding 0.0551 g of ATP to 1000 mL of DDW, subsequently, ATP standards with concentrations ranging between 0 and 1.5 μM were then prepared in PSS from the stock and used to obtain a standard working curve. To prepare the luciferin/luciferase mixture used to measure the ATP by chemiluminescence, 5 mL of DDW were added to a vial containing luciferase and luciferin. In order to enhance the sensitivity of the assay, 2 mg of luciferin were added to the vial. The chemiluminescence is measured as described in chapter 4, where the current detected by the PMT is converted to voltage which is measured in real time and plotted at a rate of 10 measurements per second for 30 seconds. A period of 15 s was allowed from the time of mixture of the two solutions in the cuvette to the time the measurement was taken by the PMT. This allowed for improved reproducibility and helped to ensure that all time intervals were identical for each solution.

5.5 RESULTS AND DISCUSSION

The normalized fluorescence intensity in figure 5.4 indicates that endothelium-derived NO is increased in the presence of hypoxic RBCs (2.13 ± 0.07) when compared to RBCs alone (1.00 ± 0.21). Specifically, a 3.5% RBC sample incubated in hypoxic

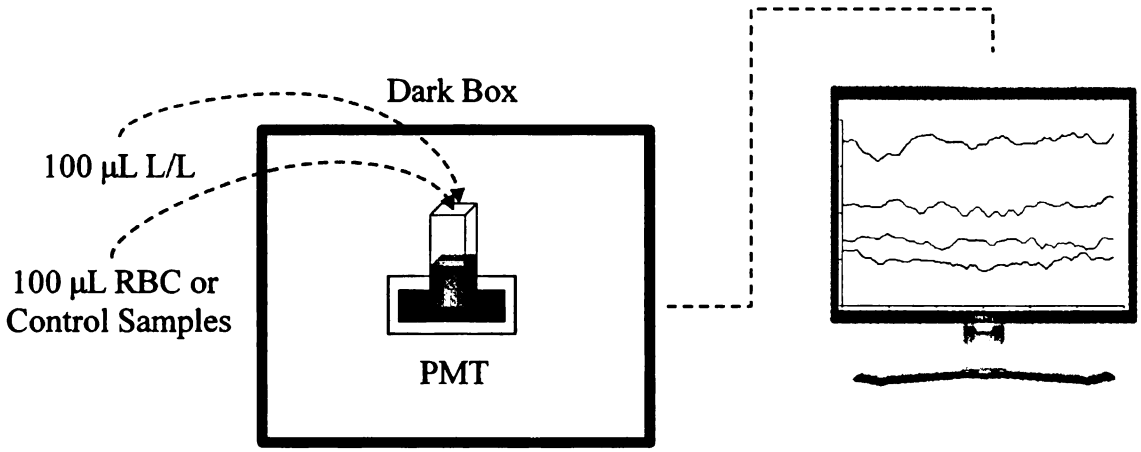

Figure 5.3 Schematic drawing of the experimental set up for determining the RBC-derived ATP release from samples incubated with trental and or iloprost to demonstrate their opposing mechanisms of action. Here, 100 µL of the luciferin and luciferase (L/L) solution is combined in a cuvette with 100 µL of each sample. The chemiluminescence is measured as before where the voltage is measured in real time and plotted at a rate of 10 measurements per second for 30 seconds onto a computer using software that was written in-house.

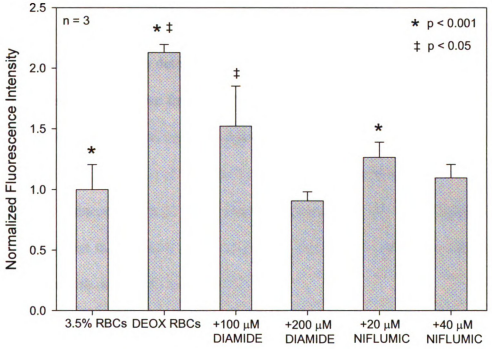

Figure 5.4 Normalized fluorescence intensity obtained from the fluorescence image of the six-channel μFA used to determine the NO produced within bPAECs cultured within the array of wells upon stimulation of various RBC samples flowing through the underlying microfluidic channels. Here, these samples include 3.5% RBCs (1.00 ± 0.21), RBCs in deoxygenated buffer (2.13 ± 0.07), and four deoxygenated samples with prior treatment of 100 μM (1.52 ± 0.33) and 200 μM (0.91 ± 0.07) diamide and 20 μM (1.27 ± 0.13) and 40 μM (1.10 ± 0.11) niflumic acid. Here the intensities are reported as averages of each well, providing triplicate measurements, and the error is reported as the standard error of the mean.

buffer stimulated more than a 2-fold increase in fluorescence intensity when compared to RBCs alone, which is directly proportional to the intracellular NO production within the bPAECs. The fluorescence intensity resulting from the RBCs hypoxic environment is decreased by 28.6% and 40.4% when RBCs are first incubated with 100 μM diamide or 20 μM niflumic acid prior to introduction into the hypoxic buffer. Demonstrating the ability to reduce this NO production even further, incubation with 200 μM diamide and 40 μM niflumic acid correspond to a decrease of 57.3% and 48.4% respectively, when compared to hypoxic RBCs.

Using the same methodology as for the hypoxic study, figure 5.5 represents the preliminary data obtained to determine the increased NO production within bPAECs due to an increase in ATP release from the RBCs incubated with metal-activated C-peptide. The normalized fluorescence intensity reported for RBCs (1.00 ± 0.05) incubated with the metal-activated C-peptide (1.31 ± 0.05) was increased by 31.0%. This intensity was consequently reduced (1.10 ± 0.20) upon prior treatment of 1 mM glybenclamide, demonstrating that the increase in fluorescence intensity was not due to cell lysis upon the incubation with metal-activated C-peptide.

Finally, the non-flow system and the luciferin/luciferase ATP assay was used to show that without subjection to mechanical deformation, the RBCs treated with trental does not elicit an increased ATP release. Figure 5.6 shows that the combination of both trental and iloprost will result in an increased RBC-derived ATP release even in a non-flow system. Here, the increase from RBCs (0.098 ± 0.006 μM) in response to iloprost (0.327 ± 0.070 μM) was three-fold, and the combination of both trental and iloprost

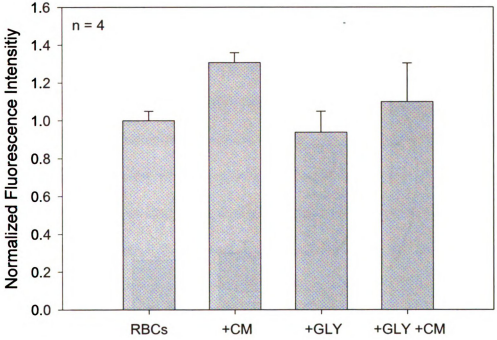

Figure 5.5 Initial results of the fluorescence intensity observed when addressing bPAECs within the μFA with RBC samples alone (1.00 ± 0.05) and with the incubation of metal-activated C-peptide (1.31 ± 0.05), 1 mM glybenclamide (0.94 ± 0.11), and 1 mM glybenclamide and metal-activated C-peptide sequentially (1.10 ± 0.20). Here the intensities are reported as averages of each well, providing triplicate measurements, and the error is reported as the SEM where the increased fluorescence intensity of RBCs incubated with metal activated C-peptide is statistically different from RBCs alone ($p < 0.05$).

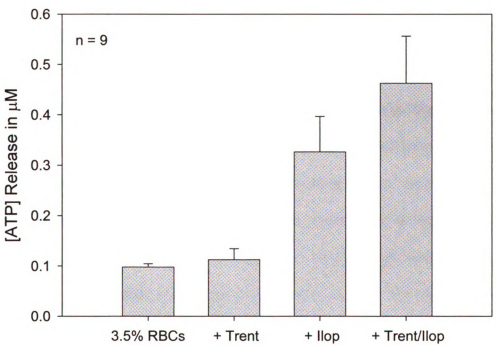

Figure 5.6 Summarized data for the measurement of RBC-derived ATP release in a non-flow system employing the luciferin and luciferase assay. Here, ATP concentrations in micromolar are reported for 3.5% RBCs (0.0981 ± 0.0063 μM), with the incubation of each 5 μM trental (0.1126 ± 0.0218 μM), 1 μM iloprost separately (0.3265 ± 0.0702 μM) and combined with 5 μM trental (0.4628 ± 0.0935 μM). The average concentration of ATP released from each RBC sample is reported where the error is represented by the SEM.

(0.463 ± 0.094) was more than four-fold, while no statistical difference in RBC-derived ATP release was observed for trental (0.113 ± 0.094 μM) when compared to RBCs alone.

5.5.1 VASODILATION MIMIC FOR MECHANISMS OF ACTION

Employing the μFA allows for the ability to better mimic the *in vivo* circulation system, specifically for the determination of hypoxia- and C-peptide-induced RBC-derived ATP release resulting in increased NO production in bPAECs cultured in the μFA. While research has previously determined that both hypoxia[1] and C-peptide[13] will increase the RBC-derived ATP release, this is the first demonstration that this will induce an increased NO production within bPAECs when compared to RBCs alone. Thus, demonstrating the multicellular mechanism of action for each hypoxia and metal activated C-peptide to elicit the production of endothelium-derived NO production.

Preliminary results demonstrate the need to examine the mechanisms of action within an appropriate system, as it is shown here, trental does not elicit a response in RBC-derived ATP release in a non-flow system. Similarly, the combination of each trental and iloprost induces an even greater ATP release from RBCs than with iloprost alone. This indicates that while iloprost will stimulate RBC-derived ATP release through IPR and the activation of the G_s-coupled signal transduction pathway within the cell, trental could possibly increase membrane flexibility, and has been demonstrated to require the shear-aspect of flow to induce ATP release.[3] Hence, the combination of these two pharmaceuticals, acting each in their own way, elicit an even greater increase in ATP release.

It has been shown that RBCs obtained from diabetic patients are stiffened[27,28] due to a reduced antioxidant ability and intracellular GSH concentrations,[29-33] as well as a reduction in the expressed G_i that is involved in the signal transduction pathway for ATP release.[9] With this in mind, the ultimate objective of this research is to provide a more appropriate analytical tool to provide individualized medicine, effectively putting the right drug into the right patient. This μFA allows for a more systems biology approach to drug discovery and clinical testing by mimicking the resistance vessels found *in vivo*, providing a means to better understand the multicellular mechanism of action as it pertains to vasodilation. Specifically, iloprost may be limited in alleviating the complications associated with diabetes for a patient with a reduced G_i expression, however addition of trental as well, may allow for increased vasodilation by increasing the RBC deformability as well.

REFERENCES

1. Faris, A. & Spence, D.M. Measuring the simultaneous effects of hypoxia and deformation on ATP release from erythrocytes. *Analyst* **133**, 678-682 (2008).

2. Kosower, N.S., Kosower, E.M., Wertheim, B. & Correa, W.S. Diamide, a new reagent for the intracellular oxidation of glutathione to the disulfide. *Biochem Biophys Res Commun* **37**, 593-596 (1969).

3. Carroll, J.S., Ku, C.-J., Karunarathne, W. & Spence, D.M. Red Blood Cell Stimulation of Platelet Nitric Oxide Production Indicated by Quantitative Monitoring of the Communication between Cells in the Bloodstream. *Anal Chem* **79**, 5133-5138 (2007).

4. Sprague, R.S., Ellsworth, M.L., Stephenson, A.H. & Lonigro, A.J. ATP: the red blood cell link to NO and local control of the pulmonary circulation. *Am J Physiol* **271**, H2717-H2722 (1996).

5. Sprague, R.S., Ellsworth, M.L., Stephenson, A.H., Kleinhenz, M.E. & Lonigro, A.J. Deformation-induced ATP release from red blood cells requires CFTR activity. *Am J Physiol Heart Circ Physiol* **275**, H1726-1732 (1998).

6. Olearczyk, J.J., Stephenson, A.H., Lonigro, A.J. & Sprague, R.S. Receptor-mediated activation of the heterotrimeric G-protein Gs results in ATP release from erythrocytes. *Med Sci Monit* **7**, 669-674 (2001).

7. Sprung, R., Sprague, R. & Spence, D. Determination of ATP release from erythrocytes using microbore tubing as a model of resistance vessels in vivo. *Anal Chem* **74**, 2274-2278 (2002).

8. Fischer, D.J., Torrence, N.J., Sprung, R.J. & Spence, D.M. Determination of erythrocyte deformability and its correlation to cellular ATP release using microbore tubing with diameters that approximate resistance vessels in vivo. *Analyst* **128**, 1163-1168 (2003).

9. Sprague, R.S., Stephenson, A.H., Bowles, E.A., Stumpf, M.S. & Lonigro, A.J. Reduced expression of Gi in erythrocytes of humans with type 2 diabetes is associated with impairment of both cAMP generation and ATP release. *Diabetes* **55**, 3588-3593 (2006).

10. Carroll, J. et al. An altered oxidant defense system in red blood cells affects their ability to release nitric oxide-stimulating ATP. *Mol Biosyst* **2**, 305-311 (2006).

11. Genes, L.I., Tolan, N.V., Hulvey, M.K., Martin, R.S. & Spence, D.M. Addressing a vascular endothelium array with blood components using underlying microfluidic channels. *Lab Chip* **7**, 1256-1259 (2007).

12. Sprague, R.S., Stephenson, A.H. & Ellsworth, M.L. Red not dead: signaling in and from erythrocytes. *Trends Endocrinol Metab* **18**, 350-355 (2007).

13. Meyer, J.A., Froelich, J.M., Reid, G.E., Karunarathne, W.K.A. & Spence, D.M. Metal-activated C-peptide facilitates glucose clearance and the release of a nitric oxide stimulus via the GLUT1 transporter. *Diabetologia* **51**, 175-182 (2008).

14. Kunt, T., Forst, T., Pfützner, A., Beyer, J. & Wahren, J. The physiological impact of proinsulin C-peptide. *Pathophysiology* **5**, 257-262 (1999).

15. Furchgott, R.F. & Zawadzki, J.V. The obligatory role of endothelial cells in the relaxation of arterial smooth muscle by acetylcholine. *Nature* **288**, 373-376 (1980).

16. Ignarro, L.J., Buga, G.M. & Chaudhuri, G. EDRF generation and release from perfused bovine pulmonary artery and vein. *Eur J Clin Pharmacol* **149**, 79-88 (1988).

17. Moncada, S., Palmer, R. & Higgs, E. The discovery of nitric oxide as the endogenous nitrovasodilator. *Hypertension* **12**, 365-372 (1988).

18. Palmer, R.M.J., Ashton, D.S. & Moncada, S. Vascular endothelial cells synthesize nitric oxide from L-arginine. *Nature* **333**, 664-666 (1988).

19. Moncada, S., Palmer, R.M.J. & Higgs, E.A. Nitric oxide: physiology, pathophysiology, and pharmacology. *Pharmacol Rev* **43**, 109-142 (1991).

20. Sobey, C.G. Potassium channel function in vascular disease. *Arteriosclerosis, Thrombosis, and Vascular Biology* **21**, 28-38 (2001).

21. Webb, R.C. Smooth Muscle Contraction and Relaxation. *Adv Physiol Educ* **27**, 201-206 (2003).

22. Tuteja, N., Chandra, M., Tuteja, R. & Misra, M.K. Nitric oxide as a unique bioactive signaling messenger in physiology and pathophysiology. *J Biomed Biotechnol* 227-237 (2004).

23. Martínez-Morales, M.E.D.-E.a.F. Pentoxifylline Diminishes the Oxidative Damage to Renal Tissue Induced by Streptozotocin in the Rat. *Exp Diabesity Res* **5**, 245-251 (2004).

24. Gunduz, Z. et al. The Effects of Pentoxifylline on Diabetic Renal Changes in Streptozotocin-Induced Diabetes Mellitus. *Ren Fail* **26**, 597 - 605 (2004).

25. Navarro, J.F., Mora, C., Muros, M., Macia, M. & Garcia, J. Effects of pentoxifylline administration on urinary N-acetyl-beta-glucosaminidase excretion in type 2 diabetic patients: a short-term, prospective, randomized study *Am J Kidney Dis* **42**, 264-270 (2003).

26. Radfar, M. et al. Effects of pentoxifylline on oxidative stress and levels of EGF and NO in blood of diabetic type-2 patients; a randomized, double-blind placebo-controlled clinical trial. *Biomed Pharmacother* **59**, 302-306 (2005).

27. MacRury, S.M., Small, M., Anderson, J., MacCuish, A.C. & Lowe, G.D. Evaluation of red cell deformability by a filtration method in type 1 and type 2 diabetes mellitus with and without vascular complications. *Diabetes Res* **13**, 61-65 (1990).

28. Schwartz, R.S., Madsen, J.W., Rybicki, A.C. & Nagel, R.L. Oxidation of spectrin and deformability defects in diabetic erythrocytes. *Diabetes* **40**, 701-708 (1991).

29. Costagliola, C. Oxidative state of glutathione in red blood cells and plasma of diabetic patients: in vivo and in vitro study. *Clin Physiol Biochem* **8**, 204-210 (1990).

30. De Mattia, G. et al. Influence of reduced glutathione infusion on glucose metabolism in patients with non-insulin-dependent diabetes mellitus. *Metabolism* **47**, 993-997 (1998).

31. Dincer, Y., Akcay, T., Alademir, Z. & Ilkova, H. Effect of oxidative stress on glutathione pathway in red blood cells from patients with insulin-dependent diabetes mellitus. *Metabolism* **51**, 1360-1362 (2002).

32. Constantin, A., Constantinescu, E., Dumitrescu, M., Calin, A. & Popov, D. Effects of ageing on carbonyl stress and antioxidant defense in RBCs of obese type 2 diabetic patients. *J Cell Mol Med* **9**, 683-691 (2005).

33. Nwose, E.U., Jelinek, H.F., Richards, R.S. & Kerr, P.G. in Redox Report, Vol. 11 99-104 (Maney Publishing, 2006).